TOOLS AND METHODS FOR STUDYING VASCULAR PHYSIOCHEMICAL FORCE TRANSDUCTION AND MECHANOBIOLOGY

A Dissertation

by

BRANDON KURT WALTHER

Submitted to the Graduate and Professional School of
Texas A&M University
in partial fulfillment of the requirements for the degree of

DOCTOR OF PHILOSOPHY

Chair of Committee,	Abhishek Jain
Co-Chair of Committee,	John P. Cooke
Committee Members,	Anthony Guiseppi-Elie
	Carolyn Cannon
	Reza Avazmohammadi
Head of Department,	Mike McShane

May 2023

Major Subject: Biomedical Engineering

ABSTRACT

Cells reside in complex physicochemical environments which provide forces acting as cues that influence the molecular physiology. However, the mechanisms and interactions between the various physical forces and the resultant downstream phenotype still have significant gaps in knowledge. This dissertation focuses on implementing tools and protocols to investigate how vascular cells respond to specific external forces and how these engineered approaches can facilitate new understanding. Three specific approaches and findings will be highlighted.

The first approach entails using engineered in vitro systems to study the interactions of two key physical forces in vascular health: shear stress and matrix stiffness. These vessel-chip systems allow for investigating often confounding variables, finding that matrix stiffness impedes the protective effect of shear stress on endothelial cells.

The second approach uses a tailored electroculture ware system to study how external electrical fields influence endothelial cell growth and biology. This work demonstrates that electric impulses accelerate proliferation and potentiate YAP activity.

The third approach establishes a pipeline for accessing subcellular biomechanics, that is, it is a protocol which provides the full mechanical properties of individual cells. Using combined Atomic Force Microscopy and Structure Illumination Super Resolution Microscopy, individual endothelial cells can be modeled, with applications to investigating physical changes in the context of aging.

Altogether the methods and approaches described here provide a foundation for studying how endothelial cells respond to physical stimuli, how external forces interact and result in biological phenomena, and whether mechanical shifts due to disease states can alter these processes from a physical perspective. Further understanding of cellular force transduction is facilitated by these interdisciplinary approaches.

DEDICATION

To my mother, father, and brother, whose support throughout this time period made this work possible.

ACKNOWLEDGMENTS

There are many people I would like to thank for their support during my thesis writing.

I would like to thank my supervisors Drs. John P Cooke and Abhishek Jain for their expertise, guidance, advice, and willingness to let me explore the fields of mechanobiology and biophysics. Their support made this work possible.

I would also like to thank my committee member and previous supervisor Dr. Anthony Guiseppi-Elie, whose insight and advice was invaluable from both a technical engineering side to the art of writing and communication.

I would also like to thank my committee member Carolyn Cannon for her time and willingness to answer my questions and support me throughout the MD/PhD training process; her help and advice were integral to my completion of this work.

The many people I worked with made this dissertation possible, and without their collaboration and enthusiam, this work would not be. I would like to thank Jacques Ohayon for his mentorship and expertise in biomechanics, and for our many conversations about science and mathematics. I would like to thank Dr. Adam Sears, Dr. Sara Abasi, Dr. Karli A Gold, and Navaneeth Krishna Rajeeva Pandian, people with whom I worked closely with on this academic endeavor.

I would also like to thank my family - my mom, dad, and brother, for their unending love and support throughout my training.

And lastly, I would like to thank God, for a peace which carried me through.

CONTRIBUTORS AND FUNDING SOURCES

Contributors

This work was supported by a thesis committee consisting of Dr. John P. Cooke [advisor], Dr. Abhishek Jain [co-advisor] and Dr. Reza Avaz Avazmohammadi of the Department of Biomedical Engineering, Dr. Carolyn Cannon of the Department of Microbial Pathogenesis and Immunology, and Dr. Anthony Guiseppi-Elie of the Department of Biomedical Engineering at Anderson University.

The fluid dynamics computations in Chapter 2 were conducted by Navaneeth Krishna Rajeeva Pandian of the Department of Biomedical Engineering (Jain). The bulk mechanical moduli in Chapter 2 were collected by Karli A. Gold of the Department of Biomedical Engineering (Gaharwar). The ECSARA system, viability studies, and equivalent circuit analysis in Chapter 3 were performed by Dr. Sara Abasi of the Department of Biomedical Engineering (Guiseppi-Elie). The representative biomechanics images in Figure 4.1 in Chapter 4 were supplied by Dr. Reza Avazmohammadi of the Department of Biomedical Engineering and Dr. Jacques Ohayon of the Department of Mechanics at the University Savoie Mont-Blanc. The contouring code and Figure 4.7c in Chapter 4 were written and supplied by Dr. Adam Sears of the Department of Biomedical Engineering.

All other work conducted for the thesis (or) dissertation was completed by the student independently.

Funding Sources

Graduate study was supported by a fellowship from Texas A&M University MD/PhD program. Grant funding sources were the NIBIB Award R21EB025945, NSF CAREER Award 1944322 and Texas A&M University Presidents Excellence in Research Award (X-Grant) to A.J.; and by funding from the National Heart Lung and Blood Institute, 1R01HL148338 and 1R01HL133254 to J.P.C. Graduate work was additionally supported by the Texas Engineering Experiment Station (TEES).

NOMENCLATURE

AFM	Atomc Force Microscopy
SIM	Structured Illumination Microscopy
STORM	Stochastic Optical Reconstruction Microscopy
VC	Vessel-Chip/Vessel-on-a-Chip
EF	Electric Field
ECSARA	Electrical Cell Stimulation And Recording Apparatus
EIS	Electrical Impedance Spectroscopy
TEER	Trans-Endothelial Electrical Resistance
EC	Endothelial Cell
HUVEC	Human Unbilical Vein Endothelial Cell
HGPS	Hutchinson-Gilford Progeria Syndrome
iPSC	Induced Pluripotent Stem Cell
RS	Replicative Senescence
YAP	Yes-Associated Protein 1
TAZ	Transcriptional Coactivator with PDZ-Binding Motif
eNOS	Endothelial Nitric Oxide Synthase
VEGFR2	Vascular Endothelial Growth Factor Receptor 2
USS	Unidirectional Shear Stress
OSS	Oscillatory Shear Stress
E-Cadherin	Epithelial-Cadherin
CD-(number)	Cluster of Differentiation-(number)
VE-Cadherin	Vascular Endothelial-Cadherin (CD-144)

PECAM-1	Platelet Endothelial Cell Adhesion Molecule-1 (CD-31)
TGF-1	Transforming Growth Factor 1
cGMP	Cyclic Guanosine Monophosphate
PIEZO1/2	Piezo Type Mechanosensitive Ion Channel Component 1/2
LATS1/2	Large Tumor Suppressor1/2
CTGF	Connective Tissue Growth Factor
ANKRD1	Ankyrin Repeat Domain 1
ICAM-1	Intercellular Adhesion Molecule 1 (CD54)
VCAM-1	Vascular Cell Adhesion Molecule 1
vWF	von-Willebrand Factor
Rho	Ras Homolog Family Member
JNK	c-Jun N-Terminal Kinase
NO	Nitric Oxide
IL-(number)	Interleukin-(number)
hTERT	Human Telomerase Reverse Transcriptase
PDMS	Polydimethylsiloxane

TABLE OF CONTENTS

Page

LIST OF FIGURES

FIGURE Page

1. INTRODUCTION AND LITERATURE REVIEW

1.1 Endothelial Mechanobiology: Cellular Physiochemical Force Transduction

Endothelial cells reside in complex environments which include a combination of chemical and physical cues which influence their overall phenotype, however, the mechanisms by which cells transduce these physical stimuli into biochemical responses is only recently being elucidated. It has been understood for over a century, however, that mechanical forces can affect cellular processes as early as 1892, it was reported that bone trabeculae aligned along an axis of stress [1]. Incidentally, there would be a long delay between this first finding and any further investigation into how cells take a physical input and alter their biology, and the field of mechanobiology would take form. In the mid-1980s, studies on vascular endothelial cells reporting alignment under shear stress were published [2, 3], opening up the field yet again to studying the importance of how cells respond to physical cues. Eventually, mechanobiology in the context of the cardiovascular system would proceed to take form.

Mechanobiology is the study of how cells respond to physical cues and alter their phenotype [4–6]. The field itself is quite young, and matured in the last 10-15 years only in parallel with the development of technologies enabling researchers to test hypotheses relating physical forces and biological responses [7–9]. These technologies include but are not limited to: advanced imaging (super-resolution imaging); atomic force microscopy; engineered, tunable matrices such as hydrogels; engineered in vitro systems; and biological force responsive sensors such as FRET tension sensors highlighting the interdisciplinary nature of require techniques for tackling these questions.

Since these pioneering findings and technological advancements, the importance of physical inputs on endothelial cell health and maintenance has been clearly established. Endothelial cells are constantly subject to several different forces; they are exposed to pulsatile shear stresses from blood flow, cyclic strain from vascular stretching, and varying matrix stiffnesses originating from

the structural components making up the vascular tissue itself, each able to affect the endothelial phenotype. This dissertation introduction will first review mechanisms of force transduction in a general sense, approaches to study these phenomena, and then discuss vascular mechanobiology with a clinical focus to describe how the tools employed here can answer outstanding questions.

1.2 Key Mechanisms of Biological Force Transduction

Physiochemical force transduction requires a biological transducer to convert a physical force into a biochemical reaction. On a fundamental level, this requires that a responsive biological entity, such as a protein or protein complex, undergoes a physical or chemical change that induces signal cascade when the stimulus is present. Several parts of this paradigm have been described, ranging from the transducer itself (integrins, cadherins, and mechanically sensitive ion channels) to mechanically controlled signaling pathways that influence gene expression and cell behavior (YAP/TAZ being a primary one of interest here).

1.2.1 Integrins

Integrins are transmembrane proteins consisting of non-covalently bound α and β subunits, which, in mammals, give rise to approximately 24 different integrin complexes [10]. Well understood to bind to several extracellular matrix components to mediate adhesion [11], with the advent of mechanobiology they have emerged as key force sensors that relay external physical cues into the cell. Integrins experience and transmit force crosstalk between cells and their matrix attachments via focal adhesions [10–13].

Integrin signaling is thought to function through a few specific steps. Surface integrins can exist in 3 general states: an inactive form; an active, talin-bound form; and a clustered, ligand-bound form [14]. Downstream of integrin signaling includes several relevant signaling pathways such as Rho kinase signaling and YAP/TAZ signaling, among others [14]. Integrins are connected to the cytoskeleton via several different proteins, including talin and vinculin [15]. Of particular importance in discussing mechanotransduction pathways is the stretch responsiveness of talin itself. Talin binds to integrins and thus can experience forces applied across the cell membrane. These

forces can induce stretching of talin, altering its confirmation and exposing previously sequestered hydrophobic residues. In turn, these newly exposed domains can bind to vinculin, providing a biophysical transducer in the form of a protein confirmational change [15]. Other studies have demonstrated that vinculin itself also experiences forces, with high tension forces promoting integrin assembly and focal adhesion enlargement [16, 17].

1.2.2 Cadherins

Cadherins are a large class of cellular adhesion molecules that play an important role in cell-cell junctional architecture [18]. There are several classes of cadherins. Classical cadherins are the most studied they are Ca2+-dependent and homophilic, with cytoplasmic binding to α/β-catenin and directly linked to the actin cytoskeleton [18]. Several well-known cadherins belong to this family, such as the prominently studied E-cadherin (epithelial) which plays an important role in cellular junctional formation, development, and tumor suppression [19]. Found exclusively in the endothelium, VE-cadherin (vascular endothelial) is a divergent classical cadherin which plays an integral role in endothelial adherens junction formation and mechanical sensing [20, 21]. Other classes of cadherins include the desmosomal cadherins that bind to intermediate filaments, protocadherins with several different interacting proteins, and ungrouped cadherins [18]. Of particular interest in the context of cardiovascular mechanobiology is, of course, VE-cadherin.

The general mechanism of force transduction via classical cadherins shares many biophysical mechanisms with that of integrins. Cadherins associate with β-catenin, which then binds to α-catenin. It is α-catenin which is stretch sensitive, much like talin. In the resting state, α-cadherin is folded and the vinculin binding domain is associated with an inhibitory domain on α-cadherin [22, 23]. When a tension force is applied across α-catenin, the protein unfolds and the vinculin binding domain disassociates with the inhibitory domain, allowing for vinculin binding and downstream signal transduction. VE-cadherin plays a role in mechanical sensing in the endothelium and is critical for vascular development and homeostasis, however the mechanism is significantly more complex. VE-cadherin forms a mechanosensory complex with two other proteins, PECAM-1/CD31, and VEGFR2 [21]. Here, VE-cadherin functions as an adaptor, while CD31

directly experiences force however application of shear stress increases tension across CD31, but decreases it across VE-Cadherin [24]. This mechanosensory also appears to play a convoluted role in fluid shear sensing, as knockdown of this complex promoted atherosclerosis where sites of protective shear occurred, but inhibited atherosclerosis at sites of disturbed flow [25, 26].

1.2.3 Ion Channels

Mechanically sensitive ion channels were established in 1988 as a way endothelial cells respond to shear stress [27, 28]. Both potassium and calcium were implicated. The potassium current was then tied to nitric oxide production by work by Cooke et al. [29] The calcium current appears to be tied to both influx and release from intracellular stores, but also increases nitric oxide production [30]. Like the other two transducers discussed, ion channels play an important role in mechanotransduction, but the wide diversity of different ions precludes a complete review. Rather, some general mechanisms will be discussed, and the importance with regards to endothelial biology will be highlighted. There are two general mechanisms described for mechanosensing via ion channels. The first is a membrane tension model, where a tension force along the cell membrane causes ion channels to open. The second gating model is a tethering model where another molecule is connected to the ion channel, and force applied along it is transmitted to the ion channel [31]. However, these are only general sketches of how the channels work and each ion channel itself has a unique structure which confers its open/close architecture.

The early response of endothelial cells to shear stress implicates a potassium efflux triggering a cascade of intracellular processes [30]; this potassium current was established early on by several research groups [28, 29, 32–34]. This potassium channel is classified as an inward rectifying channel, meaning that activation of the channel facilitates potassium entry into the cell more easily that it facilitates potassium efflux, although the actual ion flow is strongly dependent on the resting potential of the system. The specific identity of this channel is mostly strongly supported as KIR2.1 [35–37] a channel which appears to be mechanically sensitive and responds to fluid flow when expressed in several cells. Somewhat counterintuitively, though, is that the inward rectifying channels in ECs (and other tissues) are responsible for an outward potassium flow at resting mem-

brane potentials, participating in hyperpolarization [30, 36] (despite functionally supporting larger inward currents at voltages more negative than the resting potential). The precise mechanism by which this works is not yet well understood, although can be rationalized using the previously discussed general mechanisms: shear stress induced tension opens these channels which, at the resting potential of the endothelial cell, yields outward potassium current and hyperpolarization. Potassium efflux from endothelial cells then results in more calcium influx and additionally is directly tied to TGF-β1 and cGMP production as well as eNOS regulation [29, 33, 34].

A highly impactful discovery more recently was the characterization of the PIEZO1 and 2 channels. The mechanically gated calcium channels provided an important hinge point for uncovering the mechanisms of mechanotransduction. PIEZO channels (here the focus will just be on PIEZO1) are unique proteins in that they share no structural similarity with any other known protein [38–40]. These channels consistent of a tri-blade structure with long, spiraled arms that converge into a central ionic pore [41–43]. It is thought that these long arms alongside a beam mechanism controls the open and close states of the channel, although the precise mechanical gating mechanism is not clearly understood [38, 39, 41, 43, 44]. Piezo1 has a diverse set of roles. Most notably in the vasculature, it is a shear stress sensor and is required for vascular development in mice [45, 46]. It also appears to have roles in innate immune activation [47], bone development [48], lymphatic development [49], and epithelial division [50].

One such comment which will be conceptually returned to later in this dissertation is that each of these mechanosensing regimes possess a dependence on the ionic properties of the system. This is most evidenced by each ion channel being described by its current/voltage sweep curve (such as, for example, inward rectifying) at different voltages the ion channels behave differently. This would suggest that external electrical fields which alter the potential driving force for ionic currents can influence cellular behavior. Several studies have explored this, most often known via the electroceutical industry (pacemakers) [51–53], as well as studies on the influences of electric fields on cell biology [54–60]. Mechanisms by which this occurs are poorly understood, and it remains an open question.

1.2.4 YAP and TAZ

Unlike the previously discussed proteins and complexes, Yes-associated protein (YAP) and transcriptional coactivator with PDZ-binding motif (TAZ; collectively, YAP/TAZ) are paralog transcriptional co-activators which serve as downstream effectors to orchestrate cellular mechanotransduction [61–64]. In the context of mechanobiology, YAP/TAZ serve as the biochemical response elements to the physical stimulus rather than the transduction agents themselves. Their importance in mechanobiology, however, is multifaceted as they mediate responses to an enormous number of mechanical cues including matrix stiffness [65], cell-cell contact [66], cellular strain [67], cell size and geometric cues [68], and fluid shear stress [69, 70]. Originally studied in the context of the Hippo pathways and organ growth, interest in YAP/TAZ as mechanoresponsive elements has divulged biochemical pathways separate from Hippo. Stiff matrices, low cell confluency, high cellular strain, large cell sizes, and low or oscillatory shear stress all serve to activate YAP/TAZ and induce cell cycle progression and proliferation [71]. Conversely, YAP/TAZ activity is shut off by soft matrices, cell confluence, low strain, cell size restriction, and high laminar shear stress. More abstractly speaking, YAP/TAZ can serve as a readout for the cellular response to various mechanical cues, provided that each contributor to its activity is appropriately controlled for [62]. Compared to the cadherin mechanosensory complex, YAP/TAZ signaling in the vasculature is relatively simple: physical inputs which are associated with or promote plaque progression (such as disturbed flow or stiff matrices) cause YAP/TAZ activation and endothelial dysfunction. Physical inputs known to be protective inhibit YAP/TAZ activity.

YAP and TAZ are regulated by a variety of upstream biochemical signals. Their activity is, generally speaking, controlled by their phosphorylation state, with activating signals inducing dephosphorylation and nuclear translocation, and inactivating signals inducing phosphorylation and cytoplasmic retention or degradation [64]. Via the Hippo pathway, the upstream kinase which inhibits YAP/TAZ is large tumor suppressors 1 and 2 (LATS1/2), while the Wnt pathway is mediated by the destruction complex with similar outcomes [64]. The exact mechanism by which YAP/TAZ are regulated by mechanical cues, however, remains incompletely characterized. Generally speak-

ing, there are a few paradigms and pathways which have been proposed. One such fundamental mechanism explains YAP/TAZ nuclear translocation as a function of nuclear pore stretching as it was demonstrated that force application by AFM caused nuclear accumulation of YAP [72]. Incidentally, this picture is likely incomplete, as fluid shear stress, itself a force on the nucleus, induces YAP/TAZ inactivation via an integrin/G-protein signaling as mediated by Ras homolog family member A (RhoA) [70]. This indicates, at a minimum, that biochemical cues may override physical explanations for the behavior of YAP/TAZ in response to external forces. Other studies implicate cytoskeletal architecture as a main mechanical stimulus, as cytoskeletal strain activates YAP/TAZ [73]. Additionally, YAP/TAZ play a key role in focal adhesion assembly, ultimately affecting cell geometry [74]. Altogether, fundamental mechanisms which provide a complete picture of the mechanobiological regulation of YAP/TAZ are still being described.

Some further notes on YAP/TAZ function and activity are that while for the duration of this discussion and dissertation they will be referred to collectively (as they largely act in tandem), YAP and TAZ are distinct proteins with, interestingly, some differing functions which serve to delineate them. YAP and TAZ have slightly divergent structures; YAP has 5 serine residues available for phosphorylation, while TAZ possesses only 4 [75]. YAP appears to exert more influence over cellular processes (i.e. cell geometry and proliferation) when knocked out in comparison to TAZ, although they appear to share several functions [76]. And, recently, both YAP and TAZ have been studied as phase separation components which facilitate gene expression, however TAZ is a native orchestrator while YAP only mimics such function under osmotic stress or macromolecular crowding [77–79].

1.3 Current Approaches for Studying Mechanobiology

Much of mechanobiology has advanced in tandem with the technology require to study the phenomena [7]. Each of the pivotal approaches will be discussed briefly in this section, and in each chapter, a more in-depth historical context and literature review will be provided.

1.3.1 Tunable Matrices

One of the first ways mechanobiology was studied was using tunable matrices with various properties such as stiffnesses or viscoelastic properties. The matrices may be synthesized with chemical properties that impart specific interactions to study how a cell responds to the environment it has been demonstrated that substrate stiffness influences cellular differentiation and proliferation [9,65,80–88]. Incidentally, this is not a unidirectional communication and cells themselves apply forces and interaction with their environment as well, suggesting a complex crosstalk which is fundamentally governed by both the cell and the matrix composition. Once such method which uses tunable matrices is traction force microscopy, which measures the forces a cell exerts on its surroundings [89–91]. Thus, a closed loop is formed between designing a material of precise properties (such as measuring the stiffness of a material) and the response of the cell to the material both physically (traction) and biologically (e.g. YAP/TAZ biology). There are several materials used in the engineering field which are tailored for specific uses and a full treatment here is not feasible. However, common materials which repeatedly show up in literature due to their tunable material properties and ease of chemical modification include polyacrylamide [72, 89] and polydimethylsiloxane [92]. Beyond mechanical properties, these systems can then be extended to include cross-talk between a physical input and a chemical/biological one to study interactions in a quantized manner [81]. A step further than passive matrices would be tension or compression systems designed to apply a direct force to a cell and then measure the response. Examples of these system may include the Flexcell systems [93, 94], or any other systems designed to induce stress/strain. These systems have been directly applied to mechanobiological systems to test the effects of strain on YAP activity [65,67], vascular inflammation [95], and cellular alignment [96,97].

1.3.2 Microfluidic and Engineered *In Vitro* Systems

Another approach to study mechanobiology is to engineer the physical stimuli and interactions directly into a 3-dimensional culture system. Shearing systems have been present for several years [3, 98, 99] and microfluidic system development to study flow patterns, magnitudes, and ge-

ometries is ongoing [100–104]. The translation of these systems to vascular biology is immediately tangible, as modeling physiologic and pathologic flow has yielded considerable insight as to the mechanisms of vascular homeostasis. Parallel to this field is the research into organ-on-a-chip systems: devices where specific organ or tissue level functions are directly integrated into the culture environment [105–107]. Devices tailored for studying the vasculature are often termed vessel-on-a-chip devices [108–111] and can provide an alternative avenue for studying fluid and matrix mechanobiology. Specific systems have even been devised to study specific mechanobiological pathways, with devices tailored for studying YAP emerging recently [104, 112].

1.3.3 Atomic Force Microscopy

Atomic Force Microscopy (AFM) is an imaging method that operates based on interactions between a probe and the material itself. AFM has expanded beyond its imaging capacity to include force measurements as well as the ability to do chemistry as mediated by probe and material functionalization. AFM has seen several applications in biology based on these key abilities. First, it has allowed for biological mechanical measurements, allowing for the mechanical properties of individual cells, and even subcellular components, to be extracted and quantified [113–115]. It has also allowed for biophysical mechanism elucidation via its ability to support chemistry. To illustrate, AFM chemical bonding was exploited to study talin stretching mechanics and observe the changes in vinculin binding [15]. AFM is also combined readily with several other advances methodologies, such as computational modeling or super-resolution imaging to yield combined information about the system [114]. Overall, AFM is a powerful, common tool employed throughout mechanobiology.

1.3.4 Super Resolution Imaging Techniques

Any imaging technique which bypasses the theoretical diffraction limit of light is termed super resolution imaging. There are two general approaches seen in literature. The first class uses structure light to reconstruct images in Fourier space using Moiré fringes, termed structured illumination microscopy (SIM) [116]. The second class uses any method of object localization and

point spread function fitting to remove system impulse that blurs the image to improve resolution (e.g. stochastic optical reconstruction microscopy; STORM) [117]. While a complete treatment on the theory requires a sophisticated dive into optic theory [118], the applications are immediately tractable. With access to information in the nanometer range, molecular interactions, cellular architectures, and precise geometric measurements are now attainable, all of which provide insight into cellular mechanobiological processes. As an exemplar, super resolution imaging uncovered the periodic actin/spectrin structure in neuronal axons [119], information not accessible using conventional imaging methods. This structural information is invaluable for describing force transduction through cells as mechanical properties, force transduction, and cytoskeletal architecture are intimately connected. Furthermore, it would aid in computational modeling of mechanotransduction.

1.3.5 Electroculture Systems

The last of the methods discussed here which are of relevance to the dissertation, electrical stimulation of cells and the resulting biology is a long-studied field used to interrogate biological systems [120–123]. This technique, however, is more commonly used to describe certain tissues, cell populations, and disease states rather than study precise biological mechanisms. There are reports that electric fields influence cell behavior, such as that seen in wound healing, and also sees direct clinical application with cardiac pacemakers [55, 57–60, 124]. Due to the connections between mechanosensing, ionic channels, and electric fields, this dissertations uses an electrocultureware system [54] to study how electric fields may influence mechanobiological pathways pertaining to YAP.

1.4 Vascular Mechanobiology and Homeostasis

Vascular biology has been profoundly impacted by these advances in mechanobiology thanks to the uniquely complex mechanical environments the cardiovascular system possesses. It was during the early to mid-1980s (facilitating the end to the silence on biomechanical forces and cell behavior) where work from Peter Davies demonstrated that vascular endothelial cells respond to fluid shear stress [98]. Their preliminary observations reported cellular alignment and actin cy-

toskeletal changes. In the following years, other groups would report similar findings, confirming that shear stress can influence cytoskeletal mechanics in endothelial cells [3, 99, 125]. Shortly following, in 1986, Peter Davies then demonstrated that turbulent shear stress accelerates endothelial cell turnover [2], providing what would be the first evidence of a physical input that would be understood to be detrimental to endothelial cell health. As it would turn out, this general concept of countervailing physical inputs which can influence cell health positively or negatively would prove to be a fundamental underpinning of vascular biology and disease progression.

Nonetheless, this pioneering work still provided only a correlative observation, and closing the loop via a full mechanobiological pathway (as would be understood today) would follow with the work of John Cooke. In 1988, Peter Davies established that shear stress actives a potassium channel in endothelial cells [28]. In 1990 and 1991, this was tied specifically to endothelial release of nitric oxide (NO) by John Cooke, where his work demonstrated that 1) endothelial cells release a vasodilator in response to fluid flow (NO release) and that 2) this release was blocked when the mechanically active potassium channels were inhibited [29]. This then provided a complete mechanobiological pathway, connecting a physical stimulus (fluid flow) to a biological response (NO release) via a biological transducer (the potassium channel).

In more recent years, the compendium of knowledge on how physical forces influence vascular biology has grown and improved in resolution. Several different mechanical stimuli are known to influence blood vessels, including shear stress, wall strain, and matrix stiffness. It is now understood that several patterns of shear stress have differing effects on the endothelium which are dependent on the pattern and the magnitude. In the arterial system, pulsatile, unidirectional shear stress of high magnitude (10-30 dynes/cm2) is atheroprotective [26, 126–130]. The term atheroprotective specifically means stimuli (which includes physical, chemical, and biological although each of these in the field of mechanobiology blend together) which prevent vascular pathology, specifically atherosclerosis. Or, more simply, stimuli which promote vascular health. In contrast, several fluid shear patterns induce endothelial dysfunction and disease progression, all of which are termed collectively disturbed flow. Disturbed flow includes oscillatory or turbulent flow pat-

terns, recirculating flow, and low magnitude shear stress that is either unidirectional and laminar or oscillatory [26, 103, 128, 131–134]. These flow patterns instead induce endothelial inflammation, increases in vascular tone, and atherosclerotic progression, and are termed atherogenic inputs. Clinically, this paradigm intimately ties common sites of plaque development with the branch points of the vasculature, where disturbed flow patterns are most common [127]. There are two well studied mechanobiological pathways which mediate these effects in endothelial cells, the CD31/CD144/VEGFR2 complex [21], and the integrin/JNK/YAP pathway [69, 70].

Strain caused by the pressure exerted from cardiovascular pumping is another physical parameter which influences vascular cell behavior. Here it is briefly reviewed as this dissertation does not primarily focus on this parameter, however it remains an important physical stimulus in its own right and is worth mentioning. Endothelial cells align when subject to cyclic strain, however unlike the parallel alignment to shear stress, they align perpendicular to the stretching force vector [87, 135]. Notably, physiologic shear and strain work synergistically to align endothelial cells parallel to the fluid flow vector. These straining forces activate mechanosensitive transducers (such as integrins or ion channels) [136]. Mechanical strain has complex effects on the vasculature, inducing oxidative stress and C-reactive protein expression [137, 138], but also increasing eNOS expression in endothelial cells [139]. Overall, physiologic strain is important for vascular homeostasis, while excessive strain leads to pathological states [140].

Lastly, matrix stiffness plays an integral role in vascular health and disease progression. However, unlike the previous two parameters which have constantly varying parameters and ranges over which they occur even in healthy vessels, high matrix stiffness generally only presents in pathological vessel tissue [141]. There are some exceptions which are present most notably in the coronary arteries which are subject to constant muscular forces that exert external stiffening upon contraction [142–145]. Nonetheless, vascular tissue is most commonly soft (50-500 kPa; increasing within the coronary arteries or large conducting vessels [141, 144, 146–148]). Diseased vasculature or plaques, conversely, has a significantly wider range of moduli, going from extremely soft (1 kPa) to extremely stiff (>3 MPa) [143]. These associations have been understood as strongly

correlated for a long time [149], with diseased vasculature being associated with vessel stiffening. However, the connection between these two parameters clinically remains difficult to quantify and it is not clearly understood whether matrix stiffening itself induces further disease progression or if the stiffening is purely orthogonal and a consequence of plaque development [148]. There are several notable observations to discuss. First, in the coronary system, the sites which had the high probability for plaque development were located at overlapping sites of low wall shear stress and high wall stiffness [142, 144]. Second, YAP mechanobiology, now directly implicated in plaque progression [69,70], is a key mechanobiological pathway that is responsive to both shear stress and matrix stiffness. Matrix stiffening activates YAP and increases cellular proliferation, a process tied to cancer progression [65]. Furthermore, one elegant study has demonstrated that elevated matrix stiffness attenuates the release of eNOS and elevates RhoA activation from endothelial cells subject to shear [150]. And lastly, studies have reported that YAP is activated in diseased vasculature with stiffening in pulmonary hypertension [151, 152]. Thus, this suggests that mechanobiology may be a route to answer this clinical question, and is one such subject addressed in this dissertation.

1.5 Dissertation Focus

This dissertation work focuses on using these engineered approaches for studying vascular physiology and pathology. The first two chapters described tailored systems used to explore YAP mechanobiology when influenced by shear stress and stiff (Chapter 2) and exogenous electric fields (Chapter 3). These works are connected by a common theme: mechanobiology is a multidisciplinary field where the approach must be engineered to answer a given hypothesis, even when the primary implications are clinical in nature. Atherosclerosis, as an example, is a complex process in patients with significant disease progression, as affected blood vessels have altered structure and mechanical properties that are deeply intertwined with one another [142–145]. Thus, deconvoluting the contributions of these processes in pre-clinical and human patients is difficult however the in vitro vessel-chip systems offer an avenue to test this hypothesis and connect paradigms via, in this work, YAP biology. A similar essence is apparent in the electromics work: a uniquely designed culture system [54] is used to stimulation endothelial cells and study YAP behavior. In

contrast to the microfluidic work, YAP behavior here is more tied to its proliferative capacity, with electrical stimulation having potential clinical applications in wound healing [55, 153].

The final work, currently ongoing, is a more fundamental approach to mechanobiology in disease (Chapter 4). Rather than study tissue level physiology (such as an endothelial monolayer or a specific biological pathway), this work focuses on characterizing subcellular mechanical properties in healthy and aged endothelial cells to explore how geometric and elastic modulus changes influence the ability of a cell to sense shear stress. Much of literature on cellular AFM has several fundamental assumptions which do not necessarily hold true in aging [154, 155]. Thus, we established a correlative approach using AFM and SIM imaging to computationally extract the mechanical properties of the cytoplasm and nucleus of individual cells using the geometry from imaging. This work also seeks to harmonize the discrepancies in literature on whole cell measurements using AFM by describing the importance of cell geometry, a variable generally not addressed.

Altogether, these works focus on studying endothelial shear sensing and/or YAP mechanobiology, and form a set of illustrative examples for approaching these questions using engineered tools.

2. VESSEL-CHIP SYSTEMS FOR STUDYING YAP MECHANOBIOLOGY AND INTERACTIONS BETWEEN MATRIX STIFFNESS AND SHEAR STRESS*

2.1 Introduction

Mechanobiology is a discipline of physiology which focuses on how physical environments and mechanical stimuli influence cell behavior and downstream biochemical responses [126, 156]. Endothelial cells (ECs) form 3-dimensional lumenized structures and respond to physical cues such as varying matrix stiffnesses and fluid shear stresses which play a vital role in modulating endothelial homeostasis, preventing atherosclerotic progression and adverse cardiovascular events [128]. Perturbation of these atheroprotective physical inputs results in EC activation and inflammation. However, flow patterns and magnitudes which induce EC activation (and atherosclerotic progression) are termed disturbed flow [131–133] and contain varying parameters depending on the site occurrence, such as insufficient magnitude (low shear) or stark directional changes (oscillatory or recirculating flow). At sites of disturbed flow, atherosclerotic progression is exacerbated [127].

Matrix stiffening is the other primary physical parameter clinically correlated with adverse cardiovascular events, with sites of arterial stiffening associated strongly with atherosclerosis [149, 157]. Furthermore, computational studies on fluid dynamics in the coronary arteries have associated sites of high wall stiffness and low or disturbed shear as primary predictors of where atherosclerotic plaques developed [142–144]. Together, these correlations indicate that aberrant physical cues from substrate stiffness and shear promote vascular disease. However, the interaction of these vascular parameters in modulating signaling pathways and biological response are difficult to elucidate with current experimental models [148].

Recent work on endothelial mechanobiology has highlighted the Yorkie associated homologue proteins YAP (yes-associated protein) and TAZ (transcriptional coactivator with PDZ-binding mo-

*Text and figures reprinted with permission from "Mechanotransduction-on-chip: vessel-chip model of endothelial YAP mechanobiology reveals matrix stiffness impedes shear response" by B.K. Walther, N.K.R. Pandian, K.A. Gold, E.S. Kiliç, V. Sama, J. Gu, A.K. Gaharwar, A. Guiseppi-Elie, J.P. Cooke, A. Jain, 2021. *Lab on a Chip*, 21, 1738-1751, Copyright 2021 by the Royal Society of Chemistry.

tif; collectively referred to as YAP/TAZ or YAP alone) as mechanosensitive, biological sensors which are regulated in endothelial cells by mechanical cues like substrate stiffness [64] as well as shear stresses [69, 70, 158]. Extensively studied in the context of cell growth and apoptosis via the Hippo pathway [63], a variety of biochemical and mechanical cues regulate YAP/TAZ activity [61–63, 65, 68–70, 158–160] apart from Hippo. Unidirectional, high, laminar shear stress; soft substrates; and cell confluence serve to deactivate YAP activity and cause cytoplasmic retention. Conversely, disturbed flow, stiff matrices, and lack of cellular confluence serve to activate YAP and induce nuclear translocation. Importantly, the cell confluence pathways are tied to Hippo signaling, while substrate stiffness and shear stress (mechanobiology pathways) that affect YAP activity are not [61–63, 65]. Highly relevant to EC YAP mechanobiology and vascular homeostasis is that activation of YAP (nuclear partitioning) via any of these physical cues is associated strongly with EC activation, vascular inflammation, and atherosclerotic progression [26, 69, 70, 127, 128, 144, 149, 161]. As a result, YAP/TAZ activity has been implicated in atherosclerotic progression as a key biological event and specific downstream targets of its activity contribute to plaque progression [162, 163]. Altogether, this paradigm highlights YAP/TAZ as major endothelial mechanical and biochemical sensors important for maintaining homeostasis. Notably, YAP/TAZ responds to both stiffness and shear, suggesting that the connection between the clinical paradigms of stiffness and endothelial dysfunction or inflammation may be explained in part via dysregulated YAP activity, with shear stress and substrate stiffness interacting to generate the biological response. Thus, we hypothesized that increasing substrate stiffness affects the EC shear mechanoresponse by upregulating YAP activity, connecting vascular stiffness with endothelial activation (causing atherosclerotic progression).

Testing this hypothesis and precisely controlling for all the physical parameters to study YAP activity is non-trivial [61–63, 68], and systems to study YAP mechanobiology are in clear demand [71]. Furthermore, there are relatively few studies which precisely isolate the interactions of these parameters in vessels to establish a mechanistic connection between them [150], and elucidating this further has several implications in cardiovascular medicine. Thus, to explore

whether there exists a connection between the physical parameters of stiffness and shear stress via EC YAP mechanobiology, we employed organ-on-a-chip technology. Organ-on-a-chip (organ-chips) systems have emerged as biomimetic in vitro models of human physiology designed to reproduce physiologically-relevant environments and to replicate tissue- and organ-level functions [105–107, 164, 165]. Work from our group and others has shown that organ-chips may be an exceptional tool to isolate and elucidate the biological effects of a range of cellular, chemical, and physical parameters [105, 106, 164, 166]. These vessel-chips facilitate the study of endothelial pathology by supporting system interrogation wherein each degree of freedom may be allowed to vary individually [108, 167]. Currently, there are few engineered systems which are reported for the study of YAP/TAZ [104, 112], which focus either on the development of the system, cyclic strain, or developmental biology. Several microfluidic shearing systems exist which are focused on studying ECs with design and development ongoing [100–103], however, these systems do not currently incorporate relevant, interacting physiological forces (e.g. stiffness and shear stress) to study how they collaboratively influence endothelial biology. In this work, we employ a vessel-chip to study the interaction of clinically relevant physical parameters (stiffness and shear) to yield novel biological insights into endothelial mechanobiology.

Our vessel-chip model integrates three-dimensional (3D) luminal geometry, dynamic range of uniform and oscillatory shear stress, and variable matrix stiffness that replicates the physiological and pathophysiological range of these parameters in the human vasculature [141,143,144,146,147] facilitating the study of how these parameters interact and influence the EC mechanoresponse. We extensively validate our model from a biological perspective to show that it captures the in vivo behavior of YAP/TAZ accurately in previously studied regimes while additionally exploring shear stress patterns not commonly addressed. We further tie the YAP behavior in the system to established biological paradigms, demonstrating EC inflammation under regimes which upregulate YAP activity, relevant modulation of gene expression, and confirm the findings via pharmacologic inhibition of YAP. Lastly, we vary shear stress and substrate stiffness together to explore how convoluting physical inputs affects ECs, in which we demonstrate that substrate stiffening results

in upshifted YAP nuclear partitioning under high shear, connecting the two physical paradigms. We discuss several novel biological findings during validation and the implications of YAP in EC mechanobiology throughout. Holistically, this work demonstrates use of engineered organ-chip systems as tools to construct biology in a bottom-up fashion resulting in novel biological findings previously inaccessible via conventional methodology.

2.2 Materials and Methods

Channel Fabrication: Vessel-chips were fabricated according to our previous work [110]. Briefly, positive channels were designed in Solidworkső, acquired from OutputCity Inc., and photolithographically printed onto silicon wafers (University Wafer Corp.). The upper chamber of vessel-on-a-chip devices were fabricated via soft lithography using polydimethylsiloxane (PDMS, Dow Corning) and then bonded to a borosilicate glass (BSG) slide or cover slip (75 mm x 25 mm) which was either spin-coated with self-consistent PDMS (uniform channel) or left uncoated for stiff BSG controls (stiffness studies). Bonding was performed following O_2 plasma treatment (Thierry Zepto, Deiner Plasma) in a dedicated clean room.

Stiffness Measurements: Substrate stiffness was varied by changing the crosslinker concentration of the PDMS formulationA49. Compressive data was collected for the combination of PDMS with 5%, 7.5%, and 10% by weight of crosslinker. First, samples were punched into 10 mm diameter discs using a biopsy punch and heights measured using digital calipers. Samples were compressed to not greater than 20% of the measured height at a strain rate of 1 mm/min utilizing an ADMET MTEST Quattro eXpert 7600 Single Column Testing System with a 25 lb load cell. The raw data collected was processed into MS-Excel to calculate the compressive moduli as the slope of the linear region of the strain vs. stress graph. For atomic force microscopy validation studies on ECM functionalized and non-functionalized PDMS thin films, a Catalyst Biomicroscope (Bruker) was employed. MLCT conical probes (0.01 N/m; Bruker Nano) were used to measure elastic moduli pre- and post-ECM functionalization. The AFM scanning frequency used was 1 Hz in PBS. All data was processed using Nanoscope Analysis 1.50r1 (Bruker). Sneddons conical fitting was used on thin films, taking from 0-10% [168] of the full AFM force curve for at least 15

technical replicates. Iterative outlier analysis was used to remove any technical replicates which deviated strongly from the spread, and the group was averaged to yield the stiffness of the PDMS film.

Cell Culture: Human umbilical venous endothelial cells (HUVECs, Lonza) were cultured in endothelial growth media (EGM-2, Lonza) using an endothelial cell supplement EGM-2-M (Lonza). Cell culture washes were performed using pH 7.2 phosphate buffered saline (PBS, Gibco), and cell passaging was performed using 1x 0.25% Trypsin-EDTA (Gibco). HUVECs used were all between p4 and p6, passage matched for each experiment.

Channel Functionalization and Lumenization: After fabrication of the Vessel-Chips, each channel was treated with O_2 plasma (PDC-32G, Harrick Plasma) for 5 minutes, and then an extracellular matrix (ECM) solution of 100 ţg/mL rat tail collagen type I (Corning) and 50 ţg/mL human fibronectin (Sigma Aldrich) was perfused through the channel and incubated for 30 minutes at 37^{o}C, 5% CO_2. Plate controls reported were done on BSG cover slips, or 10% PDMS spin-coated glass cover slips using the same plasma treatment procedure and ECM solution. Afterwards, each channel/cover slip was then placed in an incubator at 37řC and 5% CO_2 for 30 minutes. The ECM solution was subsequently removed by perfusing EGM-2-M media through the chamber, or via washing of the cover slips. On the fully assembled vessel-chip devices, HUVECs were seeded onto the top and bottom faces of the chamber and allowed 1 hour for attachment. After the seeding period, the seeded vessel-on-a-chip devices were attached to a syringe pump (PHD ULTRA 4400, Harvard Apparatus) using a Luer curved dispenser tips (Qosina) and 20 tubing (0.094 ID, 0.145 OD; Qosina) and operated in suction mode. Media reservoirs were made from 5 mL syringes (BD). To allow for lumen formation, each chamber was then placed in shearing flow overnight at a flow rate of 1 ţL/min before each experiment was conducted (post-lumenization; t = 0). For the quasistatic control, HUVECs were seeded and cultured under extremely low shear (<2 ţL/hour) using two 1-mL pipets as reservoirs for 48 hours such that cellular confluence was achieved.

Flow Rates: Flow rate shear stresses were calculated numerically using the finite element method in Ansys Fluent v29R1 from Solidworks v19 models. Cell culture media (comparable

to water) was used as the fluid for modeling (density: 0.998 g/cm^3; viscosity: 0.001 Pa*s). A flow rate of 1 ţL/min was calculated to be 1.12 dynes/cm^2 (low/venous shear), and 10 ţL/min was calculated to be 11.2 dynes/cm^2 (high/arterial shear). Values are reported as exact calculations at the center of the XZ planes (top/bottom wall shear) distant from the corner. Disturbed flow was induced via an oscillatory flow pattern of 1 or 10 ţL/min, 2 seconds of withdrawal and 1 second of infusion (100% duty cycle, 0.33 Hz) to deliver fresh media. Each of these regimens were run for 3 hours and 6 hours after appropriate lumenization.

Verteporfin Treatment: Verteporfin was purchased from Millipore Sigma ($\geq$94% HPLC) and dissolved into a 1 mM stock in dimethyl sulfoxide (DMSO; Millipore Sigma) and stored at -20řC until use. The stock solution was diluted into 2 mL of EGM-2-M media for the corresponding experiment. Each concentration was supplemented with DMSO to ensure each flow chamber received the same amount of DMSO regardless of dilution. Verteporfin was introduced into the chamber in a dose-dependent manner. DMSO controls were media and the total DMSO volume required for dilution only.

RNA Isolation and Gene Expression: HUVECs in each channel were trypsinized and cells pelleted for RNA extraction and lysed with 10 minutes of detachment. Note that YAP is rapidly inactivated upon trypsinization and gene expression is thus dependent on the half-life of the mRNA [66]; cells must be lysed quickly and RNA extraction begun immediately. RNA was extracted using an Arturus^{TM} PicoPure^{TM} RNA Extraction Kit (Applied Biosystems, Thermo Fisher Scientific). The cDNA was synthesized from the extracted RNA using a 5x iScript Reverse Transcriptase Supermix (Bio-Rad Laboratories, Inc.). The cDNA was then diluted to a volume of 100 ţL for qPCR. For each qPCR reaction, a volume of 20 ţL was used consisting of 10 ţL of Power SYBRő Green Master Mix (Applied Biosystems, Thermo Fisher Scientific), 7 ţL of H2O (DNAse/RNAse free, molecular grade), 1 ţL of the gene specific primer, and 2 ţL of the sample cDNA. All primers were purchased as validated 20x SYBRő Green assays for glutaraldehyde 3-phosphate dehydrogenase (GAPDH), endothelial nitric oxide synthase (eNOS), connective tissue growth factor (CTGF), ankyrin repeat domain 1 (ANKRD1), intercellular adhesion molecule 1 (ICAM-1), vascular adhe-

sion molecule 1 (VCAM-1), vascular endothelial growth factor receptor 2 (VEGFR2), and interleukin 6 (IL-6), (Bio-Rad Laboratories, Inc.). RT-qPCR was performed on a QuantStudio 12K Flex (Applied Biosystems, Life Technologies) with the following pre-set settings: 96-Fast Well Plate 0.1 mL, Relative Quantification (-$\Delta\Delta$Ct), SYBR$\H{o}$ Green Reporter, and Standard Run Time. All gene expression results were reported as a fold change with respect to the denoted control and the housekeeping gene, GAPDH [169].

Immunohistochemistry: Each sample was fixed with 16% formaldehyde (Thermo Fisher Scientific) for 20 minutes at 4^{o}C and then blocked and permeabilized with 2% bovine serum albumin (BSA, Sigma Aldrich) and 0.1% Triton X-100 (Thermo Fisher Scientific) in PBS (blocking buffer) for 1 hour at 4^{o}C. Channels were then stained with either rabbit anti-YAP (Abcam), rabbit anti-VCAM1 (Abcam), rabbit anti-vWF (Dako), or mouse anti-CD144 (BD Pharmigen) in blocking buffer (1:100) overnight at 4^{o}C. Secondary staining was performed with donkey anti-rabbit Alexa Fluor^{TM} 555 (Invitrogen Molecular Probes, Thermo Fisher Scientific) for 1 hour at room temperature. Actin was stained with phalloidin Alexa Fluor^{TM} 488 (Invitrogen Molecular Probes, Thermo Fisher Scientific). Nuclei were stained with 4,6-diamidine-2-phenylindole dihydrochloride (DAPI, Roche Diagnostics).

Imaging and Analysis: Image acquisition was performed on an FLUOVIEW FV3000 confocal microscope (Olympus Corporation). Analysis was performed on the associated software (cellSens, Olympus Corporation) for YAP partitioning and circularity index by denoting regions of interest and extracting the raw fluorescent values and measurements. YAP partitioning was calculated as the nuclear YAP signal divided by the total cellular YAP signal for 60 cells. Circularity index was calculated via 4π(area/perimeter^2) for 60 cells. Actin alignment images were grayscaled in GIMP or ImageJ, and analysis was performed using the directionality function in Fiji (ImageJ) using Fourier component analysis for 0^{o} to 90^{o}. The values were reported in vector notation of the form(r,θ), where r corresponds to the relative density (magnitude) of observations for a given angle calculated from the directionality function, and θ (phase) is the angle itself. Thus, angular preferences are visualized as radial spikes or peaks, and random organization is a radially homogenous

distribution. Five or greater fields of view were taken for each experimental condition in the study of actin alignment (indicated). Color mapping was performed using OrientationJ [170].

Statistics and Data Visualization: All data was analyzed using either an appropriate Students t-Test or ANOVA with post-hoc Tukeys/Scheffs test. Statistical significance was set as $p < 0.05$, however all p-values are reported as their exact calculated value. All data visualization (except bar graphs) was performed in Python 3.7 using Matplotlib [171] with Seaborn packages. All scripts are available upon request; examples scripts are included in supplementary material.

2.3 Results and Discussion

Design of the Microfluidic Vessel-Chip System: In order to design a microfluidic culture environment conducive to studying endothelial mechanobiology, we first engineered the key physiologic parameters directly into the system and developed protocols to study ECs under different shear patterns. We employed the anatomy of a typical vessel-chip consisting of a microfluidic channel with a rectangular cross section providing a 3D culture environment for lumen formation (**Figure 2.1a-c**), where HUVECs cultured within the chamber formed a circular monolayer around the inner walls of the chamber (**Figure 2.1d**) after 18-hour incubation under a low shear rate (1 ţL/min; **Figure 2.1e**). Next, to determine the shear regimes studied during the experimental portion of the protocol (t=0; **Figure 2.1e**), we used shear stresses and patterns which are known to be protective or inflammatory. To this end, we imposed a low shear (inflammatory) regime, a high shear regime (protective), and oscillatory versions of both (inflammatory) [132]. As the HUVEC response to shear has been extensively characterized [130, 172, 173], in that they respond favorably to arterial range shear (10 30 dynes/cm^2) [162], we selected a flow rate of 10 ţL/min (11.2 dynes/cm^2) as our model of high shear. Conversely, low shear regimes (1-3 dynes/cm^2) are activating for endothelial cells thus we selected a flow rate of 1 ţL/min (1.12 dynes/cm^2) as our low shear regime (**Figure 2.1f**). To then model disturbed flow, we imposed a flow reversal pattern (oscillatory flow) to induce EC activation (**Figure 2.1g**), based on flow patterns known to cause activation [131, 174, 175]. Within our model, in order to deliver media over the course of the experiment, a net positive flow vector was required, and thus the oscillatory regime displayed

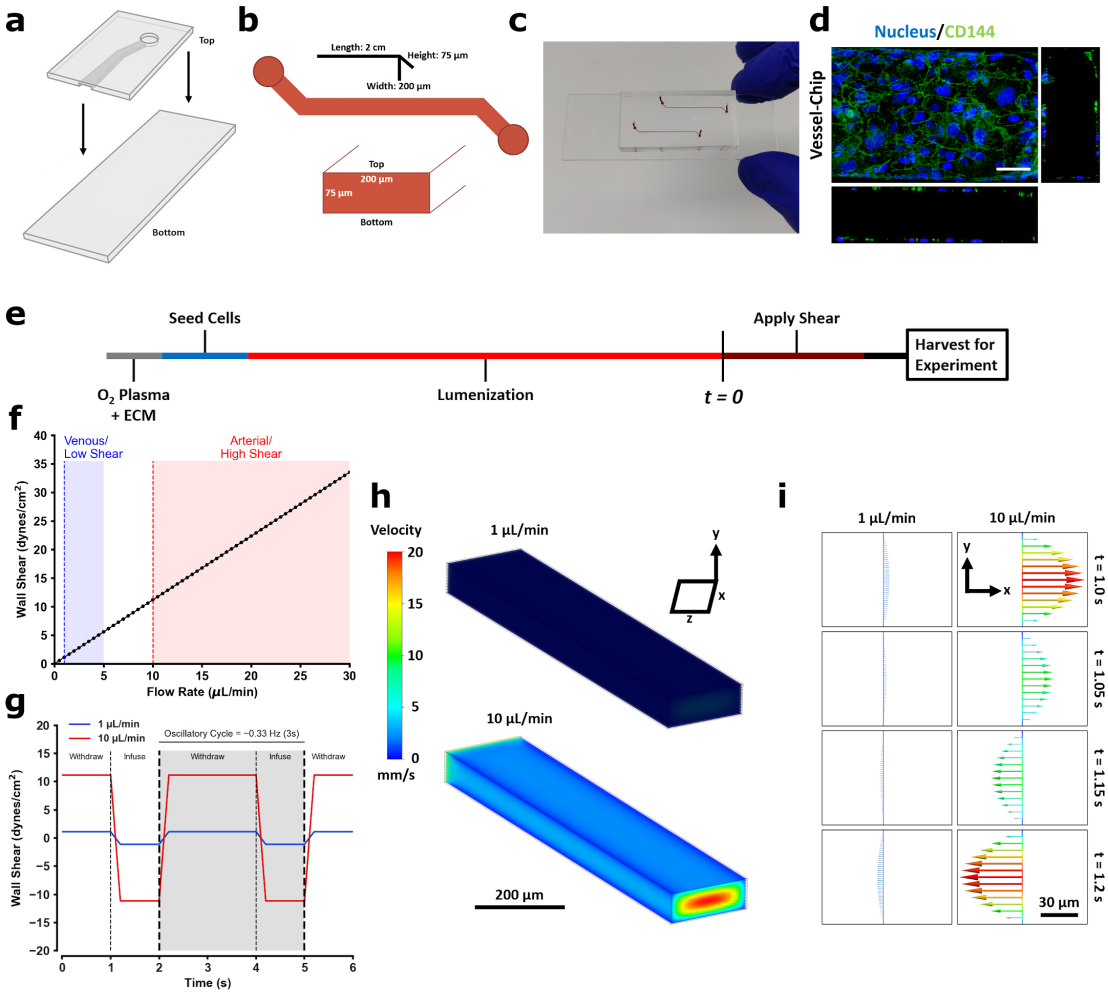

Figure 2.1: Fabrication of the vessel-chip microfluidic device for endothelial mechanobiology and preliminary quantification. **a** details the parts of the device bonded together to form a microfluidic channel. **b** lays out the dimensions of the channel. Each channel is 2 cm long, has a height of 75 ţm, and a width of 200 ţm. The PDMS upper comprises the top face of the channel, while the bottom glass slide is the bottom; these faces are referred to when seeding cells in the device as both faces are seeded prior to experimentation. **c** are pictures of a fully fabricated device. **d** is a representative confocal maximum Z-image of a HUVEC lumen formed on the device using this protocol (Flow Rate: 10 ţL/min). **e** is a graphical schematic of the cell culture protocol used for each experiment. 3-dimensional computation fluid analysis of the applied wall shear stress based on the flow rate with corresponding physiological ranges are shown in **f**, while **g** details the oscillatory flow pattern used to induce activation (0.3 Hz cycle, 2 seconds withdraw, 1 second infuse). Flow velocity heatmap profiles are shown in **h** for the unidirectional regimes and the corresponding flow rate, and **i** details the velocity profile during an oscillatory cycle, showing the 1-dimensional change in flow direction and magnitude.

a frequency of 0.3 Hz (2 second withdrawal, 1 second infusion). 3D fluid modeling confirmed conventional laminar regimes within the cuboidal chamber and presence of a flow reversal in the oscillatory regimes which remained entirely laminar (**Figure 2.1h-i**). It is beneficial to note that in the context of the model, disturbed flow is isolated to being comprised of only flow reversal. While from a fluid mechanics perspective this is trivial, biologically the scenarios which activate ECs are complex, and several fundamental flow patterns may activate ECs, of which flow reversal is one. Other patterns such as recirculating flow also induce activation, and are classified as disturbed flow, and additionally disturbed flow need not be laminar [103, 133, 134, 158]. Lastly, to complete our protocol development, our experiment duration (t=0, Figure 2.1e) was set to follow the onset and stabilization of EC gene expression under shear, starting within an hour and stabilizing by 6 hours [176]. Thus, we selected an experimental duration of 6 hours. We confirmed this time point using gene expression of various shear sensitive genes (**Figure 2.2**).

Endothelial YAP/TAZ Mechanobiology in the Vessel-Chip: Our next goal was to establish that our vessel-chip model recapitulated known patterns of YAP/TAZ biology in endothelial cells: cytoplasmic retention under high, unidirectional (atheroprotective) laminar shear and nuclear partitioning when exposed to disturbed flow [69, 70]. We began by setting a quasistatic control baseline for HUVECs cultured on the chip (flow <2 ţL/hour), as cells cultured in the vessel-chip require perfusion to remain alive and fully static state is not relevant. At these quasistatic conditions, partial YAP nuclear partitioning was observed (nuclear YAP/total YAP; **Figure 2.3a-b**). HUVECs elongated and aligned weakly along the flow vector, both attributable to culture under flow (**Figure 2.3c-d**). This baseline established, we moved to study and compare physiologic/pathologic conditions. We examined YAP partitioning via immunofluorescence after 6 hours of the different flow regimes detailed earlier (**Figure 2.4a-b**). In all disturbed flow regimes (low shear 1 ţL/min and both oscillatory regimes), we observed strong nuclear partitioning of YAP, while under the high atheroprotective regime, YAP was retained strongly in the cytoplasm (**Figure 2.4c**). We note that the quasistatic control YAP partitioning values were statistically identical to that of the oscillatory regimes ($p = 0.9$), indicating the strong influence of protective shear on YAP cytoplasmic

retention and importance of fluid flow. Altogether, all parameters which conventionally classify as disturbed flow strongly induced YAP nuclear partitioning. Although this observation is consistent with previous studies [69, 70] reporting that disturbed flow results in YAP activation in ECs, we have added some greater resolution to the mechanosensing paradigm, as few studies have explored differences between unidirectional and oscillatory flow at low levels of shear stress. We observed that the flow pattern appears to be the dominant determinant of YAP localization in high shear regimes (10 ţL/min unidirectional vs. oscillatory). By contrast, when the shear stress is low, ECs are comparably activated by unidirectional or oscillatory flow.

Within our vessel-chip model, we additionally observed common morphology changes associated with disturbed flow. HUVECs exposed to high shear became elongated, while in all disturbed flow regimes cells remained rounded (**Figure 2.4d**). Although EC exposed to both unidirectional regimes aligned primarily along the 0ř flow vector, those exposed to high shear displayed a much more prominent alignment peak (Frequency peak: 1 ţL/min=0.13 vs. 10 ţL/min=0.23). HUVECs exposed to oscillatory flow regimes all displayed a blunted alignment (**Figure 2.4e**). Representative color mapping of actin alignment (from **Figure 2.4a**) demonstrates the wide distribution of angles seen in the oscillatory regimes (**Figure 2.4f**). Taken together, our data suggests that the key observations of in vivo YAP behavior are captured within the vessel-chip system, while additionally facilitating novel findings pertaining to the relative influence that shear stress magnitude and pattern have on endothelial activation. Moreover, morphological characteristics of ECs subject to (disturbed) flow were readily captured and shown to be consistent with current understanding [177, 178].

Endothelial Activation and Inflammation in the Vessel-Chip: In the context of vascular mechanobiology, drawing connections between the detrimental mechanoresponse from disturbed flow (YAP nuclear localization and increased activity) and the clinical implications (atherosclerotic progression and vascular disease) would be vital to capture within our model to ensure the mechanobiological changes parallel alterations in endothelial activation. Specifically, does nuclear YAP partitioning (with disturbed flow) parallel endothelial activation and inflammation? Accord-

ingly, we selected an atheroprotective regime (unidirectional high shear) and the corresponding disturbed flow pattern (oscillatory high shear), and assessed the relative level of two molecules known to be induced under disturbed flow and integral to atherosclerotic progression: vascular cell adhesion molecule 1 (VCAM-1) and von Willebrand Factor (vWF) [175, 179–184]. We observed reduced levels of both VCAM-1 and vWF when HUVECs were subject to unidirectional high shear, whereas high oscillatory shear greatly increased the levels of both VCAM-1 and vWF (**Figure 2.5a-d**), illustrating the connection between the EC mechanoresponse and EC inflammatory activation.

Gene Expression Analysis: Subsequently, we examined gene expression of ECs subject to the various fluid shear stress parameters. The first two genes examined, connective tissue growth factor (CTGF) and ankyrin repeat domain 1 (ANKRD1) are downstream targets of YAP/TAZ activity known to be upregulated by its transcriptional co-activation [69, 70]. The second two genes, endothelial nitric oxide synthase (eNOS) and vascular endothelial growth factor receptor 2 (VEGFR2), are shear responsive genes [21, 134, 185–189] not directly tied to YAP activity. Unidirectional high shear downregulated expression of CTGF compared to unidirectional low shear, however ANKRD1 remained relatively unchanged (**Figure 2.6a**). Under the conditions of high oscillatory shear, CTGF and ANKRD1 were both dramatically upregulated (**Figure 2.6b**), consistent with previous reports [69, 70]. By contrast, at low levels of shear stress, there was no difference between unidirectional and oscillatory shear stress in expression of CTGF and ANKRD1 (**Figure 2.6c**). Taken together, this data suggests than CTGF expression is highly sensitive to both the magnitude and pattern of shear stress. By contrast, the expression of ANKRD1 is not affected by difference in the magnitude of unidirectional shear stress, but is affected by the flow pattern at higher levels of shear stress. Notably, the sensitivity of CTGF to the magnitude of unidirectional shear stress has been previously reported [172]. Changes in other known mechanosensitive genes (eNOS and VEGFR2) were modest but in the expected directions (**Figure 2.6d-f**). Summarizing, these data confirm that our chip model replicates the known biological effects of laminar and disturbed flow (i.e. response of eNOS and VEGFR2) and provide new insights into the flow response

of genes downstream of YAP/TAZ activation (i.e. CTGF and ANKRD1). Notably, CTGF is highly expressed in atherosclerotic plaques [190–192] and knockdown greatly reduces plaque progression [193]. This is consistent with our data that CTGF is upregulated by patterns of disturbed flow, which hemodynamic condition is associated with sites in the vasculature that are predisposed to atherosclerosis.

Pharmacologic Inhibition of YAP Activity: To confirm the importance of YAP activity on the flow-mediated regulation of mechanosensitive genes, we employed verteporfin, a potent YAP inhibitor [194–197]. We assessed a dose response to verteporfin (0.125 1 ţM; **Figure 2.7a-b**) and assessed YAP nuclear localization of treated cells subject to 10 ţL/min oscillatory shear. We observed increasing cytoplasmic retention of YAP with increasing concentrations of verteporfin, with 1 ţM verteporfin treatments resulting in cytoplasmic retention of YAP comparable to that of ECs subject to high unidirectional shear (**Figure 2.8a-b**). Notably, concentrations above 1 ţM induced excessive cellular detachment (**Figure 2.7c**), which is attributable to verteporfins ability to potently induce apoptosis and cell death at high concentrations [198]. Additionally, verteporfin treatment did not rescue cell circularity/morphology nor alignment (**Figure 2.8c-d** and **A4d**). As concentrations of 1 ţM demonstrated the highest tractable cytoplasmic retention, we selected 1 ţM as the concentration to examine inhibition of downstream YAP gene expression. Compared the DMSO controls (required for verteporfin solubility), verteporfin strongly suppressed expression of CTGF, however, strikingly ANKRD1 expression was not affected (**Figure 2.8e**). We note that this mirrors the finding of Wang et al. [70] when they reported pharmacological inhibition of c-Jun N-terminal kinase (downstream of YAP/TAZ activity) greatly modulated CTGF expression, but minimally affected ANKRD1 [70]. Thus, this supports that CTGF is predominantly regulated by upstream YAP activity (and thus the EC mechanoresponse), however ANKRD1 is likely to be associated with other regulatory pathways. More generally, these pharmacological studies performed using the vessel-chip system in this manner demonstrate how chemical intervention can influence and reverse the biological response to mechanical cues, and how organ-chip systems support these preclinical and potentially translational studies in a controlled manner.

Substrate Stiffness Impedes the Shear Mechanoresponse: As YAP is responsive to both substrate stiffness and shear stress, we hypothesized that stiffening the substrate matrix impedes the ability of ECs to fully respond to shear stress, upshifting YAP nuclear localization. The stiffness of the PDMS substrate was modified by varying the crosslinker concentration [92]. Arterial stiffnesses range from 50 kPa up to roughly 600 kPa [141, 146, 147]. Complicating this paradigm is that diseased vasculature and atherosclerotic plaques have a significantly higher range of stiffnesses, from 1 kPa up to 5 MPa [143, 144]. Thus, we explored a stiffness of the same order of magnitude as those reported in normal muscular arteries (300-500 kPa; such as the coronary arteries) [142] as well as stiffness in the range of atherosclerotic vessels (>1 MPa). Accordingly, we reduced the crosslinker density to 7.5% (to yield 1 MPa) and to 5% (500 kPa); ECM functionalization did not alter the PDMS materials properties (**Figure 2.9**). We subjected endothelial cells grown on these matrices to unidirectional low or high shear and measured YAP localization (**Figure 2.10a-b**). Consistent with our previous experiments, all low shear groups displayed elevated YAP nuclear partitioning consistent with EC activation under flow. Furthermore, all high shear groups displayed significantly decreased nuclear YAP localization. However, higher levels of stiffness attenuated the effect of high shear to reduce YAP nuclear partitioning (**Figure 2.10c**), indicating that stiff matrices impede the protective EC shear mechanoresponse. Also, of note, there was no difference in the nuclear localization with increasing stiffness when shear stress was low. This finding indicates that low shear stress (such as that found at sites of disturbed flow in the large and medium arteries) is strongly activating and a dominant stimulator of YAP activity, EC activation, and vascular inflammation. Interestingly, high shear was sufficient to induce YAP cytoplasmic retention on borosilicate glass (Youngs Modulus 64 GPa), displaying a value statistically indistinguishable from the 10% PDMS (10% PDMS=0.32ś0.1; BSG=0.32ś0.1; p=0.7), which suggests the influence of matrix stiffness on the shear mechanoresponse plateaus past some highly stiff threshold (**Figure 2.11**). Altogether, this data suggests that ECs reside in a complex physical environment where they balance different physical cues and respond biologically to the convolution of the stimuli (**Figure 2.10d-e**). The protective signals from high shear stress are attenuated by increasing matrix stiff-

ness to a certain threshold, while low shear is universally activating. Notably, this data supports a biological link associating matrix stiffness and flow patterns to EC dysfunction, inflammation, and atherosclerotic progression, consistent with clinical data.

2.4 Conclusions

Here, our report describes the use of a vessel-chip model to arrive at novel understandings of the interaction of physiological forces which conventional methods or models may not facilitate. This type of bottom-up engineering approach to biology, combined with insights from current in vitro and in vivo models, may provide a more comprehensive understanding of forces acting on cells in a concerted fashion to result in a single biological response.

In the context of vascular mechanobiology, our vessel-chip model yielded several new insights into the physical cues which govern EC health and homeostasis. First, our data reveals that shear stress magnitudes and patterns are a dominant signal in EC phenotype maintenance. The most dramatic differences were observed between unidirectional and oscillatory flow patterns at high levels of shear. Interestingly, the pattern of flow (unidirectional v. oscillatory) did not appreciably modulate gene expression when ECs were subject to low levels of shear. Thus, low levels of shear (which promote atherosclerosis in the arterial circulation) dominate over the flow pattern with respect to EC signaling. Gene expression analysis across flow regimes and inhibitor studies highlighted CTGF as a highly sensitive measure of the EC mechanoresponse to shear and flow pattern. CTGF was upregulated with disturbed flow, consistent with its increased expression in atherosclerotic vessels. By contrast, ANKRD1 was only affected by the flow pattern at high levels of shear stress. Verteporfin studies confirmed that CTGF but not ANKRD1 is significantly downregulated by YAP inhibition, emphasizing the distinction between these genes.

The most significant finding of this report is the interaction of substrate stiffness with shear stress to modulate the EC YAP mechanoresponse. Here, we observed that increasing the substrate stiffness increased the levels of YAP localized to the nucleus under high shear, however low shear was strongly activating across varying stiffnesses. Our work is consistent with prior studies associating coronary wall stiffness and shear patterns with development of atherosclerosis [142–144].

Indeed, the data suggests a feedforward mechanism of EC activation and atherosclerotic progression (**Figure 2.10f**) where some inciting event (either physical or chemical [133, 199]) induces YAP activation in ECs. This, in turns, causes endothelial activation and vascular inflammation, as reported previously [69, 70]. The endothelial activation and vascular inflammation then drive atherosclerotic progression, which may further stiffen the vascular architecture, activating YAP further. Kohn and colleagues observed that stiffer substrates resulted in lower eNOS production and increased RhoA activation [150], the latter of which interacts with YAP/TAZ [200]. Together, their work and ours strongly suggest that matrix stiffness attenuates the endothelial response to physiological shear stress. The combination of a decrease of eNOS (also atherogenic [127]) and increases in RhoA and YAP/TAZ activity all serve to suggest that matrix stiffening is not only a correlative consequence, but a cause of vascular disease. Indeed, other recent reports indicate that YAP activation is associated with vessel stiffening in the context of pulmonary hypertension [151, 201], though do not explore fluid shear stress as deeply.

There are model limitations and interpretation qualifiers important to discuss. Our current vessel-chip model does not incorporate strain, which is known to activate YAP activity as well [112]. Furthermore, we have not incorporated a vascular smooth muscle cell layer in our model, which also contributes to vascular disease [202, 203]. Thus, some of the biological implications of our model findings require additional study to incorporate the interaction of these biological variables with stiffness, shear stress, and flow patterns. Also of note is that the ECM chemical composition itself influences EC behavior [204], which was not a variable considered in our work. We also assumed that the matrix is a uniform, isotropic material, however, blood vessels are composite and anisotropic [141]. Lastly, our work focuses on modeling mechanobiological response in the arterial circulation (using HUVECs) which may not be entirely reflective of the venous mechanoresponse. As an example, recent work, including our own, highlights that low (1 dyne/cm^2) recirculating flow in vein leaflets is protective [205, 206], rather than activating. Thus, our conclusions are only appropriately applied to arterial biology while venous mechanobiology requires more investigation.

Nonetheless, we believe the methods and resulting conclusions emphasize how engineered organ-chip models can be used in such a manner as to draw upon biological knowledge and facilitate new findings. As evidenced by the work here, organ-chip systems support biological inquiry that fills the gaps between the in vitro models and animal models. Further extension or applications of this work include system sophistication to incorporate additional geometries or cellular layers to study an additional interface, or the inclusion of iPSC-derived ECs or diseased cell models to study perturbations of the shear response induced by internal, cellular dysfunction.

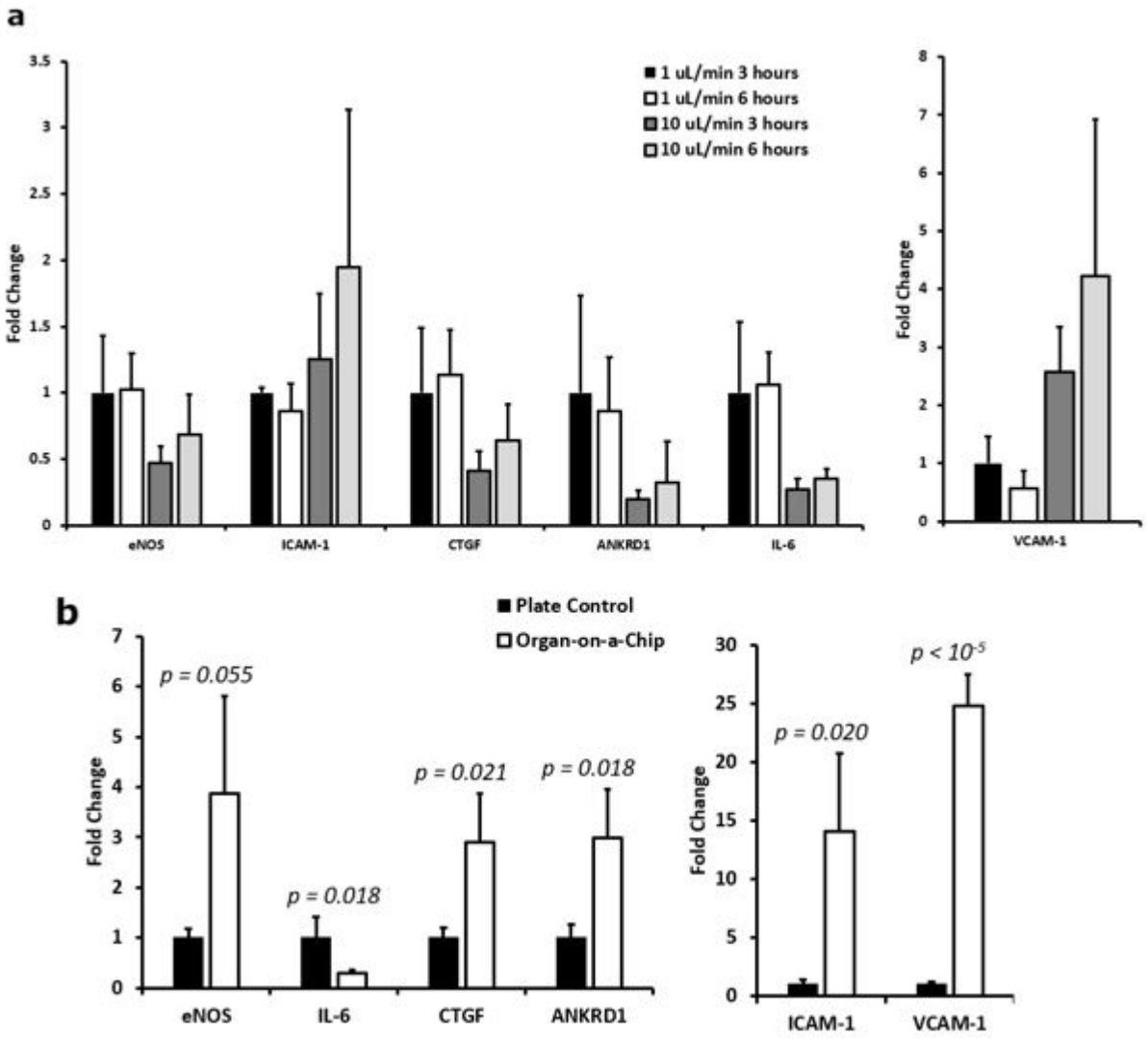

Figure 2.2: RTqPCR gene expression analysis of various endothelial genes at 3- and 6-hour timepoints for venous and arterial shear (**a**). Each group for each gene was run n=3. Note that in the manuscript proper, the 1 vs 10 ţL/min regimes were repeated an addition 4 times, and the n=3 from this graph were analyzed together with the repeat for the n=7 in the main manuscript. The data here is intended only to illustrate the timepoint trends. A fundamental limitation but repeatable observation for the vessel-on-a-chip model was that the arterial shear regime displayed upregulated surface adhesion molecules (ICAM-1 and VCAM-1). RTqPCR gene expression analysis of the vessel-on-a-chip system at 72 hours incubation total (**b**). Each group performed at n=3. This figure highlights than, in comparison to a plate control, longer incubation times seem to aberrantly regulate gene expression contrary to the expected patterns. Notably, surface adhesion molecules and targets of YAP/TAZ are all upregulated in the vessel-on-a-chip system vs. the polystyrene plate controls. This is remedied by the lumenization protocol established, and was the main driving force for developing a rigorous protocol.

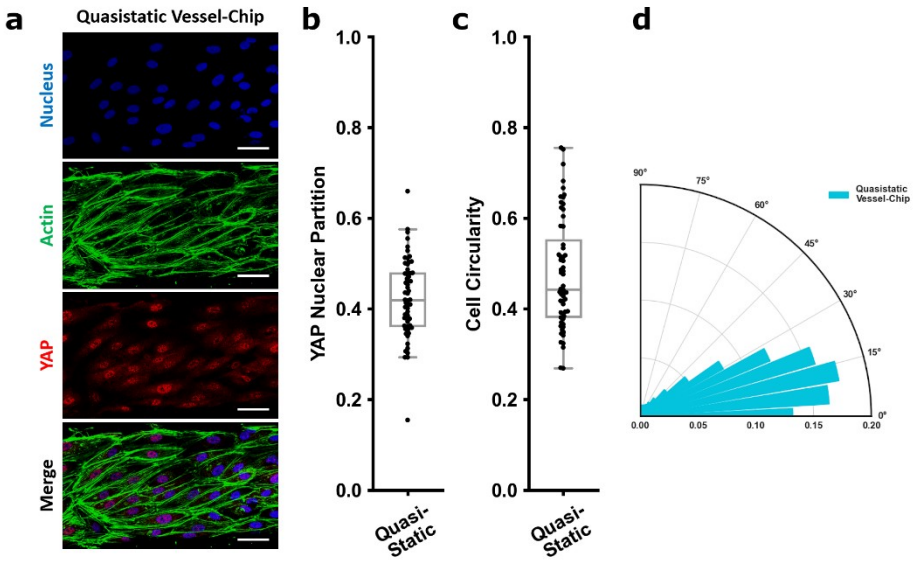

Figure 2.3: Quasistatic control IF is shown in **a** (scale bar: 50 ţm). YAP partially partitioned to the cytoplasm (**b**). Cells elongated and aligned under flow (**c-d**). This control set required 48-hour culture under <2 ţL/hour to achieve confluence and lumen formation.

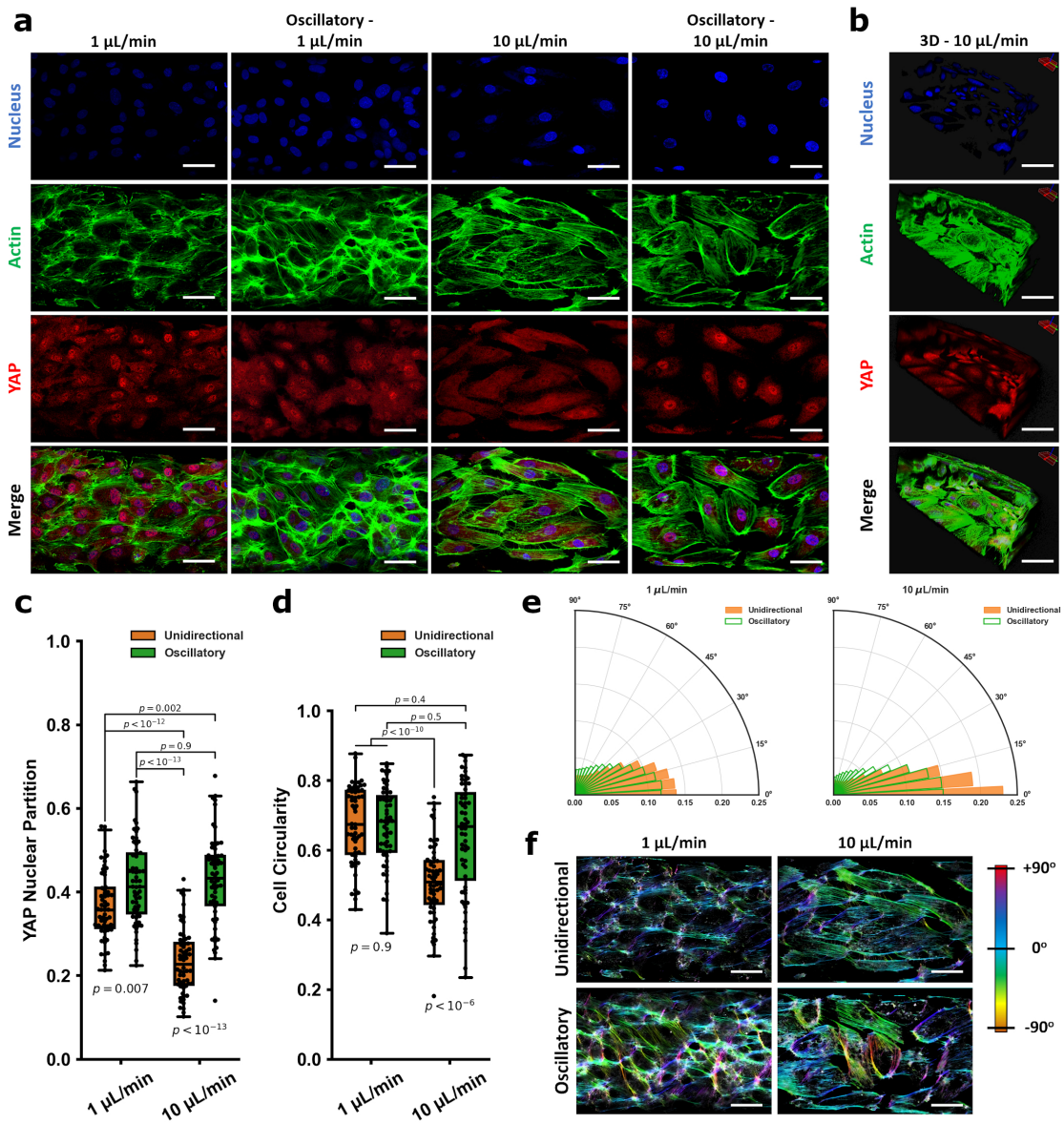

Figure 2.4: YAP mechanobiological model validation of the vessel-chip system for studying endothelial mechanobiology. In **a** are representative fields of view within the vessel-on-a-chip device. **b** is a Z-stack image of a section of a vessel-on-a-chip showing lumen formation). Scale bars in **a** and **b** are 50 ţm. YAP partitions for each group are: 1 ţL/min: 0.37 ś 0.08; oscillatory 1 ţL/min: 0.42 ś 0.1; 10 ţL/min: 0.23 ś 0.08; oscillatory 10 ţL/min: 0.43 ś 0.11 (**c**). The cellular morphology (circularity) is quantified in **d**: 1 ţL/min: 0.67 ś 0.11; oscillatory 1 ţL/min: 0.67 ś 0.11; 10 ţL/min: 0.51 ś 0.11; oscillatory 10 ţL/min: 0.64 ś 0.16. Directionality assays based on actin alignment are shown in **e**. For 10 ţL/min, HUVECs aligned strongly along the flow vector. The effect was attenuated in the 1 ţL/min regime. HUVECs in both oscillatory flow fields showed markedly decreased alignment. Color mappings from **a** are visualized in **f**. For YAP partition experiments and CSI experiments, n=60 cells. Alignment polar histogram plots are comprised of an average of 5-6 fields of view, directionality calculated from 0° to 90° binned 15 times in ImageJ. Statistics performed using a single factor ANOVA with post-hoc Tukeys test. Significance is taken at $p < 0.05$. All values reported as mean ś standard deviation.

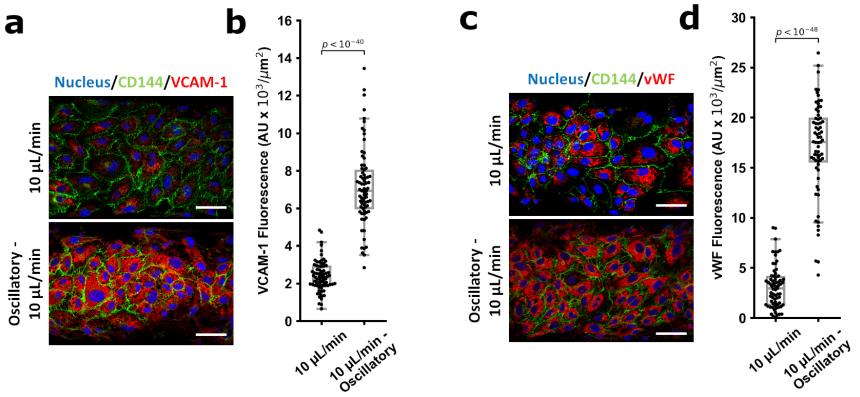

Figure 2.5: Endothelial activation studies between the different shear regimes. 2 markers of endothelial inflammation (VCAM-1 and vWF) were examined under the laminar and oscillatory flow conditions. For both markers, oscillatory flow patterns resulted in marked intensity increases for VCAM-1 (**a-b**, Fluorescence: 10 ţL/min 2.4 ś 0.8 AUx10^3/ţm^2, Oscillatory 10 ţL/min 7.1 ś 2 AUx10^3/ţm^2) and vWF (**c-d**, Fluorescence: 10 ţL/min 3.1 ś 2 AUx10^3/ţm^2, Oscillatory 10 ţL/min 17 ś 5 AUx10^3/ţm^2). For VCAM-1, n=74 cells; for vWF, n=69 cells. Statistical analysis was performed using an unpaired Students t-test, significance taken at $p < 0.05$. Data is reported as the normalized intensity (to cellular area), mean ś standard deviation.

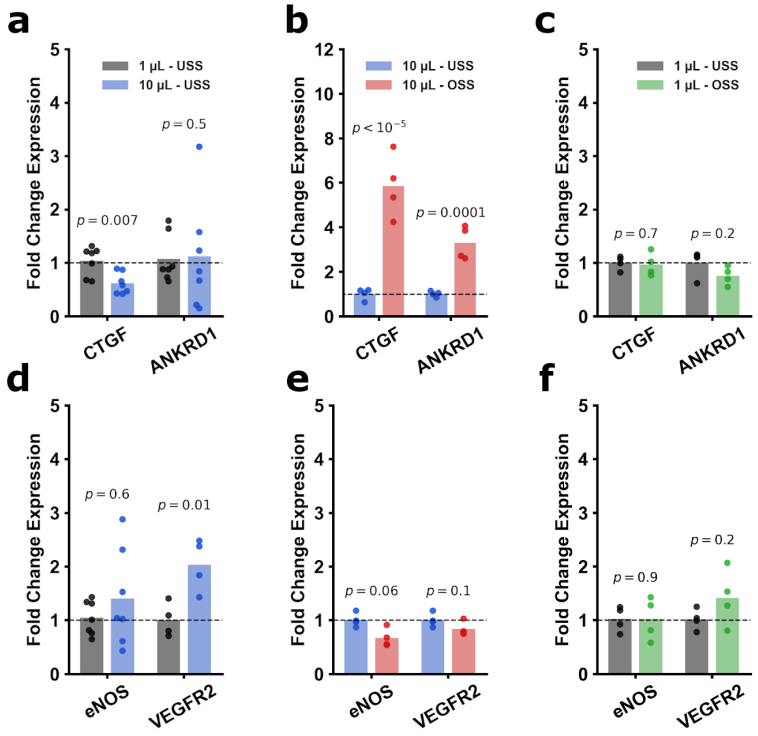

Figure 2.6: Gene expression for key mechanosensitive genes were selected as transcriptional readouts (CTGF, ANKRD1, eNOS, and VEGFR2). CTGF expression was significantly decreased from 1 µL/min to 10 µL/min (**a**, FC = 0.6) while ANKRD1 was not changed (FC = 1.1). However, oscillatory 10 µL/min vs. 10 µL/min displayed a marked upregulation of both CTGF and ANKRD1 (**b**, respectively FC = 5.9 and FC = 3.3). Conversely, expression of CTGF and ANKRD1 in the oscillatory 1 µL/min vs. 1 µL/min regime was not changed (**c**, FC = 0.97 and FC = 0.76). With regards to eNOS and VEGFR2, from 1 µL/min to 10 µL/min, eNOS was not appreciably changed, though VEGFR2 saw modest upregulation (**d**, FC = 1.4 and FC = 2.0, respectively). Oscillatory 10 µL/min vs. 10 µL/min shown downward trends for both genes (**e**, FC = 0.67 and FC = 0.83) without reaching significance. Oscillatory 1 µL/min compared to 1 µL/min showed minimal changes (**f**, FC = 1.0 and FC = 1.4). For a and d CTGF, ANKRD1, and eNOS, n=7; all other genes performed n=4. Statistical analysis was performed on the ddCts for each group using an unpaired Students t-test. All p-values are reported natively, significance taken at $p < 0.05$. Values are reported as FC. GAPDH was selected as the housekeeping gene for all experiments.

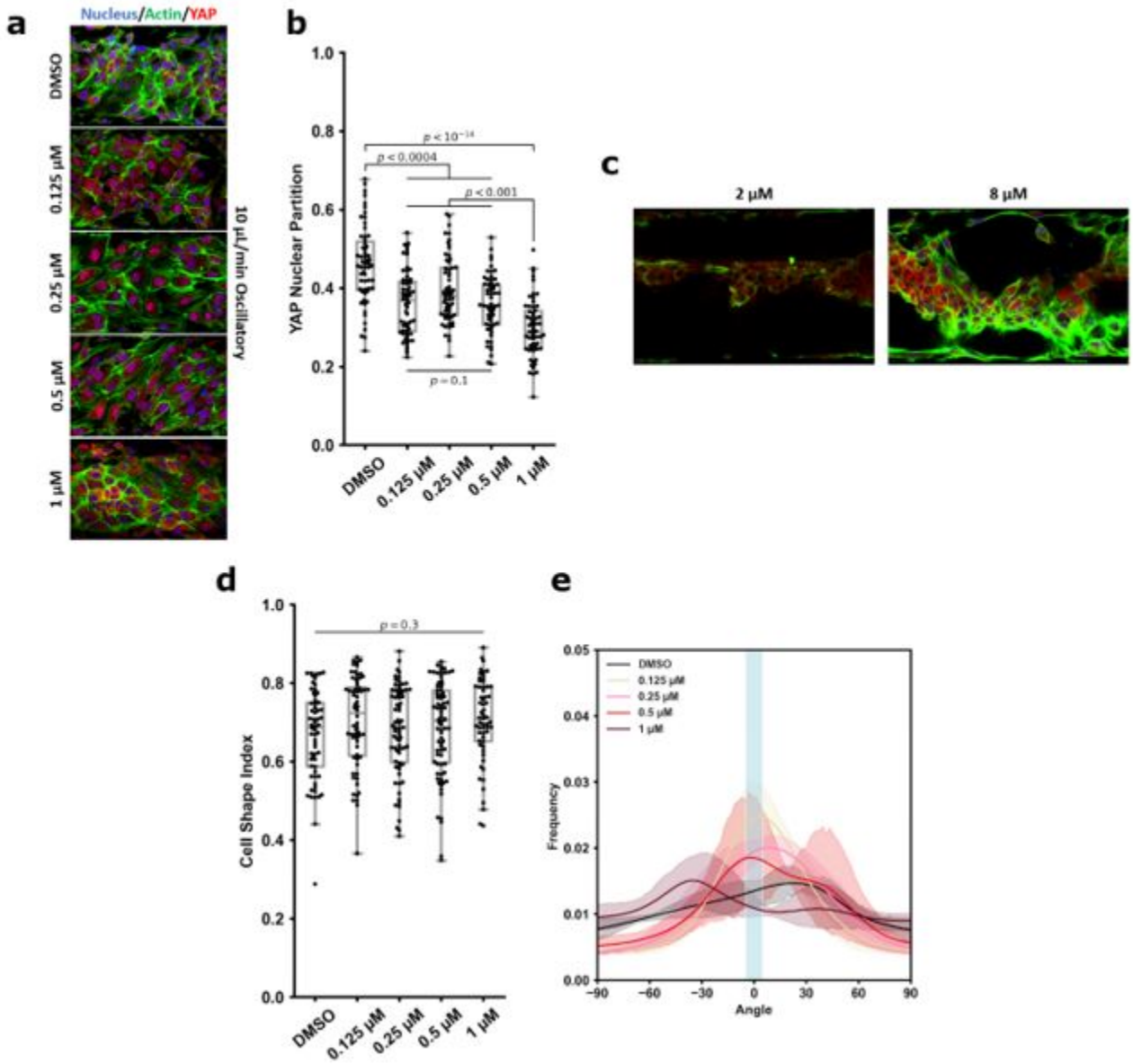

Figure 2.7: Full verteporfin dose response curve with ECs subject to 10 ţL/min oscillatory shear, showing the inhibition of YAP nuclear localization with increasing concentrations (**a-b**). In **c**, representative high concentration regimes are shown to highlight how excessive verteporfin induces excessive cellular detachment. Both the cell circularity (cell shape index) and alignment are not affected by verteporfin (**d-e**). The manuscript displays the data seen here only from DMSO and 1 ţM.

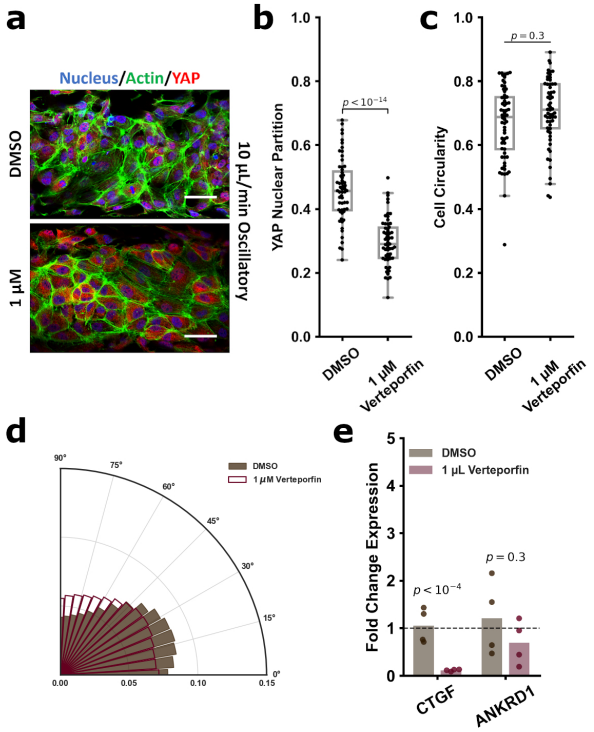

Figure 2.8: Verteporfin immunofluorescence (for nuclei (DAPI, blue), actin (phalloidin, green,) and YAP (red), **a**) showed decreasing YAP nuclear partitioning in the 1 ţM group vs. DMSO control (DMSO: 0.46 ś 0.1; 1 ţM: 0.30 ś 0.1, **b**). Verteporfin treatment did not rescue cellular morphology or alignment under oscillatory flow (**c-d**). Cell circularity indices for the DMSO and 1 ţM Verteporfin groups were respectively 0.67 ś 0.1 and 0.71 ś 0.1. Gene expression analysis of CTGF and ANKRD1 post-verteporfin treatment (**e**) showed significant downregulation of CTGF (FC = 0.11) and insignificant modulation of ANKRD1 (FC = 0.70). Verteporfin treatment IF and circularity performed on n>59 cells. Gene expression performed n=4. Statistical analysis was performed on the calculated normalized IF values or ddCts for each group using an unpaired Students t-test. All p-values are reported natively, significance taken at $p < 0.05$. Values are reported as circularity, FC, or normalized intensity, mean ś standard deviation. GAPDH was selected as the housekeeping gene for all experiments.

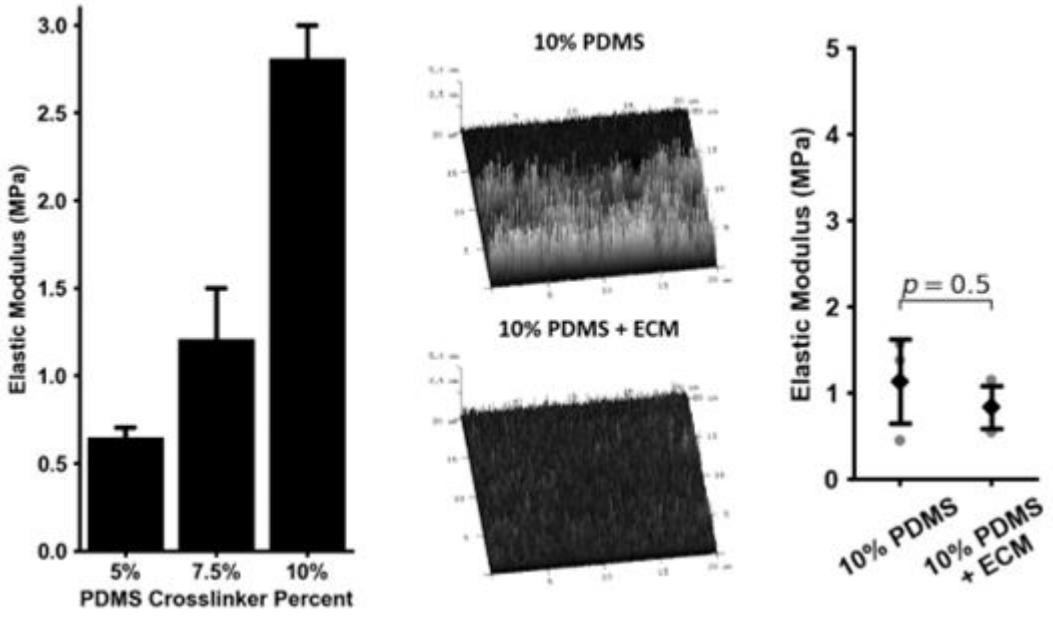

Figure 2.9: Elastic moduli of the various PDMS formulations and confirmation via AFM that chemical modification of a 10% PDMS thin film does not alter the mechanical properties. Conical fit using 0-10% of the AFM curve was used to fit data of PDMS thin films, >15 technical replicates taken per sample with iterative outlier analysis to remove technical replicates with large deviations.

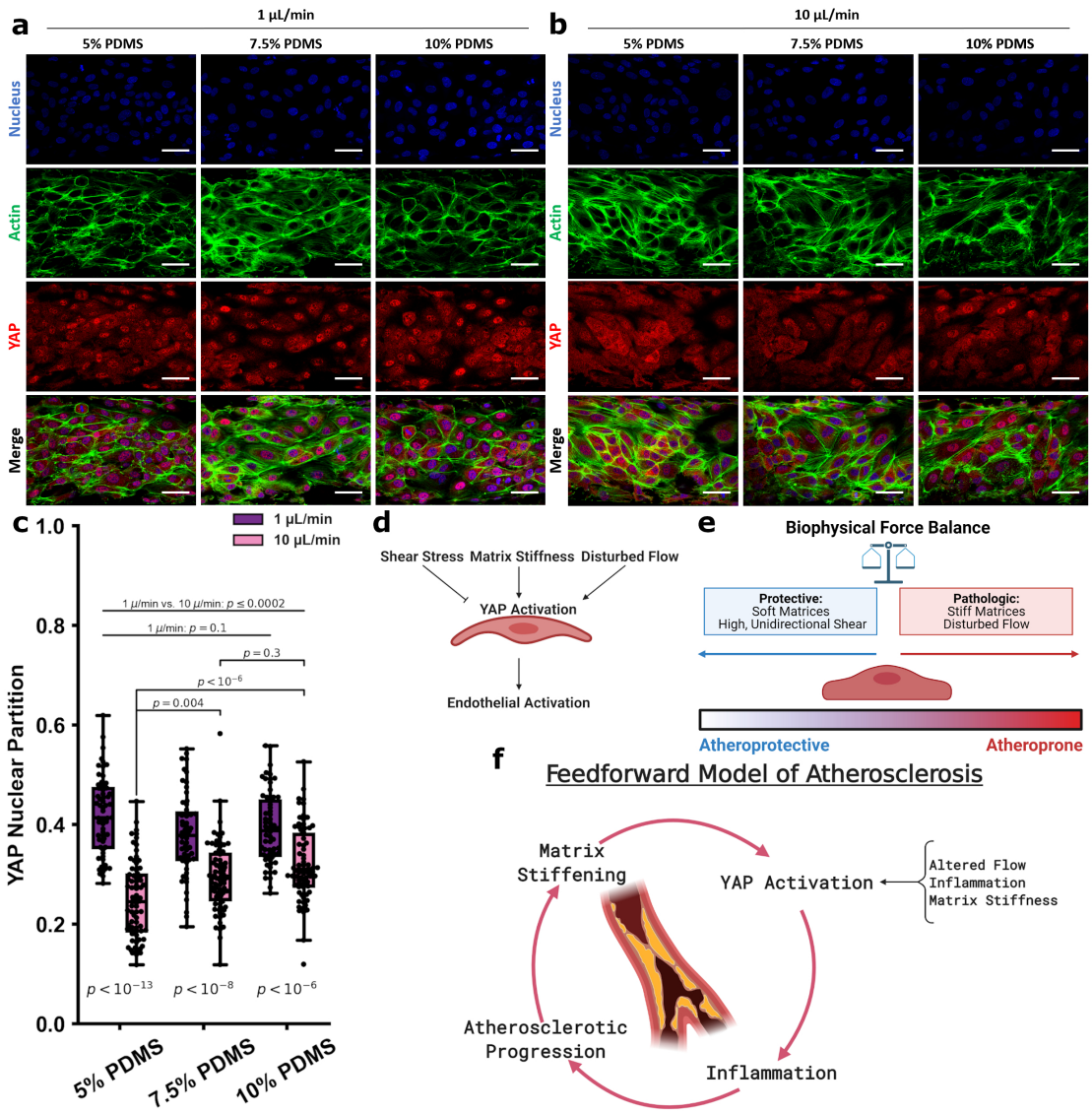

Figure 2.10: Varying device stiffness to modulate the HUVEC endothelial mechanoresponse. Experiments were performed in devices made form the varied crosslinker concentrations of 5%, 7.5%, and 10% and under the unidirectional shear regimes of 1 ţL/min and 10 ţL/min. Cells were stained for nuclei (DAPI, blue), actin (phalloidin, green,) and YAP (red), shown in **a-b**. Across the 1 ţL/min groups, YAP partitioning was not affected by substrate stiffness (5%: 0.42 ś 0.1; 7.5%: 0.38 ś 0.1; 10%: 0.39 ś 0.1), while those subject to 10 ţL/min showed increasing YAP partition as the substrate stiffened (5%: 0.25 ś 0.1; 7.5%: 0.29 ś 0.1; 10%: 0.32 ś 0.1, **c**). YAP nuclear partitioning between the 1 ţL/min and 10 ţL/min groups were significantly different between any 2 groups from different shear regimes. This suggests that ECs respond to a variety of mechanical cues which can either be protective or inflammatory (**d-e**). The physical regimes of stiffness and shear stress may be connected via YAP mechanobiology in a feedforward manner where an initial incident can result in propagating stiffening and YAP activity (**f**). For the 1 ţL/min groups, n = 56 cells, for the 10 ţL/min groups, n = 71-73 cells). Statistics performed using a single factor ANOVA with post-hoc Tukeys test for significance. Each p-value between groups is reported natively as calculated, significance taken at $p < 0.05$. All values reported as mean ś standard deviation.

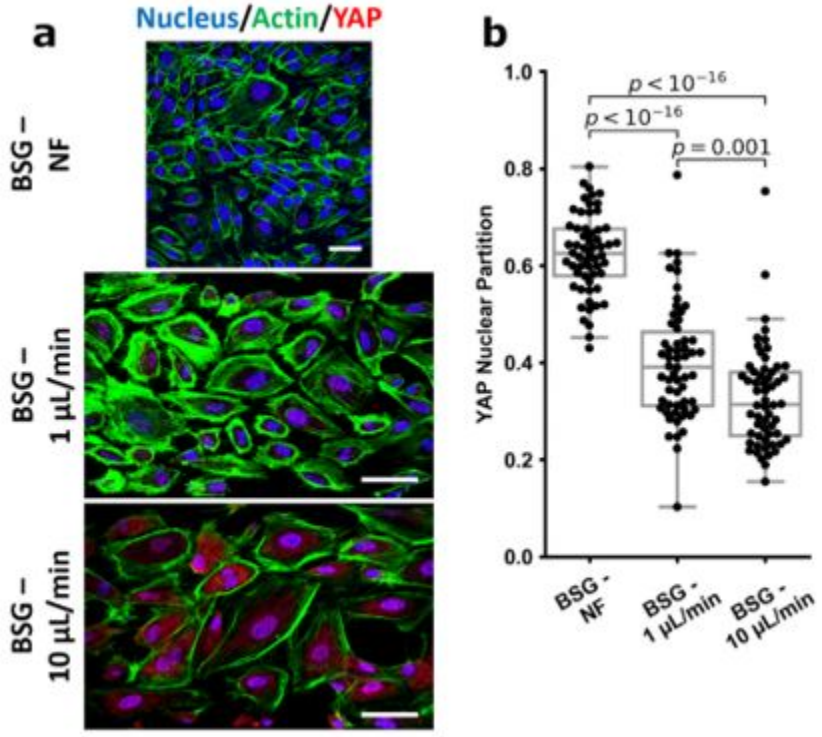

Figure 2.11: Borosilicate glass (BSG) studies demonstrating that high shear can downregulate YAP activity when HUVECs are culture on glass. The NF (no flow) control is conventional glass coverslips used commonly in cell culture, HUVECs within the device require delivery of media, and static controls within the flow chamber is suboptimal. Flow experiments are performed using non-coated BSG glass as the vessel-chip bottom. Note that YAP partitioning on BSG is statistically identical to the 10% PDMS group (**Figure 2.4b** in manuscript, 10% PDMS=0.32ś0.1; BSG=0.32ś0.1; p=0.7). Note the coverslip control is a conventional glass coverslip as perfusion is required on the chip to maintain EC media delivery however the morphology of HUVECs grown in conventional culture is different from those grown under shear fundamentally, and this control only illustrates changes in YAP partition.

3. THE INFLUENCE OF ELECTRIC FIELDS ON YAP MECHANOBIOLOGY PATHWAYS AND VASCULAR PROLIFERATION

3.1 Introduction

Electric field biology, the influence of external electric fields on biological processes, or electrobiology, has long been a source of fascination [207, 208]. Electric fields, voltage differentials, and membrane potentials are an integral part of cellular and tissue physiology [209]. Cellular electrical potentials play an important role in spatially delocalized, time-resolved signaling as observed in the nervous system and cardiovascular system. In these systems, cells generate action potentials, traveling waves of charged ion gradient changes [210–212], which alter membrane potentials and result in biochemical responses and alterations in gene expression [213–217]. The physiology of these electrical potentials is formed and sustained by membrane-confined proteins that serve as ion channels and active transporters which maintain a balance of electrical and chemical potentials such that a specific voltage is maintained across the cell membrane [218–221]. The membrane potential of cells, ranging between 0 to -100 mV, varies in proliferating versus non-proliferating cells and suggests the possible role of external fields on critical cellular performance during the cell cycle [222]. Such an intimate connection between cellular function and electric potentials suggests that cellular behavior may be modulated by application of an external field to induce or inhibit a specific response. This endeavor is realized in the development of electric field chemistry, oriented external-electric-fields (OEEF) that alter structure and chemical reactivity [161, 167], electroceuticals, nascently-produced biochemicals whose levels may be altered with the use of an electric field [63] and so influence cell behavior [51–53], and in the many clinically relevant electrostimulation devices [64, 166]. Applied electric fields may also induce physicochemical changes to transmembrane potentials, alter membrane permeability, or change the electroactivity of receptors or ligands [54, 70]. Electric fields have likewise been shown to influence the cytoskeleton and inhibit growth in cancer cell lines [223–225]. Indeed, there are several approved approaches already

a mainstay in the clinic, such as cardiac pacemakers and antiarrhythmic devices [226, 227]. Here, a new term is defined, electromics, which is the study of cellular gene expression profiles and their implications under the influence of exogenously applied electric fields. This field is a synthesis of bioelectronics and molecular biology, and this report describes preliminary work at this frontier through studies of YAP and CD144 expression biology in HUVECs.

Electric fields are normalized electrical forces per unit charge with the Lorenz force:

$$\vec{F} = q\vec{E} + q\vec{v} \times \vec{B} \tag{3.1}$$

aptly describing the influence of an electric field $\vec{E}$ on a charged entity, q, moving at velocity, $\vec{v}$, in a magnetic field, $\vec{B}$. This relationship suggests that electric fields apply forces throughout systems with charged species in abundance a property which characterizes all biological systems [228], implying that electrostatic interactions and the resulting forces are a fundamental part of molecular biology beyond, but including, the action potential. These electrical forces share an analogy with mechanical forces, such as those arising from shear stress or substrate stiffness, and thus may have similar avenues of cellular expression. Tangibly, ion channels and electrical potentials have been tied to molecular processes, outside of action potentials, to connect these paradigms; ion channels in endothelial cells have been shown to be mechanosensitive and responsive to shear stresses [229] with examples including the recently elucidated piezo channels [40–42,44,230,231]. Electro-mechanical coupling in tissue maturation is well known for maturing cardiomyocytes from neonatal rats or from hiPSC differentiation; such maturation being facilitated by electrical or mechanical stimulation [165]. Beyond the connection between mechanobiology and electrobiology (electrical stimulation), electrical fields have also been shown to influence gross cellular behavior in wound healing, influencing cell proliferation and migration [55, 57–60, 124, 232]. Taken together, this suggests a deep connection between the voltage potentials and forces induced by electrical fields, ion channel signaling, and the influence these may have on cellular genetics and biochemistry. Thus, there is considerable interest in harnessing the power of electric impulses to aid healing of chronic wounds, reduce pain, and restore neurological activity. However, fundamental under-

standing of the role of such electric impulses on cellular activity remains elusive. Yesassociated protein 1 (YAP) and WW-domain-containing transcription regulator 1 (transcriptional coactivator with PDZbinding motif) (TAZ) are the main effectors of the Hippo pathway, pivotal to tissue growth, and their nuclear localization is a well-established signature of the regulation of their transcriptional activity and role in signal transduction [164, 233]. Shuttling between the nucleus and the cytoplasm, nuclear YAP/TAZ promotes cell proliferation, organ overgrowth, survival to stress and dedifferentiation of post-mitotic cells into their respective tissue progenitors [160]. Such localization is well known to be influenced by external mechanical forces in pathways distinct from Hippo [64], including shear stresses, such as in 3D printing of suspended cells or arising from flow over adherent cells [234], and substrate stiffness [235]. Acting as transcriptional co-activators [64], several genes are regulated by YAP/TAZ activity. Two such commonly used targets include connective tissue growth factor (CTGF) and ankyrin repeat domain 1 (ANKRD1) [62, 236], which are positively regulated by increasing YAP/TAZ activity. Thus, the relative expression of these genes may be used as a readout for the level of YAP/TAZ activation in parallel to its nuclear partitioning. The downstream regulation of YAP/TAZ via several plasma membrane domains [237] suggests that membrane potentials and electrical influences that affect the plasma membrane [184] may similarly and likewise affect YAP/TAZ localization.

Isolating such interactions between electric fields and its downstream influence on cellular processes requires precise engineering of the system. Certain reports have described directly using electrodes or electrode arrays to stimulate cells [238–240], after which cells may be harvested and characterized. Additional reports use conductive scaffolds, polymers, or hydrogels [241–245] to engineer a more biomimetic environment for cell growth which facilitate advanced fabrication techniques such as 3D printing [241, 246, 247].

To facilitate electromics, a cell culture system to culture and monitor the cellular response to uniform electrical fields in real time, termed the electrical cell stimulation and recording apparatus (ECSARA), was previously designed, fabricated, tested and reported [54]. The primary advantage of this system is its use of conventional 24-well cell culture plate format while enabling the inves-

tigations of gene expression under a uniform electric field orthogonal to the cell growth plane of trans-well cell culture inserts. This design separates the cells from direct contact with the titanium oxide-coated titanium electrodes thus assuring isolation of the cells from any effect other than the field-effect, and as modeled, uniformly applies the same electric field to all cells cultured on the trans-well inserts [54]. This approach eliminates any perturbation of the cells by non-electric field aspects of the system. Moreover, the design based on 24-wells allows for simultaneous, multiplexed interrogation and investigation of both stimulated and control groups to be run in parallel and in replicates which enhances the statistical power to resolve small differences not readily discerned in single lab-on-a-chip type constructs. Thus, using this previously validated ECSARA system supports quick transition into the intended biological inquiry.

In this study, ECSARA was used in a novel application to specifically study YAP expression biology and CD144 expression under electrical field influence. The effect of electrical stimulation on human umbilical endothelial cells (HUVECs) was studied by applying an electrical field under three regimens alongside separately prepared, non-stimulated, negative controls for each regimen. ECSARA allowed parallel real-time monitoring of trans-endothelial electrical resistance (TEER; a resistance measure that assesses CD144 enabled tight junction formation between HUVECs) by electrical impedance spectroscopy and equivalent circuit analysis (EIS-EQCRTA). Using ECSARA) [54], cells were stimulated with programmed stand-off electric fields. HUVECs were exposed to electric fields of 0 (non-stimulated, negative control), 2 mS pulses of amplitude 162 mV/mm (1.2 V) at 1.2 Hz (T1), 81 mV/mm (0.6 V) at 1.2 Hz (T2), and 162 mV/mm (1.2 V) at 0.6 Hz (T3) over a 48 h period where 1.2 Hz corresponds to a heart rate of 72 beats/min. The range of electric field strength was chosen to induce no temperature or pH change to the incubated (constant 37^{o}C) and highly buffered cell-culture medium. Hence, all observed cellular responses would be related solely to the electrical stimulation [248]. In a parallel and separate group of experiments, the viability (alamarBlue^{TM}) of stimulated and control HUVECs was measured, to allow the construction of a temporal viability profile under stimulation. The impedance of cells was measured and analyzed with an equivalent circuit to monitor cell growth, proliferation, and formation of a

confluent monolayer. Trans-well EIS-EQCRTA was performed over the range 10 mHz 1.0 MHz and over a 72 h period to reveal changes in TEER performance under the different cell stimulation conditions and these were evaluated relative to negative controls. The EIS data were collected from the cells every 6 h and were modeled using an $R_S(Q_{CELL}R_{CELL})(Q_{OX}R_{OX})(Q_{DL}R_{CT})$ equivalent circuit wherein R_S represented the resistance of the solution or media, R_{CELL} and Q_{CELL} represented the insert-supported cell monolayer with R_{CELL} specifically being reflective of TEER. Due to the non-ideal capacitive behavior of the bioelectrochemical system, the capacitance (C) was represented by a constant phase element (CPE or Q). The impedance of the CPE $[= 1/C)(j\omega)^{-n}]$, where for the case of n=1, Q presents the behavior of an ideal capacitor. The subscript OX stands for oxide layer and characterizes the electrochemical contribution of the titanium oxide layer formed on the interrogating titanium electrodes. The Q_{DL} and R_{CT} terms reflect the double layer (DL) capacitance and charge transfer (CT) resistance of the electrochemical system. Over similar periods, separately stimulated cells were isolated for total RNA extraction followed by gene expression via real time quantitative polymerase chain reaction (RTqPCR). The expression of downstream targets of the transcriptional coactivators, YAP/ TAZ, were assessed by RTqPCR. Of specific interest was gene expression of connective tissue growth factor (CTGF) and ankyrin repeat domain 1 (ANKRD1) (downstream targets of YAP activation) and VE-Cadherin (to assess endothelial junctional formation). Confocal microscopy was performed to assess YAP nuclear partitioning. Inclusion of negative controls within the same plate as the EF stimulated group ensured precise evaluation of cellular response to EF.

3.2 Materials and Methods

Electrical Stimulation: Electrical Cell Stimulation And Recording Apparatus (ECSARA), designed and developed in the C3B lab, was used in this study. The design, fabrication, testing, and validation of the system were reported in detail previously. The system employs a pair of titanium oxide-coated titanium electrodes positioned above and beneath the cell culture inserts hence the applied EF is orthogonal to the cell growth plane [54].

Cell Culture: RFP-expressing HUVECs (Angio_Proteomie) were cultured and expanded per

standard protocols. Cells at passage number $\leq$8 were used. Following expansion, cells were seeded on gelatin-coated 0.4 ţm PET (Polyethylene terephthalate) inserts (Corning, Millipore) at a density of 2.5 x 10^5 cells/ml (equal to 7.5x10^4 cells/cm^2) and 1000 ţL of media was added to the reservoir. One hour following seeding, the TEER measurement was performed, t0, at an interrogation voltage of 20 mV p-p over the frequency range of 0.01 Hz-1 MHz. Simultaneously, in a triplicate group of wells, the media was replaced with media containing 10% Alamar Blue reagent, incubated for 2 h and the absorbance was subsequently measured with a Synergy HT plate reader (BioteK) at 570 nm and 600 nm wavelengths.

Electrostimulation of cells was performed 1 h post seeding. An electrical pulse of T1 = 1.2 V magnitude (162 mV/mm), 2 mS width and 1.2 Hz, T2 = 1.2 V magnitude (162 mV/mm), 2 mS width and 0.6 Hz, T3 = 0.6 V magnitude (81 mV/mm), 2 mS width and 1.2 Hz, where 1.2 Hz resembles heart rate of 72 bpm, was applied continuously to cells except for 30 min duration when the TEER was measured by EIS-EQCRTA and the results were compared with cells at electric fields of 0 (non-stimulated control). The EIS data were collected from the cells every 6 h in the first 24 h and then every 12 h and were modeled using an $RR_S(Q_{CELL}R_{CELL})(Q_{OX}R_{OX})(Q_{DL}R_{CT})$ equivalent circuit where the changes in R_{CELL} represented the transmembrane epithelial/endothelial cell resistance (TEER) of the monitored HUVECs. The viability of the EF stimulated and control groups were likewise measured at 1 h post seeding (t0), 12 h, 24 h, and 48 h following t0.

cDNA Synthesis and Gene Expression: Extracted RNA was converted to cDNA in a 20 ţL reaction using 5x iScript Reverse Transcriptase Supermix (Bio-Rad Laboratories, Inc.). The reaction volume was then diluted to 100 ţL using DNAse/RNAse-free water. For each qPCR reaction, a volume of 10 ţL was used consisting of 5 ţL of Power SYBRő Green Master Mix (Applied Biosystems, Thermo Fisher Scientific), 3.5 ţL of H2O (DNAse/RNAse free, molecular grade), 0.5 ţL of the gene specific primer, and 1 ţL of the sample cDNA. All primers were purchased as validated 20x SYBRő Green assays for qPCR (Bio-Rad Laboratories, Inc.). Primers used were glutaraldehyde 3-phosphate dehydrogenase (GAPDH), connective tissue growth factor (CTGF), ankyrin repeat domain 1 (ANKRD1), and VE-Cadherin (CD144). RT-qPCR was performed using

a QuantStudio 12K Flex (Applied Biosystems, Life Technologies) with the pre-set settings of: MicroAmpő EnduraPlate Optical 384-well plate (Applied Biosystems, Thermo Fisher Scientific), Relative Quantification (-$\Delta\Delta$Ct), SYBRő Green Reporter, and Standard Run Time. Statistics were performed on ΔCt values. All gene expression results were reported as a fold change with standard deviation with respect to the denoted control and the housekeeping gene, Glyceraldehyde-3-Phosphate Dehydrogenase (GAPDH).

Immunofluorescence: Each trans-well insert was placed into a new 24-well plate, washed with PBS and fixed using 4% paraformaldehyde (Thermo Fisher Scientific) for 20 min at room temperature. Cells were washed afterwards twice with PBS and then blocked and permeabilized with 2% bovine serum albumin (BSA, Sigma Aldrich) and 0.1% Triton X-100 (Thermo Fisher Scientific) in PBS (blocking buffer) for 1 h at 4^{o}C. Each insert was then stained with rabbit anti-YAP (1:100) in blocking buffer overnight (16 hours) at 4^{o}C. The next day, inserts were washed twice with PBS and secondary staining was performed with donkey anti-rabbit Alexa Fluor^{TM} 555 (Invitrogen Molecular Probes, Thermo Fisher Scientific) in blocking buffer for 1 h at room temperature. Actin was stained with phalloidin Alexa Fluor^{TM} 488 (Invitrogen Molecular Probes, Thermo Fisher Scientific) in PBS for 30 min. Each trans-well insert was then carefully cut out to be mounted on a glass slide. Nuclei were stained with 4,6-diamidine-2- phenylindole dihydrochloride (DAPI, Roche Diagnostics), contained within the coverslip mounting media.

Imaging and Imaging Analysis: Slides were imaged at 40x oil immersion (ULSAPO40XS NA: 1.25, Airy Disk: 1) on a FLUOVIEW FV3000 confocal microscope (Olympus Corporation). Each condition was imaging using the Z-stack function and analysis was performed using maximum Z-projections on the associated software (cellSens, Olympus Corporation) for YAP partitioning. YAP partitioning was calculated as the nuclear YAP signal divided by the total cellular YAP signal using regions of interesting manually created in the software for n = 15 cells.

Data Visualization: All data visualization was performed in Python 3.7 using Matplotlib [171] with Seaborn packages or with GraphPad Prism. All scripts are available upon request; examples scripts are included in supplementary material.

3.3 Results

Viability Assay: The alamarBlue™ cell viability assay was performed with the intent of monitoring cell growth and any unfavorable side effect of EF on cells in comparison to a non-stimulated control group. As shown in Figure 3.1, during the first 24 h, the viability of the EF stimulated group followed the control group very closely for T1 and T2 EF stimulation regimens and outpaced the control thereafter. The average growth index after 48 h was 37.5% and 5% higher than control for T1 and T2 regimens, respectively. After 12 h under the T3 stimulation regimen, the growth index of EF the electro-stimulated group fell behind the control, with the average being 5% less than control after 48 h. Considering the 24 h doubling time of HUVECs, the data suggest that within two cell generations, EF stimulation supported increased proliferation in a field dependent fashion. The data further suggest that the EF stimulation favorably altered HUVEC viability after 24 h.

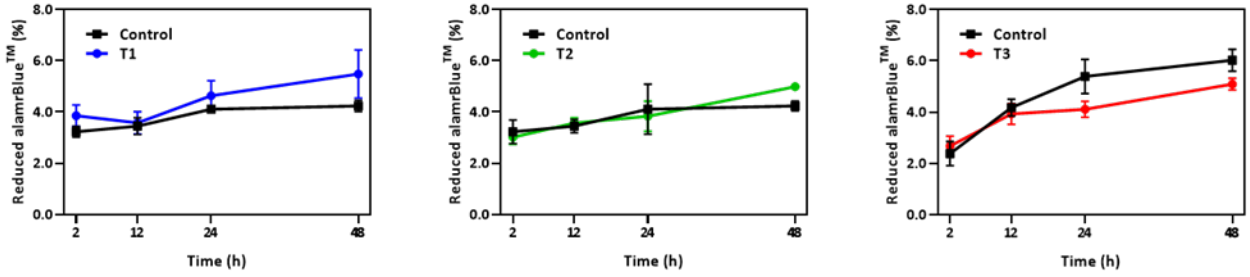

Figure 3.1: Temporal changes in alamarBlue™ viability assay over a 48h period for HUVECs receiving electrical stimulation under T1, T2, and T3 electrical stimulation regimens. Percent of reduced alamarBlue™ shows the change in intensity of alamarBlue™ relative to that obtained 1h post cell seeding (n=3).

TEER Measurement: The trans-monolayer resistance of HUVECs was investigated via electrical impedance spectroscopy (EIS) using the concomitant recoding mode of the ECSARA and characterized using equivalent circuit analysis (EQCRTA) with an appropriate model to describe

the system. As in previous work, use was made of an $R_S(Q_{CELL}R_{CELL})(Q_{OX}R_{OX})(Q_{DL}R_{CT})$ equivalent circuit wherein R_S represents the resistance of the solution or medium, R_{CELL} and Q_{CELL} represent the insert-supported cell monolayer with R_{CELL} specifically being reflective of transepithelial/ endothelial resistance (TEER; a resistance measure that assesses the establishment of tight junctions between HUVECs). Due to the non-ideal capacitive behavior of the bio-electrochemical system, the capacitance (C) is represented by a constant phase element (CPE or Q). The impedance of the CPE $[= 1/C)(j\omega)^{-n}]$, where for the case of n=1, Q presents an ideal capacitance. The subscript OX stands for oxide layer and characterizes the electrochemical contribution of the titanium oxide layer formed on titanium electrodes. The Q_{DL} and R_{CT} terms reflect the double layer (DL) capacitance and charge transfer (CT) resistance in an electrochemical system, respectively.

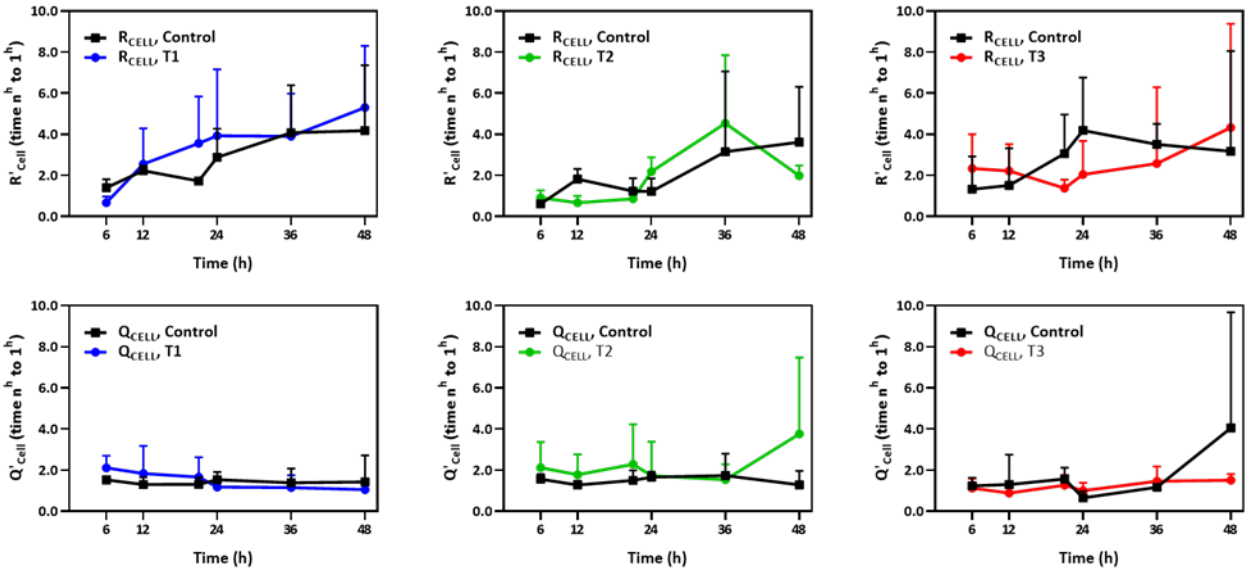

Figure 3.2: Temporal changes of R_{CELL} and Q_{CELL} derived from the $R_S(Q_{CELL}R_{CELL})(Q_{OX}R_{OX})(Q_{DL}R_{CT})$ model for T1, T2, and T3 electro-stimulated HUVECs. The Y-axis is the relative fold change in R_{CELL} (top panel) and Q_{CELL} (bottom panel) normalized to R_{CELL} or Q_{CELL} measured 1 h post cell seeding (n=3).

The temporal changes in Q_{CELL} and R_{CELL} correspond to the growing influence of tight junc-

tions formed between the adjacent HUVECs as they grew to confluency. Values of Q_{CELL} and R_{CELL} were extracted and graphed and are shown in Figure 3.2. After about 20 h the TEER, R_{CELL}, outpaced the control in both the T1 and T2 EF stimulation regimens, consistent with the viability study. A similar pattern was observed in Q_{CELL}, an element representing the number of cells in the EIS. Under the T3 electro-stimulation regimen, the pattern was reversed and both R_{CELL} and Q_{CELL} were lower than control during the later phase of culture, again, consistent with and confirming the association of TEER with the viability study.

Immunofluorescence: Previous reports have suggested that electric fields promote vascular proliferation and junction formationRN156, RN157, RN155, RN154. Effectors of the endothelial cell mechanoresponse YAP and TAZ [63, 65, 68–70, 159] are known to modulate the cell cycle and control cellular proliferation and apoptosis. YAP/TAZ displays differential activity depending on the physical and biochemical stimuli and translocate to the nucleus when transcriptionally active. To explore how electrical fields may modulate these transcriptional co-activators, YAP/TAZ localization was assessed via immunostaining and subsequent confocal microscopy detailed in Figure 3.3. Across the first 12 h of the three electro-stimulations regimens, YAP/TAZ nuclear partition was lowest in the control group and increased in all groups following electrical stimulation for 12-h. At the 12 h time point, T3 displayed the most elevated nuclear partition ($p < 0.05$). This would suggest the T3 electrostimulation regimen was a potent inducer of YAP activity and proliferation, however the proliferation data suggests otherwise, which may be tied to detrimental effects associated with elevated YAP activity (such as inflammation). When cells were again measured at 24 h, YAP/TAZ activity was not significantly different across all three electro-stimulations regimens, which suggests that the cellular monolayers had reached comparable steady states after two cell cycles. The data indicate and confirm that the timescale for YAP/TAZ translocation precedes apoptosis as evidenced from viability studies and precedes tight junction formation (TEER).

Gene Expression: To assess the effect of electrical stimulation on HUVECs at a transcriptional level, specific targets of YAP/TAZ transcriptional activity (CTGF and ANKRD1) and expression of an endothelial junctional protein (VE-Cadherin/CD144) were measured and shown in Figure

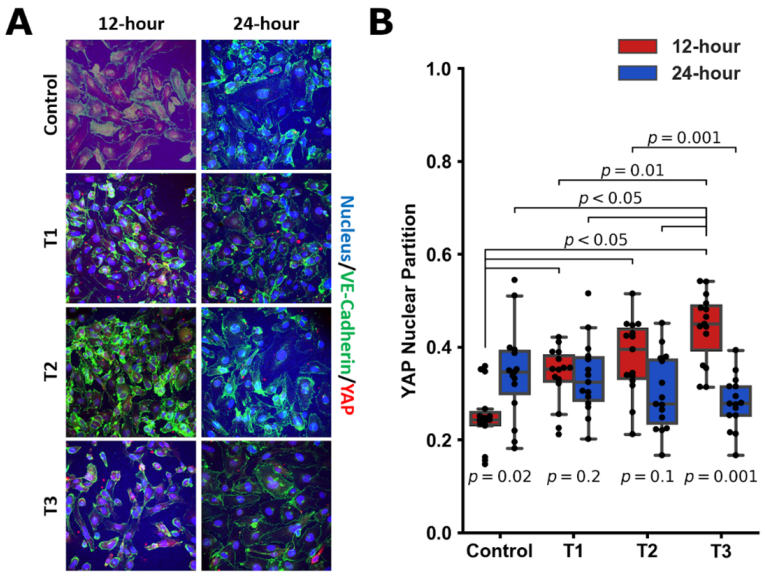

Figure 3.3: (**A**) Immunostaining of HUVECs stimulated by electric fields at three different conditions (T1, T2 and T3) at 12 and 24 h post stimulation. (**B**) Box and Whiskers plot of YAP nuclear localization obtained from immunofluorescent images, n=15 individual cells per group.

3.4. CTGF expression at 12 h was modulated modestly, with the T2 and T3 frequency regimens shown a decrease in its expression. At the 24 h mark, there was some upregulation through the different electrical stimulation regimens, although T3 was not different from the control 24 h group. However, notably, the fold changes for each of these experimental groups rarely exceeded 2-fold, suggesting overall a modest biological difference. Note this contrasts with the IF data, as the IF data demonstrated an increase in YAP nuclear localization whereas gene expression showed a small down regulation. This might be tied to specific system limitations, which are discussed further. ANKRD1 was not appreciably modulated by electrical stimulation across regimens with an exception between the 24 h control and the T2 stimulation regimen at 24 h. In summary for YAP targets, these genes do show some modulation although the expression changes are less than 2-fold. In contrast, CD144 was dramatically upregulated by the T1 and T2 regimens, although this effect was significantly dampened by the T3 regimen. We note that the T3 frequency was shown to function as more of an inhibitor of cell proliferation in the viability assays, which is captured here as well. At 24 h, there were no changes in CD144 expression, although expression

remained elevated compared to the 12 h control. This supports the view that certain electrical stimulation patterns can serve to accelerate cell proliferation and junctional format, but that after a certain time point, cells appear to proliferate and reach a steady state that is agnostic of the electrical stimulation regime. Thus, the feasibility of electrically stimulating HUVEC proliferation and junctional formation is consistent with our previous purely cellular report [54].

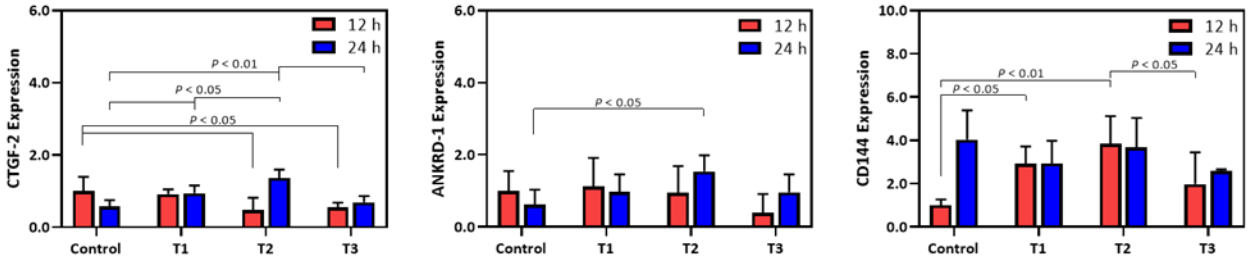

Figure 3.4: Expression fold change relative to controls of ANKRD1, CTGF, and CD144 in HUVECs stimulated with electric fields at 12 h and 24 h post stimulation. Results were obtained from RT-qPCR analysis (n=3).

3.4 Discussion

This study was inspired by investigating potential homology between electro- and mechanobiology. In response to the environmental changes, activation of ion channels of cell membranes followed by intracellular signaling determines the cell response to a stimulus. Flow sensitive potassium and chloride channels are activated in response to shear forces causing cells to hyperpolarize/depolarize. Potassium channels demonstrate the first and fastest response to the shear stress, activating at lower thresholds and saturating at high stresses [29, 34]. These channels temporally lose their sensitivity under sustained stress [28]. Similar forces result in YAP/TAZ translocation between the cytoplasm to the nucleus. The response to steady and oscillatory shear stress is very different in endothelial cells according to several reports [56, 69, 70, 184] . While a 0.2 Hz oscillatory flow resulted in full hyperpolarization (2.8 mV) and limited depolarization (1.1 mV), a 5

Hz oscillatory flow did not induce hyperpolarization nor depolarization. A 1 Hz oscillatory flow caused partial hyperpolarization (1.8 mV) and depolarization (0.6- 1.1 mV) [184]. In the case of steady shear stress, the threshold magnitude is much lower for hyperpolarization compared to depolarization. Electromechanical coupling that induces force transduction via charged surface integrin receptors was proposed by Hart in 2006 [249]. Assuming a rod shape for integrin and using theoretical models, he suggested that an alternating EF of 100 mV/mm exerts forces of 1 fN on integrin molecules, similar to a force that is applied by shear oscillatory stress of 1 N/m2 [249]. The force is independent of frequency up to a threshold before rapidly attenuating with increasing frequencies. The threshold frequency depends on the length of the charged glycoprotein, and is roughly within 0.1-1.0 Hz for glycocalyx on endothelial cells. Surface integrins are implicated in several mechanotransduction pathways, and modulating their activity via external EFs may connect the electric stimuli with the observed downstream effects. The coupling between glycoproteins on the surface of the same cell or adjacent cells signifies the efficiency and strength of the effect. In the present study, a potential difference of 1.2 V or 0.6 V corresponding to an electric field of 162 mV/mm or 81 mV/mm was applied to HUVECs. This low electric field is well within the physiological EFs (1-200 mV/mm) present in the body [56]. Applying a perpendicular EF of this range to an approximate 2 ţm thick endothelial cell monolayer [250], results in a potential difference of 0.32 mV or 0.16 mV across cells. Elucidating the exact nature of these mechanisms is an active area of research [251]. These low potential differences could affect and possibly activate some of the voltage-sensitive channels of the cell membrane and may trigger signals to induce YAP/TAZ activation via a mechanobiological pathway [251, 252]. Such potentials also likely cause electrophoretic movement of ions (Ca2+, K+, Cl-, Na+) within the cell and cell culture media, creating a local, transient imbalance of ions across the cell membrane yet to affect transmembrane channels. Lastly, there may be some level of electromechanical coupling present as charged surface receptors would experience a force when subject to an external EF (as hypothesized by Hart) . More recently, experimental evidence for direct influence of charged residues of proteins under an electric field was demonstrated [253], providing additional experimental evidence that electromechanical cou-

pling may be an important contributing mechanism. Nevertheless, the electro-stimulation was not sufficient to generate heat and/or change the local pH and/or ion concentration in a way that could not be rapidly dissipated and/or trigger a response beyond the EF stimulation [254]. During the electrical stimulation regimens employed in this work, a constant 81 mV (T2 and T3) or 40.4 mV (T1) was applied to HUVECS with periodic pulses of 162 mV/mm (T2 and T3) or 81 mV/mm (T1) strength in the opposite direction at frequencies of 1.2 Hz (T1 and T2) or 0.6 Hz (T3). The constant potential likely polarized the cell monolayer and rearranged the charge distribution across the cells. The HUVEC viability results of alamarBlue^{TM} assay, where the number of live cells in T1 and T2 EF stimulation regimens, but not that of T3, were higher than the control condition, confirmed that the T1 and T2 regimens promoted cell viability and/or proliferation while T3 suppressed the growth or possibly caused cell death. These results were similarly reflected in EIS derived TEER data. In T1 and T2 electro-stimulation regimens, the EF was applied at the same 1.2 Hz frequency with 0.6 V and 1.2 V pulse magnitude, respectively; while under the T3 electro-stimulation regimen, a 0.6 Hz frequency with 1.2 V pulse was used. These results highlight the more determinative role of frequency (within this low frequency region) compared to the voltage magnitude on cellular behavior. It can be argued that the cumulative time over which cells were exposed to a higher voltage was longer for the 0.6 Hz pulse. The magnitude of voltages used was relatively low compared to other studies to avoid any probable electrolytic splitting of water (hydrogen and oxygen evolution) that occurs at the electrode-cell culture interface. During the first 12 h, the applied electric field did not cause any difference in HUVEC population as indicated by alamarBlue^{TM} assay, yet YAP translocated and partitioned into the nucleus at a significantly higher level under all three electro-stimulation regimens compared to the control. The results of immunofluorescent staining confirmed that across all three electro-stimulation regimens, electrical stimulation for 12h increased YAP nuclear partitioning compared to the controls, while after 24 h, there were no longer significant differences. YAP/TAZ activity controls cellular proliferation, which would be supported by the general upshifting of CD144 expression in stimulated HUVECs, however, neither the alamarBlue^{TM} nor gene expression appear to follow this phenomenon on the

same time scale. Notably, YAP/TAZ partitioning occurs at a timescale significantly faster than the target gene expression (minutes vs. hours) [255], while the experiments here had a minimum time resolution of 12 h, and more definitive differences in signaling activity may be observable either at earlier time points or later ones (as supported by the alamarBlue^{TM} and EIS data). This reinforces the well-established paradigm that subcellular signaling events occur on time scales that are far shorter than changes in morphological or pathological cellular and tissue processes, in this case viability and tight junction formation among HUVECs [256]. The effect of EF on cell population was observed 12-24 h post stimulation, in accord with the cell doubling time of 24 h. Pulse frequency appears to additionally induce cell death more readily than the voltage magnitude, which may confound conclusions comparing T3 to the other electrical stimulation regimens as these regimens did not display such issues. However, at the 24-h mark, nuclear partitioning does not display significant differences, which suggests that at the 24-h mark, the endothelial monolayer has reached confluency, and thus is biologically more quiescent.

Gene expression of downstream targets of YAP was modestly regulated in the electroculture system, and in some cases were opposite to that supported by cell viability assays and IF studies. This may be due to several reasons tied to the system itself, as the culture wells are relatively non-physiologic physical environment which interferes with YAP/TAZ activity. Such outcome, however, are not likely to be related to pH/ temperature changes because of the stimulation since the field strengths applied were generally weak. Other parameters which modulate YAP activity strongly, such as substrate stiffness [65, 68] and shear stress [70], although controlled (no flow employed and the same substrate used), were not directly measured. Gene expression is notably convoluted with specific variables known to influence downstream YAP activity, which may explain the relatively low fold-change observed with CTGF, as its expression is extremely sensitive to YAP activity. Conversely, ANKRD1 has several other regulatory pathways and is not as strongly influenced by YAP activity as is CTGF [70]. However, expression of VE-Cadherin was clearly accelerated in the presence of electric fields, consistent with previous reports demonstrating that electrical stimulation increased cell proliferation and junctional formation [153, 232]. The 12

h time points associated with cellular proliferation and junctional formation in the viability and impedance studies all showed stark upregulation on qPCR, while the group that inhibited growth (T3) showed diminished CD144 expression compared to the T2 group which promoted expression most strongly. At 24 h, cells appear to have reached a steady state, and CD144 expression normalized across the three regimens regardless of the stimulation magnitude and pattern. Outside of the system limitations themselves, each experiment was conducted in the same test environment (notwithstanding the applied electric field) alongside an un-stimulated negative control group, so changes that are observed are attributable to the electrical stimuli. Together then, the data presented here is consistent with previous reports, yielding a closed system which allows for control over the electrical stimulation regimes in a precise manner. However, this report goes beyond others to confirm that electric fields share a similar influence as do mechanical forces in affecting YAP nuclear partitioning but unique in promoting CD144 tight junction formation.

3.5 Conclusions

This work presents a closed system for precise control of the frequency, magnitude, and duration of applied EFs to cells in culture and its application to explore how electrical stimuli influences gene expression. Evidenced by the increasing number of studies reporting that EFs can stimulate proliferation and expedite wound healing, the system was applied in such a manner as to study these effects on gene expression in HUVECs a path toward understanding electro-stimulated vascularization. It was found that, overall, EF stimulation expedited junctional formation, increased cellular proliferation, and increased YAP nuclear localization. Cytoplasmic localization of YAP within endothelial cells is known to occur under interfacial shear stress occasioned by steady and pulsatile flow, while nuclear localization occurs under disturbed flow, stimulating proliferation, inflammation, and vascular disease [257]. However, downstream targets of YAP were not appreciably affected, though this is likely due to limitations of the system and countervailing physical stimuli that are also known to govern YAP activity (such as substrate stiffness), which were not controlled in a manner to avoid potentiation. Moreover, despite multiple views regarding the mechanism for influence of EF stimulation on biological processes, the role of field strength, duty cycle,

frequency and duration of cellular systems is not molecularly and quantitatively fully known. Researches that deem the response on voltage-gated channel and their distribution on cell membrane, movement of ions and charged biomolecules inter- and intra-cellularly, and changes in cell signaling [248] suggest a countervailing influence of EF on cellular behavior which could be responsible for the reported trend in YAP activity and its downstream targets in this study. Regardless, the results demonstrate that electrical stimulations improve proliferative capacity, and that oscillatory frequency was more important than field strength. This is desirable in wound healing and in tissue regeneration, especially in the context of revascularization of tissues to restore blood flow. Together, these data support that EFs modulate gene expression tangibly which may see application in the clinic as electroceutical treatments in regenerative medicine. More generally speaking, this work opens the field of electromics for further investigation, or more precisely, quantifying the effect of electric fields on gene expression and cell biology to understand how this transduction occurs and the biochemical pathways that are modulated. Future work includes a holistic approach using sequencing methods to provide a global look into gene expression under electrical influence.

4. COMBINED ATOMIC FORCE MICROSCOPY AND SUPER-RESOLUTION IMAGING TO STUDY STRUCTURAL AND MECHANICAL CHANGES IN SENESCENT ENDOTHELIAL CELLS

4.1 Introduction

Mechanobiology is the study of how external physical forces and the mechanical properties of cells influence cell physiology and disease processes [5, 7, 156, 163]. Insight into mechanisms of mechanotransduction, or how biological force transducers work, is an active area of research [31, 61, 90]. Considerable light has been shed on vascular function and disease, and given that blood vessels are constantly subject to several physiological forces, it is unsurprising that mechanobiological pathways are directly implicated in cardiovascular homeostasis, disease progression, and atherosclerosis [69, 70, 193, 258]. Cardiovascular disease risk increases with aging, and senescence has been extensively studied as a propagating factor in vascular dysfunction [133]. However, only recently has the dysregulation of mechanotransduction been studied in the context of aging and senescence, and their impact on the mechanical properties of cells and the resulting pathways remains to be completely explored [259]. Previous reports have shown that the mechanical properties of senescent cells are altered in and accelerated aging disease, Hutchinson-Gilford Progeria Syndrome [260, 261], however the granularity at which this information was collected needs refinement: there appear to be several different studies reporting composite stiffnesses as measured by AFM to be higher [260–262], lower [263], and Suunchanged [264] between young and aged cells. These variations imply that underlying assumptions [154] or individual cell heterogeneity may influence the effective stiffness measurements as conducted via AFM significantly. Thus, to provide insight as to how the mechanical properties change in senescence and explore how this may affect mechanotransduction, we sought to quantify the mechanical properties of individual cells in a highly precise manner by directly accounting for individual cell geometries.

The mechanical properties of materials are dependent on several factors, including molecu-

lar composition and geometry. The major contributors to a cells measured elastic modulus, accordingly, are the cytoskeletal and nuclear architectures [265] and the relevant cellular geometries [168, 266]. Thus, altering either the amount of cellular cytoskeletal/nuclear material, the chemical composition or state of said material, or shape of a cell would alter the elastic modulus the latter of which should be corrected for to elucidate contributions from the former. In the context of aging, the nuclear [254], cytoskeletal [267, 268], and geometrical [269, 270] properties of cells are altered, suggesting that some level of mechanical dysregulation is innate to the aging process. Indeed, the alterations of the structural components in senescence paired with the dramatic increase in cell size [269, 271] necessitates a more sophisticated approach.

One commonly applied technology to study the mechanical properties of cells is atomic force microscopy (AFM) [168, 266, 272–275]. Incidentally however, these AFM measurements are strongly influenced by the location of the measurement and the system parameters, and often require mathematical correction or modeling to improve [114,275]. To address this issue, we devised a protocol to collect AFM measurements and then computationally extract the mechanical properties from the force-displacement curves using the finite element method [276]. This required establishment of a pipeline to measure live-cell mechanical properties and correlate these properties to high resolution geometric information, the latter of which we selected super-resolution microscopy to attain. The combination of AFM and super-resolution imaging is a recent approach in mechanobiology to correlate mechanical measurements with cellular structures and processes. Current research in the field has demonstrated the development of such super-resolution correlative techniques to study cellular and molecular dynamics [277–279]. Here, we present for the first time use of correlative AFM and super-resolution structured illumination microscopy (SIM) to provide all the necessary information (respectively, force-displacement and (sub)cellular geometry) for complete biomechanical modeling to study single-cell mechanics in the context of aging.

4.2 Pipeline Design and Rationale

4.2.1 Dataset Acquisition

In order to obtain the mechanical properties of a material, both a material measurement and the geometry are required. The former may be obtained as a force displacement curve via AFM. In order to facilitate computational modeling as well as use a conventional approach, we used a spherical AFM bead (radius = 1.25 ţm), commonly described using a Hertzian model corrected by Chadwicks formula [266]. Each measurement taken using AFM is raw data consisting of a calibrated force via deflection and the raw displacement. However, this data is often fit using a software program imposing a specific model (for example, Hertz) yielding what is an effective stiffness that is agnostic of the specific material composition and geometry. Thus, each AFM measurement must be carefully taken and corrected using several other pieces of information [280]. In this work, the aim was to quantify two continuum properties of a cell: the nuclear and cytoplasmic elastic moduli, using cellular measurements to augment the information attained using AFM.

When taking an AFM measurement of a cell at a specific location, it is important to recognize that each measurement is a composite measurement of several materials, then modified by the material geometry. Here, as the cytoplasm and nucleus are being model as continua, we combine the cytoskeletal elements into a single value: ECyt. This measurement is collected on a cellular region at a distance from the nucleus of the cell. Conversely, the nuclear measurement is a composite measurement of contributions of the nucleus and the cytoplasm, which also is modified by the geometry. Therefore, with two unknowns for each individual cell, at least two measurements must be taken for each cell. Each of these measurement locations are included as several replicate AFM curves are obtained, see Figure 3.1.1. In practice, the cytoplasmic measurement cannot consistently be fully decoupled from the nuclear measurement as, mathematically, this would require substantial spatial delocalization that is not always present on cells, and often these measurements may have contributions from structures not incorporated into the representative measurement.

After these measurements are taken, the (intra)cell geometry now must be obtained. As AFM

is a surface imaging technique, it cannot be used to extract the cell geometric distances of any intracellular distances, and thus imaging techniques are chosen. Although, there is an immediate obstacle which must be considered when using microscopy techniques to measure intracellular geometries: resolution limits. The theoretical limit of the most sophisticated classic imaging strategies is around 200 nm in the XY plane and half a micron or more in the Z plane [281]. This is dependent on the numerical aperture of the lens and the wavelength of light being used. The theoretical limit is known as the classical or Abbe diffraction limit, which is permanently entangled with light (given that one is using only the best lens equipment) [282]. Thus, to bypass this limit, one may either not use light, as in electron microscopy, or employ super-resolution techniques. There are two general strategies commonly used for super-resolution imaging [118]. The first is any point-emitter localization method which fits a point-spread function to randomly activated point light sources [117]. The other, used here, uses patterned or structured light to bypass the theoretical limit, and is termed structured illumination microscopy (SIM) [116, 281, 283, 284]. SIM is conducive to structural imaging owing to its ease of preparation which requires modest changes to conventional fluorescent preparations and its ability to generate Z-stack images much like confocal microscopy. These high-resolution Z-stack image sequences can then be contoured into a 3D geometry for biomechanical modeling. Each image sequence here has an XY resolution of approximately 50 nm in the image plane and a Z-resolution of 100 nm, significantly better than limits used by confocal (Figure 3.1.2). However, the actual resolution limit of SIM is not theoretically bounded by any lower value when using excitation harmonics rather the limit is now a practical one based on when the fluorophore bleaches [283].

To complete the dataset collection, the last step was to correlate the AFM measurements with the imaging techniques. To locate each individual cell, a fiduciary marker was used to ensure that AFM and image acquisition would occur in the same small region. Each cell was then imaged under brightfield so that it could be localized on the SIM microscope and its Z-stack obtained. To locate where each AFM measurement was performed on the cell itself, the brightfield images were scaled up to the same size as the super-resolution images and overlayed onto a max Z-projection

image for each cell. As both imaging setups (AFM brightfield and SIM) were conducted in a bottom-mounted fashion, the two images differed only by a rotation vector in each dataset. Thus, using any visual marker to determine the rotation, each overlay image was constructed to the resolution and pixel dimensions of the super-resolution images and the bead location extracted for each individual cell.

4.2.2 Geometric Reconstruction

Each image stack is exported as an OME file so each detector signal is stored discretely. These image stacks are first exploded to check for quality, and then imported into CellProfiler [285] to determine bounds for the objects of interest. Once this is complete, these new stacks are processed using LabelMe [286], which converts the image sequences into sets of discrete contours that determine the boundaries of the cytoplasm and nucleus. Now that a stack of contours for each cells nucleus and cytoplasm are ready, these sequences are then passed into a Python 3.7 script to convert the contours into coordinates interpretable by ANSYS. The script, conceptually speaking, first finds a center of mass using the top slice of nucleus and sets this point as the new origin. From here, the points from contouring are then converted into polar coordinates (r,θ) rotating about this new origin. Each slice of the stack is processed this way, such that the new object is a sequence of centered, polar coordinate graphs for the nucleus and cytoplasm.

In order to maintain physicality and avoid computational singularities, a few additional rules are imposed during 3D reconstruction. First, should the nucleus extend above the cytoplasm, a cytoplasmic height equal to the Z-slice increment for a given cell is added on top until the cytoplasm is above the nucleus. Second, a padding layer is incorporated to increase the distance between the nuclear contour and the cytoplasmic contour in the XY plane. The rationale for this processing choice is to avoid computational errors if the two are too close, and to correct any non-physical nucleus/cytoplasmic overlaps. Each contour is limited to 20 points to ease processing expense, and the Z-plane is sample 10 times for each cell.

The last image processing requirement is to localize the AFM probe to the newly contoured objects and export coordinates corresponding to the AFM indentation sites. Each overlay image

from the previous step is analyzed using a Canny edge detection algorithm [287] used to find the tip of the angular AFM probe. Once the tip has been detected, the pixel coordinates are extracted from the overlay image and then ported into the newly-processed contours a 1:1 translation as the overlay images and OME files are the same pixel dimensions and have the same unit/pixel physical dimensions. Once the contours and AFM probe locations have been made, these files are exported to ANSYS for biomechanical modeling.

A full pipeline schematic (including future biomechanical modeling not presented in this dissertation) is shown in **Figure 4.1**.

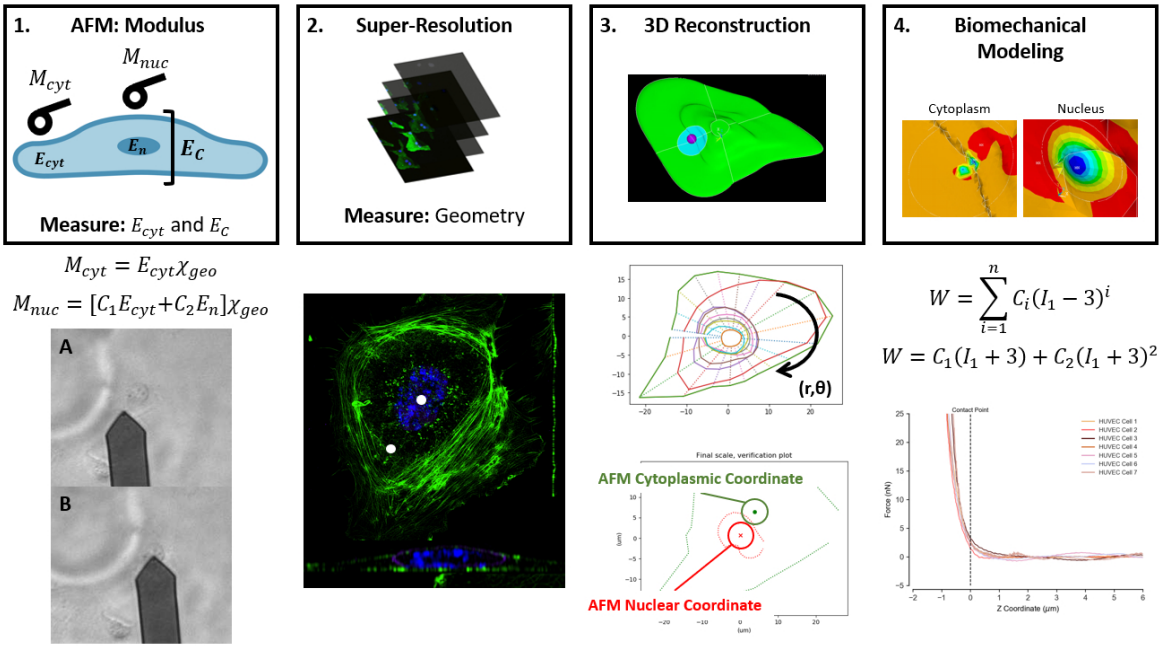

Figure 4.1: A schematic of the full pipeline for extracting the mechanical properties of cells. Two AFM measurements are taken, one at a nuclear location and one at a cytoplasmic location (**1**). These locations are saved as brightfield images and used to localize the cell on super-resolution imaging via a fiduciary marker (**2**). The Z-stack information is contoured and reconstructed using a Python 3.7 script (**3**). Overlay images of a max projection image from SIM and the AFM brightfield images yield the coordinates of the measurement. Future work includes computational biomechanics using a Yeoh hyperelastic model (**4**).

4.3 Results and Discussion

AFM Measurements of Endothelial Cells: For each cell, 2 measurements were taken, one near the top of the nucleus, termed the nuclear measurement or just nucleus, and one far from the nucleus, referred to as the cytoplasmic measurement. The most common way to extract a physical measurement from the force displacement curves is to fit the data to a Hertzian model using a software package. The Hertzian model for a spherical probe indenting a material is given by:

$$F = \frac{4}{3} E R^{\frac{1}{2}} \delta^{\frac{3}{2}} \tag{4.1}$$

Where F is the force, R is the radius of the probe, δ is the displacement in the Z-plane, and E is the elastic modulus. In reality, E is an effective elastic modulus that is a composite of the bead and material stiffness, although often a rigid bead is used such that its contribution is minimal. There is a key fundamental assumption in this equation that is implied each time AFM data is fit to it (as commonly done using software): the observed E is assumed to be of a bulk material. That is, geometric considerations are not included. Additionally, only a single, composite value comprised of all components of the material is obtained using this model. There are thin material corrections in the form of Chadwicks formula [168, 266], or a short-hand (and coarse) solution is to only fit the initial values of the indentation and ignore any values within high strain regimes. For the purposes of selecting a median, representative curve, the latter is done. Thus, when discussing the raw datasets here, it is important to acknowledge that this data is just that: raw values obtained from AFM.

Four sets of AFM curves were obtained for each cell: extension and retraction curves located at the nuclear and cytoplasmic locations. A few points are worth making about this data. The first point is that in nearly all cases, the cytoplasmic measurement is significantly higher than the nuclear measurement. This does not suggest that the cytoplasm is stiffer than the nucleus per se, but rather this highlights the very thin nature of the cytoplasmic regime (on the order of 200 nm), which would heavily influence the observed force for any given indentation, even when very

small. Also of note, all senescent cells had lower effective moduli than the control counterparts. This is a particularly interesting observation as, based on literature, it is somewhat counterintuitive. Nonetheless, there are conflicting reports as to whether these effective measurements of aged cells should be higher or lower [155]. Here, the raw data can be rationalized in a simple way: geometric changes in senescence dominate the observed elastic moduli and convolute the raw data. Senescent cells get excessively large [269], and these large volume expansions can alter the structural properties without affecting the intrinsic mechanical properties. This observation is a large motivator for the complete biomechanical treatment.

Another first order observation would be the dependence of the nuclear measurement on the cytoplasmic elastic modulus. As the measurement on top of a cell is a composite measurement of a cytoplasmic contribution and a nuclear contribution, one would expect that a higher effective cytoplasmic modulus would result in a higher nuclear modulus as the latter is a linear combination of the two. Geometric contributions notwithstanding, this relationship holds generally true globally through the dataset. This serves more as a sanity check than an observation which contains fine grain information, although intuitively the conclusion appears straightforward. Lastly, it is important to note that several of these measurements are entangled with each other to some degree. This means that the nuclear measurement is influenced by the cytoplasmic contribution (as stated previously), but also that the cytoplasmic measurement may by spatially localized close enough to the nucleus that it itself also sees contributions from it. Physically, this is a common scenario on small cells.

To address these considerations, we performed computational biomechanics using a Yeoh hyperelastic model which can incorporate parallel calculation of the cytoplasmic and nuclear moduli. There are several benefits to this model. First, all assumptions made by Hertzian contact mechanics are no longer a limitation to the work. Any geometric contributions either due to close spatial localization of the two measurements, or the influence of the substrate due to the thin-film nature of cells, are corrected to yield a final, intrinsic elastic modulus.

Adhesive Forces from Endothelial Cells: We also collected AFM retraction curves from

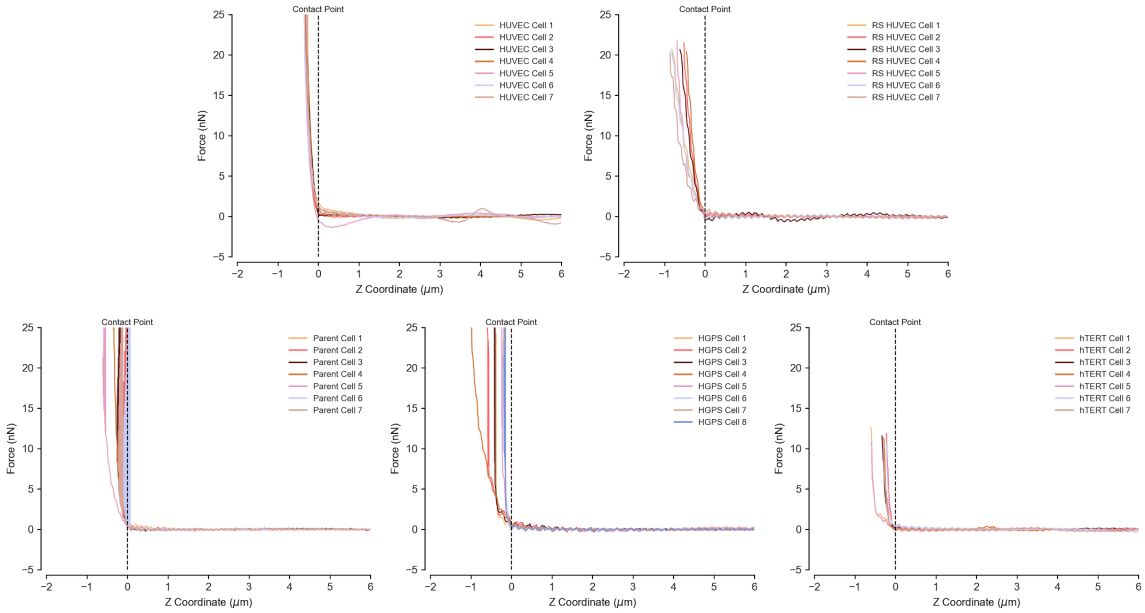

Figure 4.2: Cytoplasmic force-indentation curves for each cell from the 5 groups.

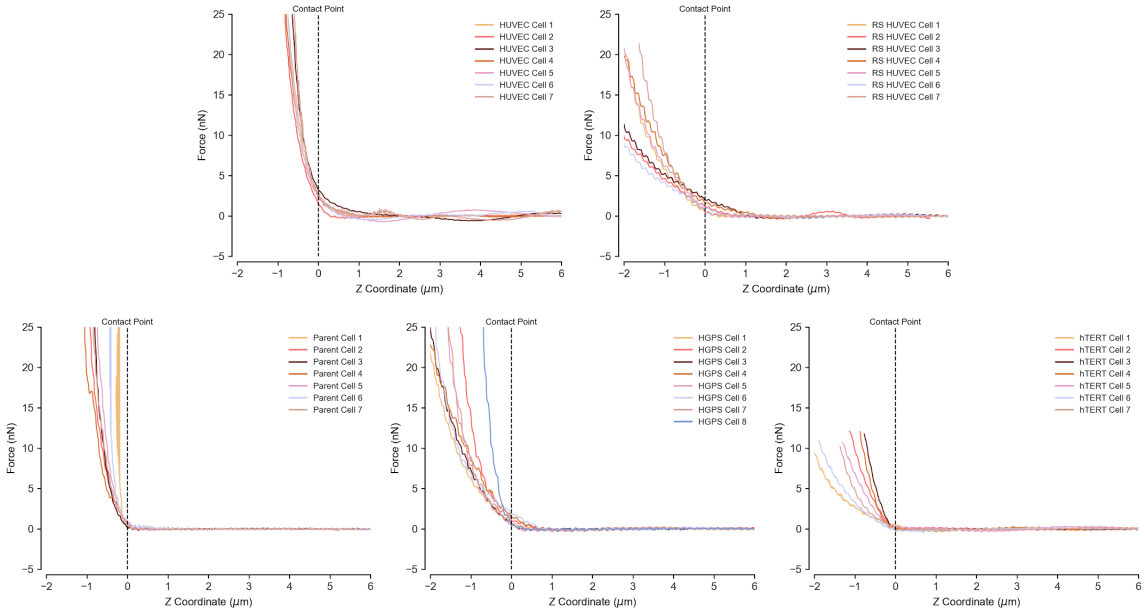

Figure 4.3: Nuclear force-indentation curves for each cell from the 5 groups.

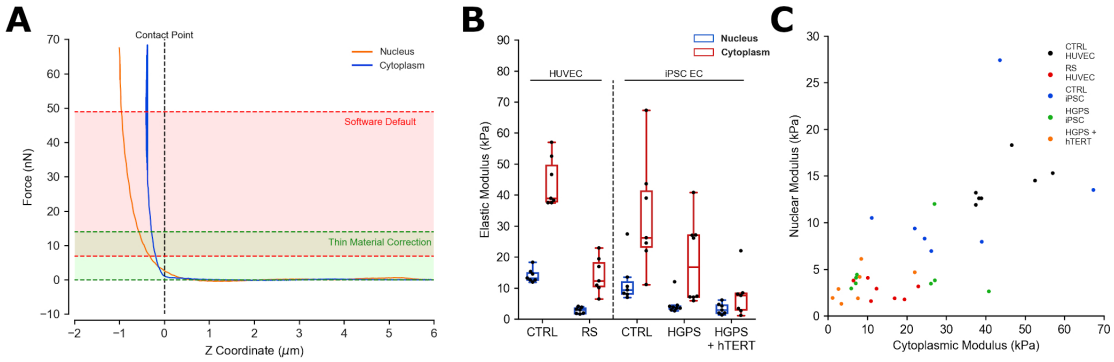

Figure 4.4: The software default for a Hertzian model fit and the thin film correction are shown in **A**. Each curve was fit from 0%-20% of the total force indentation curve to yield a preliminary, pre-processed curve. The median curve was selected for computational biomechanics. The pre-processed values are shown in **B**, while the correlation between a pair of cytoplasmic/nuclear measurements across all groups is shown in **C**.

each cell, however these curves were not used in computational modeling for several reasons. The first is that adhesive forces between the cell surface and the AFM are not indicative of the mechanical properties of a cell but the combined surface chemistries. Thus, adhesion forces have to be deconvoluted from the mechanical properties. We found that there was considerable single-cell heterogeneity presence in the retraction curves. Nuclear retraction curves displayed larger adhesive forces and a wider variance than the cytoplasmic curves on average, most likely due to the larger bead contact surface area afforded by the taller Z-plane geometries. Due to this overserved variance and its multifactorial origins, these curves are included for completeness but are not used for further computational modeling.

Cellular Cytoskeletal Components and Modifications in Aging: To explore how these measured mechanical changes may be induced by cellular structural changes, we investigated cytoskeletal components and specific post-translational modifications which (de)-stabilize the filaments. The cytoskeleton and nuclear lamina are respectively the major determinants of cytoplasmic and nuclear elastic moduli [154, 265]. To begin, we examined how much of each filament was present in each cell using confocal microscopy. Consistent with previous results, replicative senescent cells showed a dramatic increase in vimentin, while microtubules and actin filament amounts

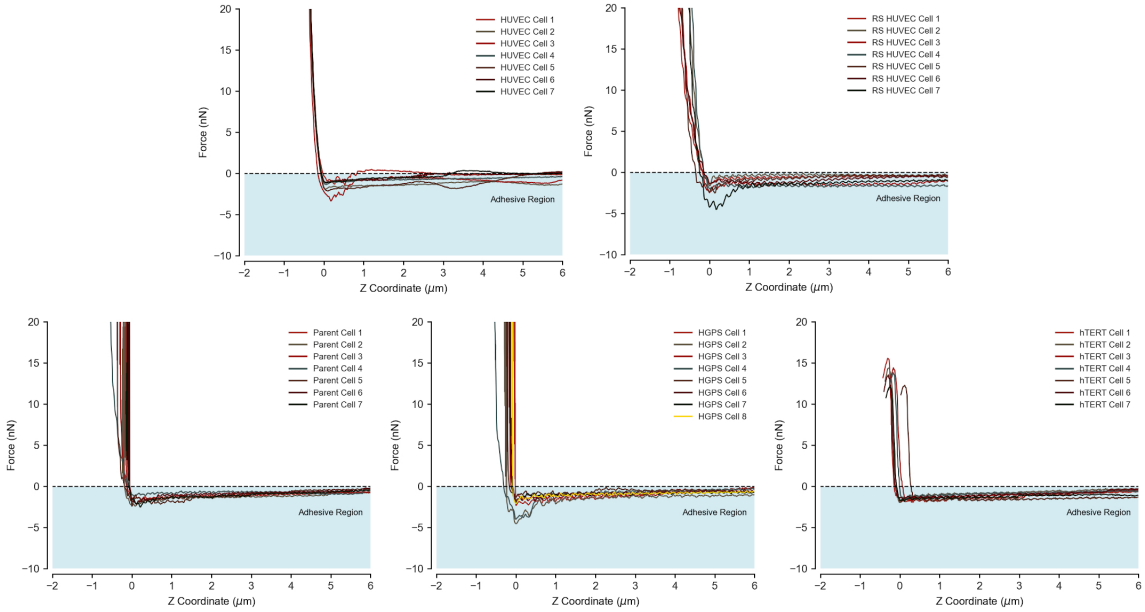

Figure 4.5: Cytoplasmic retraction curves for each cell from the 5 groups.

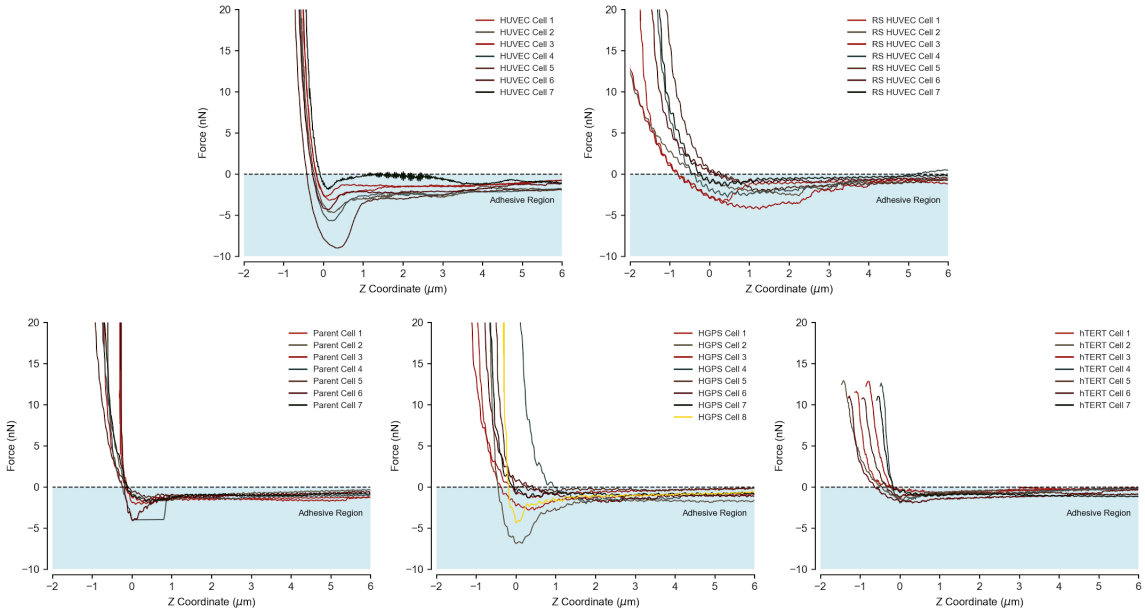

Figure 4.6: Nuclear retraction curves for each cell from the 5 groups.

were unchanged [270, 288]. However, in the HGPS model of accelerated aging, all cytoskeletal elements were dysregulated. Both vimentin and microtubules showed a large increase in their presence, while actin was less abundant compared to parent iPSC-control cells. This is a deviation from replicative aging, and differentiates between chronological changes to cytoskeletal architecture and those induced by progerin expression in HGPS. Indeed, progerin-induced laminopathy has been reported to cause severe cytoskeletal defects [260]. One of the primary determinants of cellular stiffness is the integrity of the actin cytoskeleton while the microtubule and vimentin architecture contribute significantly less [289]. Thus, changes to the observed elastic moduli, should they be based entirely on the abundance of actin filaments, would suggest that HGPS cells have lower cytoplasmic moduli compared to the parent controls, while minimal changes to the replicative senescent cells would be observed. Incidentally, this conclusion assumes that any changes to the cell geometry does not impact the finding. Intriguingly, treatment with hTERT rescued the cytoskeletal dosing problems and normalized the relative fiber abundance across the all cytoskeletal filaments, suggesting that some structural defects present in aging can be reversed by doing a first-order intervention of the senescent phenotype.

Computational Reconstruction and Correlative Microscopy: One illustrated example of reconstruction is shown in Figure 4.8, showing data for a HUVEC cell. Each cell is centered according to a new center of mass designated the new origin from the original SIM image (Figure 4.8 A). Localization of the AFM probe is done via image overlaying with precise upscaling based on the distances each pixel represents (shown in Figure 4.8 B). For each AFM measurement on a specific cell, a bright field image is taken (Figure 4.8 Bi and ii); this image is then upscaled based on the distance in ţm each pixel represents based on the scale bar to match the images from SIM. These two images (brightfield AFM and SIM) differ only by a rotation vector from mounting during the image process both the AFM brightfield and SIM fluorescent imaging are done via a bottom-mounted objective without any change to the imaging configuration (glass-coverslip facedown). Thus, all overlay images can be internally checked between each other as the image rotation is ideally identical through a dataset (Figure 4.8 Biii and iv). The AFM bead location

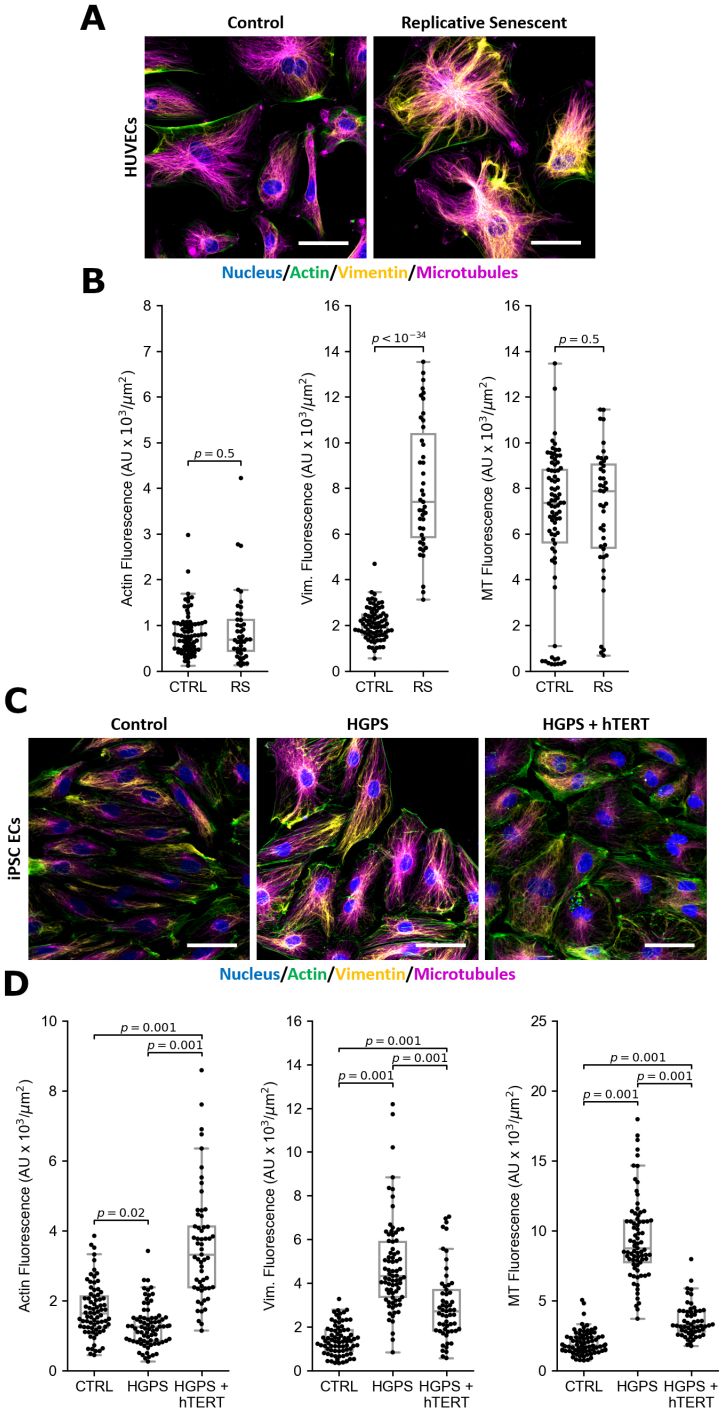

Figure 4.7: Confocal microscopy analysis of cytoskeletal elements in aging. In replicative senescence, only the amounts of vimentin are increased, while actin and microtubule amounts remain unchanged (**A-B**. In progeria, all three cytoskeletal elements are dysregulated. Microtubule and vimentin amounts are increased, while actin filament amounts are decreased **C-D**. All cytoskeletal dysregulations are partially or fully rescued by hTERT treatment, suggesting that reversing the senescent process has potential to correct structural defects in accelerated aging in progeria.

is located precisely via the Canny edge finding algorithm [287]. The bead location is manually optimized by running the algorithm iteratively and adjusting the point in the XY plane until minimal adjustments are required. Figure 4.8C illustrates the padding algorithm and subsequent bead location following padding. Here, no padding (0 pixel) and exaggerated padding (80 pixel) are shown to demonstrate how the cytoplasm is shifted away from the nucleus to obtain computational stability. The AFM bead location remains unaffected by these changes, and padding is minimized such to facilitate computation, as excessive padding unrequired for stability alters the outcome of mechanical modeling.

4.4 Future Work

This study is currently ongoing, and this thesis discussion includes the current work and demonstration of feasibility of the data acquisition protocol. Here, the remainder of this body of work will be described. The datasets, as were reported earlier, have been collected and each have been pre-processed in full. The current work to complete the pipeline is this to finish computational biomechanics, this code is still being optimized based on the parameters and complications discussed in this section. Computational stability is a primary consideration for processing this data which was the motivation for the reconstruction rules imposed. Of these rules, the padding between the cytoplasm and nucleus serves to stabilize the calculation most strongly, while the boundary condition between the nucleus and the cytoplasm (nucleus must be within the cytoplasm) is largely to maintain physicality. The mechanical properties are extracted using a Yeoh hyperelastic model.

The next step is to perform shear modeling on the reconstructed cells once the mechanical properties are obtained. To do so, a shearing force of comparable magnitude to arterial physiologic levels will be applied to 3 cells from each group to explore how these forces are transmitted to the nucleus. We hypothesize that in senescent cells, via a damping mechanism induced by the altered cytoskeletal structures and decreased mechanical properties, force transmission to the nucleus is decreased, explaining in part the poor response to shear stress observed in senescent endothelial cells. Notably, the opposite case may be true, such that the altered mechanical properties increase

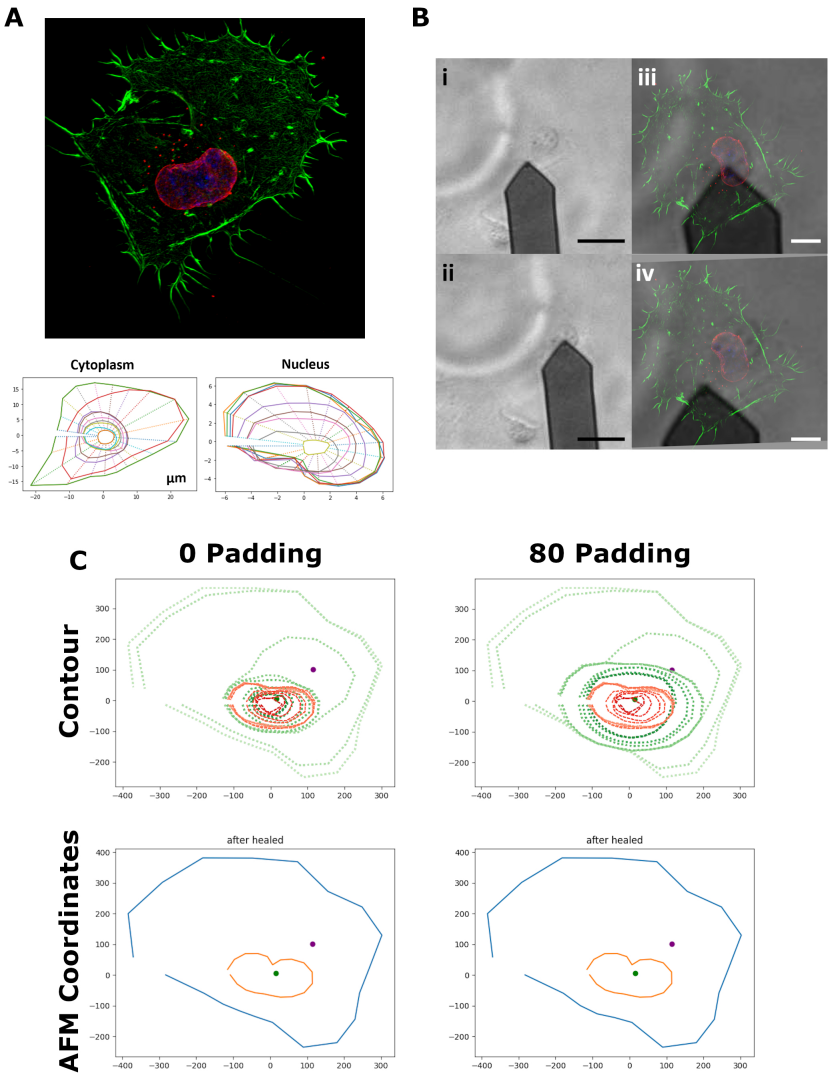

Figure 4.8: An example of a contoured cell is shown in **A**, where each Z-stack contour is superimposed on the new center of mass in a polar coordinate system. Localization of the probe coordinates is done via image overlay (shown in **B**). The two locations of AFM measurement are shown in i and ii (scale bar - 30 μm); these images are upscaled based on the distance each pixel represents and overlaid onto the SIM max Z-intensity image (ii and iv, scale bar - 10 μm). Using a Canny edge-finding algorithm, the bead XY coordinates are located and passed into the contour files. In order to facilitate computational stability, nuclear/cytoplasmic padding must be added (shown in **C**). The padding distances are denoted by pixel and are increased until no issues arise in the biomechanics portion. Padding changes the geometry of the cell and distances between the cytoplasm and the nucleus, however the XY location of the AFM probe remains unchanged.

the forces applied to the nucleus, or they may remain unchanged. In this case, the data would then suggest that the primary transduction deficit is primarily biological, rather than physical. Regardless of the outcome of this study, elucidating the cross-talk between physical and biological signal transduction in aging and the degree to which each induces dysfunction would be impactful.

There are also some confirmatory studies which would support the data presented here underway. Geometry studies on live cells from each population using AFM imaging can confirm the volume expansion seen in senescence as well as describe the heterogeneity present in these cells. The importance of these studies is two-fold. First, it confirms the datasets used here for biomechanical modeling and contextualizes their meaning holistically in aging. Second, it provides a simple way to harmonize the different observations reported in literature on the stiffnesses of senescent cells by underscoring the importance of geometry. Other imaging studies which describe the cytoskeletal state also may provide a biological snapshot of the chemical changes in senescence. Post-translational modifications of microtubules and expression of actin (de)-stabilizing proteins would provide additional evidence for the altered mechanical changes observed in aging while juxtaposing how much each influences the effective mechanical properties provided by uncorrected AFM with the contributions from cell geometry.

4.5 Conclusions

Here, we discuss the feasibility and results of a correlative microscopy approach to study cellular biomechanics in aging. Aging cells display several structural and geometric changes which alters their mechanical properties. To study these changes, we combined AFM with SIM imaging to generate several datasets comprised of individual force-indentation curves for a nuclear location and a cytoplasmic location paired with the relevant geometry for each cell. This allows for a full biomechanical treatment using a computational approach by providing the minimum information required to extract the real hyperelastic moduli of endothelial cells.

Several key observations were made during the data collection process. First, it appears that geometry and probe location strongly influence the observed modulus of live cells [168]. There is a wide variation in the raw cytoplasmic region stiffness measurements, which are a combination

of several factors. One such determinant is the actual geometry of the cell at the specified location measurements taken farther away from the nucleus are influenced less by any cellular curvatures present, however on average are also thinner in total height. Another factor which is not visualized until imaging is performed is the underlying cytoskeletal structure, which varies spatially and will alter the observed mechanical properties for a given spot. The nuclear measurements, due to a combination of being taller in height as well as a (relatively) more uniform material due to the nuclear lamina comprising a large mechanical component of the nuclear location measurement. Cytoplasmic changes in replicative senescence and progeria are different as well a key distinction to make. In replicative senescence, it appears that geometry is an important determinant of the observed measurements, as the only altered cytoskeletal component is the intermediate filament vimentin. However, in progeria, actin is decreased while microtubule and vimentin amounts are increased. With actin being a primary determinant of cellular stiffness [289], this would suggest that the cytoskeletal (and all AFM measurements) would be decreased. Several studies have demonstrated that the nucleus itself in HGPS is stiffer [261, 290], while whole cell AFM nuclear measurements on progeria cells may not necessarily reflect this until the nucleus is isolated [264]. Altogether, the data here serves to underscore the importance of various cellular structural and geometric changes influencing AFM measurements in senescence, suggesting that extracting the true mechanical properties of cells is nontrivial.

There are several study limitations and qualifying remarks to make about this work. First, AFM intervention itself can induce cytoskeletal/mechanical changes in cells [291], which requires intervention time to be kept to a minimum. Second, the correlative method itself results in information loss between AFM and SIM imaging. Brightfield imaging for AFM must be located using fiduciary markers and then overlayed onto the SIM image, requiring some form of manual alignment and determination of the relevant coordinates of measurement. Furthermore, preparation for imaging may introduce further changes to the cellular geometry that would alter the results. Nonetheless, this type of correlative approach requires tradeoffs. One such way to address the information loss between correlative microscopy is to perform simultaneous live-cell AFM/SIM

imaging, as reported elegantly by Gómez-Vrela et al. [277], although this presents a technical problem for obtaining live-cell mechanical measurements paired with high resolution Z-stack images. To get the required Z-plane resolution for a given cell (100 nm), image acquisition for a single cell is 1-2 hours, significantly longer than the time scale at which a cell may move or change its orientation. Thus, ideally cells are fixed for imaging to retain any confirmational information contained close to the AFM intervention timepoint. However, fixation before the mechanical measurements greatly alters the intrinsic elastic moduli of biological samples [292]. This presents a trade-off as live measurement is required for mechanical measurements, but the timescale for 3D imaging precludes a purely live-cell approach (until imaging modalities reach compatible acquisition times). In this work, we elect to maximize the geometric resolution by doing a complete imaging preparation protocol for 3D SIM, although this serves to highlight that other approaches with their own pros and cons are viable alternatives. Additionally, there are some variables we did not directly integrate into this work. The effects of substrate matrix and cellular attachment sites are integral to biomechanics [89, 90], whereas in this work we assumed that cells were entirely fixed entities. Furthermore, out continuum model approach, while appropriate for a global picture of a cells mechanical state, does not account for nanoscale variations in cell mechanical properties [115] all nuclear/cytoskeletal spatial information is blended into the hyperelastic properties. And, lastly, biological tissue is appropriately modeled as a viscoelastic materia [273]l, rather than a hyperelastic material. The benefit of our approach aids in cleanly contextualizing our results with the literature at large for cell measurements in disease and aging, though a more sophisticate approach would include moving beyond the commonly employed elastic models into viscoelastic regimes. Together then, here is a work which demonstrates the feasibility of correlative AFM and SIM to extract cellular mechanical properties. The results here illustrate the important of not just the biochemical composition of cells themselves but also the geometry as well. Both of these properties are altered in aging and senescence, highlighting the importance for controlling for both before conclusions can be made about altered mechanics in aging.

5. CONCLUSIONS AND FUTURE PERSPECTIVES

5.1 Mechanobiological Crosstalk Between Matrix Stiffness and Shear Stress in Vascular Biology

Clinical cardiology has long understood the associations between vascular stiffness and dysfunction [149, 293]. However, the connections between the two from a mechanistic perspective remain less characterized compared to the epidemiological understanding at hand [294]. From the physicians perspective, it is a strong indicator of eventual cardiovascular disease and organ damage [295], which suggests that there is some deep connection between this change in a physical parameter of the blood vessel and the pathophysiology it consistently induces. The changes in vascular stiffness are multifactorial, and are tied to matrix deposition and compositional changes as well as vascular smooth muscle cell mechanics (among others) [296]. However, an outstanding question is precisely how much do these two paradigms induce one another (vascular stiffness and atherosclerosis) or, does disease progression simply bring a mechanical stiffening along for the ride?

There are several observations, past the epidemiological data displaying a significant correlation, which indicate that stiffness appears to compound the issue and progress vascular disease. The first of which to be mentioned are several computational studies performed on cardiac mechanics demonstrating that sites of atherosclerosis in the coronary arteries are highly associated with sites of both abnormal shear stress and excessive matrix stiffening [142–145]. An elegant and pivotal study was published in 2015 demonstrating isolation of the biophysical parameters shear stress and stiffness, showing that increasing stiffness decreased the endothelial eNOS production in response to shear, as well as RhoA activation [150], suggesting that connections between matrix stiffness and some form of endothelial dysfunction inducing cardiovascular disease are not strictly correlative.

Reframing this question in terms of YAP mechanobiology was only recently feasible, as inci-

dentally, only in 2016 were the studies published showing that YAP mediated the protective effects of shear on endothelial cells [69, 70]. However, at first review, YAP appears to be an excellent candidate to augment the understanding of the clinical paradigm. YAP activity increases with high matrix stiffness [65], meaning vascular stiffening may affect it. High, unidirectional shear stress deactivates it, while disturbed flow activates it. Furthermore, YAP activity induces endothelial inflammation [69, 70], which in turn results in vascular dysfunction and cardiovascular disease. As far as relevant, interacting parameters go with selecting a mechanistic connection, YAP covers all bases it would not be difficult to hypothesize then that perhaps increasing vascular stiffening may activate YAP to levels higher than would be present under physiologic shear and matrix stiffness. Aberrantly activated YAP would then drive disease.

The purpose of this work was to address that question specifically here it was shown that isolating interactions between external stiffness and shear, high matrix stiffnesses impeded the endothelial shear mechanoresponse. This establishes complimentary support to the notion that vascular stiffness is, then, not just simply a byproduct of disease progression but in fact may propagate disease. We describe a feedforward model of atherosclerosis, where some inciting event may induce vascular dysfunction and matrix stiffening. This then induces further endothelial dysfunction, which then drives disease more. Notably however, is that this paradigm is not strictly limited to YAP, nor is it posited that this YAP mechanobiological pathway is the sole contributor to atherosclerosis. Indeed, other factors (such as eNOS) are implicated. Rather here the sum total of the interactions between a stiff matrix and shear stress suggests that the connections between the two are casual, rather than correlative.

Continuing the work from this point can be generally split into 2 separate endeavors that approach the question from opposite ends. The first is to gradually increase the levels of sophistication in the engineered systems such that higher levels of investigation may be performed. The second direction is to study, knowing this connection exists, what the in vivo implications are for disease progression.

5.1.1 System Sophistication

There are several approaches which would provide further insight to the connection between stiffness and endothelial dysfunction, and only some prospective studies will be proposed here. The logical next step is to introduce the other cell layer strongly implicated in vascular health and disease progression: the vascular smooth muscle cell layer [297]. Crosstalk between endothelial cells and vascular smooth muscle cells is a vital part of cardiovascular homeostasis, with vascular smooth muscle cells controlling much of the external mechanical environment endothelial cells reside in. Both extracellular matrix descriptions as well as vascular smooth muscle cell stiffening descriptions have been used to characterize vessel stiffening in disease [298, 299]. Thus, studying to what extent extracellular matrix stiffening can induce vascular dysfunction would be import to describing the course of disease progression.

Incorporating extracellular matrix interactions meaningfully into an engineered system is non-trivial, as vessel-chip systems with a smooth muscle cell layer generally exclude mechanical control over that interface. Thus, different approaches may be more optimal. One such avenue for studying this interface includes 3D printed blood vessels [300]. Cellular bioprinting facilitates incorporation of the intima layer within inks which can be designed to have varying stiffnesses after curing. With the ability to alter the mechanical environment, apply shear stress, and study the interaction between endothelial cells and vascular smooth muscle cells, a more complete picture of the pathology would be obtained. For example, varying the substrate stiffness alone would provide insight as to how much the cellular interface mitigates the detrimental effects of matrix stiffness. Additionally, each stiffness can be studied with and without vascular smooth muscle cells. Furthermore, the geometry may be match to that of the human body, allowing for complex flow patterns to be capture to study how they may compound and promote or inhibit disease progression.

Nonetheless, vessel-chip systems still are invaluable for isolating specific phenomena. One such area which may necessitate further exploration is complex flow patterns in microfluidic systems. Chamber bifurcations and obstacles are one such way to model disturbed flow in vitro that still remain relatively tractable from a computational perspective. As it is understood that sites of

low wall shear stress and high wall stiffness appear to be most strongly correlated with disease, this can be directly engineered into the chip. In the context of the work presented here, this is the most immediate next step and further work.

5.1.2 *In Vivo* Studies

The other approach to this work is exploring in vivo phenotypes now understanding the connection between matrix stiffness and shear stress. It is understood that inhibiting YAP prevents disease progession in vivo [70], although deconvoluting this process from other instances is significantly more difficult. Several pathways implicated in atherosclerotic progression, such as inflammation [235] or ROCK activation [301], appear to directly involved in mechanotransduction pathways. Furthermore, several approaches have already suggested targeting vascular stiffening as an avenue for treating vascular disease, however currently clinical realization of this endeavor remains minimal. Thus, here in vivo studies may be more appropriately designed to understand the course of disease vs. strict treatment development. And indeed, feed-forward mechanisms as suggested by the interactions between shear and matrix stiffness imply a stronger need to focus on prevention to avoid such poor outcomes.

Here, in vitro studies may guide in vivo application. As the understanding of mechanobiology increases, more pathways by which cells respond to physical cues will be uncovered. Examples exist within endothelial cells as there are 2 main shear sensing regimes CD31/CD144/VEGFR2 and Integrin/JNK/YAP/TAZ, and the interactions between such pathways (illustrative here) remains relatively poorly understood. That is to say, many other pathways by which cells respond to shear stress and extracellular stiffness may themselves provide a more complete picture and guide pharmacological development but are to be discovered.

That being said, in vivo studies can be devised to explore this mechanical interface. Correlative studies which examine tissue stiffness, modeled flow, and then investigate the relative levels of YAP/TAZ activity can be performed to explore the correlations between the 3 parameters. While extensive analysis would likely yield several useful insights, this work would ultimately be correlative in nature, and rather serve to underscore a clinical understanding already well accepted. One

approach that is relatively simple are correlations between vessel pulse-wave velocities and YAP activity, measured by either qPCR, single-cell sequencing, or histology although the preparation times for these are a consideration. Of importance here is altered pulse-wave velocities in the absence of plaque development, as geometric changes to the vessel architecture would alter flow patterns and further convolute an already entangled biology. These efforts may uncover, however, endothelial dysfunction preceding full atherosclerotic progression due to matrix stiffening.

Some more recent work has connected YAP activation in the vasculature as one such driving for disease progression in pulmonary hypertension [151, 152, 201]. Indeed, a similar type of positive feedback loop has been suggested between arterial stiffness and hypertension in a general sense [302]. They suggest that stiffness in the presence of hypertension is both a consequence of the disease and a driving force for further disease progression, a concept akin to that proposed earlier with YAP and atherosclerosis. High wall pressures increase vascular stiffness effectively, but sustained high pressures induce matrix remodeling and intrinsic stiffness increases. Stiffening of the vessel, well know to be a predictor of adverse events, then would be subject to the previous mechanisms (such as aberrantly activated YAP), further explaining in part the mechanistic connection between hypertension and atherosclerosis. Parallel to their discussion is, notably, a remark that whether stiffness is fully correlative or causal is somewhat irrelevant [302], as once the feedback loop starts, the cardiovascular dysfunction propagates itself. This serves to highlight the previous comment that prevention may be champion over intervention due to the positive feedback loops present in cardiovascular disease. Thus, the same clinical problems remain as to how best to prevent this process from starting, although further mechanistic understandings can move us ever closer to clinical therapeutics, YAP modulation being one such candidate.

5.2 Electric Field Influence on YAP Activity

The influences of exogenous electric fields on cellular behavior remains, comparatively, relatively unexplored compared to other physical stimuli. With the except, of course, of the nervous system. Physiologic voltages however, are integral to cellular health, as ion shuttling and gradients are important to membrane potential, signal transduction, and intracellular second messenger

systems [222, 303, 304]. Clinical applications of electric stimuli are focused, but common pacemakers are a mainstay in cardiology [213, 226, 227, 305]. However, beyond these paradigms, the body of knowledge becomes slimmer; this works most important conclusion is the proposal that mechanobiological pathways (shear stresses, for example) and electrical stimulation may share a convergent biology.

Electric field influence on YAP biology suggests that electromotive forces may act on upstream signal transducers to induce a biological response. On a more fundamental level, this implies electromechanical coupling some mechanism where the electric field forces can induce changes in protein conformations or drive ion gradients. Excluding a novel mechanism yet undiscovered, two likely candidates for this electromechanical coupling are ion channels responsive to shear stress and integrin-mediated signaling. Both of these are also implicated in the shear response [30, 70]. To speak to the former, electric fields exert forces on charges species via the Lorentz force, meaning that exogenous fields can change the ion gradients by altering the potential energy landscape of the system and inducing ion redistribution and potential electrophoretic movement across membrane ion channels. From that point, the signal transduction cascade may proceed as normal. The other mechanism could occur through integrin clustering in the presence of an electric field [306] forces from shear stresses and low frequency electric fields appear to apply comparable forces. Due to the charged nature of these compounds, it has been hypothesized that the mechanisms are electrophoretic or electro-osmotic, although the precise reason for surface receptor redistribution under electrical stimulation remains to be described.

5.2.1 Establishing Electromics

The clear next step for this work from a genetics perspective is to conduct a global scale omics investigation. RNASeq performed under several different electrical stimulation regimes would provide a comprehensive picture of what genes electric fields are being modulated. A specific focus on pathways associated with mechanotransduction (such as the shear response) and DNA damage, apoptosis, and inflammation would be a reasonable first set of investigations. The former is to elucidate which different pathways are being modulated (such as RhoA, integrin signaling, shear

sensing, YAP/TAZ, and more), observe the convergent biology evident, and elucidate candidates for physiochemical transduction. This would allow for the ruling in/out of different modalities by which electric fields exert their influence and would aid in the search to establish the precise type of electromechanical coupling occurring be it ion channel mediated, charged species mediated, or some other mechanism. The latter is to investigate detrimental effects of externally applied electrical fields. With the ultimate goal of clinical application, negative effects of these stimuli are important to study. Additionally, binding studies using ChIP-Seq of relevant proteins (such as YAP/TAZ) would supplement this work by further confirming the electrical influence on gene expression.

As much of the focus is on how physical stimuli influence endothelial biology, mixing electric stimuli with shear influences would also be of interest. Most vascular cells are subject to constant hemodynamic stimuli, and convoluting the two would provide insight into what stimulation regimes could be conducive to in vivo regeneration. A vessel-chip/impedance device could be envisioned for this type of work making one or two of the faces of the organ-on-a-chip model would facilitate dual stimulation. Ideally, clear electrodes (such as indium tin oxide) would be most optimal for imaging work, and real time studies could be attained using cells expressing YAP-fluorescent constructs. Together, this new system would allow an intriguing investigation into the endothelial response to combined shear and electric fields.

5.2.2 Biophysical Studies

Another main focus, although markedly divergent from the application-based studies previously mentioned, would be to investigate the biophysical mechanisms which would connect electric fields and mechanobiology. These biophysical experiments may be inspired by prior mechanotransduction studies, but rather than use mechanical force, an electric field may be applied. A few such studies will be described here. Borrowing from the study demonstrating that forces induces talin stretching [15], we can devise a similar experiment employing the photobleaching schematic using bound protein. In the absence of an external force, photobleaching events are at a minimum due to minimal talin/vinculin binding. Thus, applying an electric field and then using the

same photobleaching protocol, it can be deduced whether the electric field induced a confirmational change on the protein. There are several considerations for this general approach. The first is that this experimental schematic does not have to focus specifically on talin/vinculin binding, rather the approach itself may be applied to any force-induced binding pairs. The second consideration is that the system must be engineered to accommodate imaging in parallel with electric field application. While non-trivial, this is attainable using indium tin oxide electrodes, or even more exotic materials such as graphene [307]. Lastly, it must be accounted for that electrophoretic movement of proteins is not itself inducing a higher binding probability. This can be controlled for by performing a parallel experiment where the stretch domain is flanked by two fluorescent molecules to form a FRET pairing. In this approach, electromotive stretching of the protein would break the FRET pairing, serving as a readout for the study. This experiment must also be carefully designed as well, since new functional domains on the protein themselves are charge, and thus both experiments are ideally performed together to establish the conclusion.

Another study of interest would focus on how electric fields induce integrin grouping on the cell membrane [306]. This study can be completed using conventional imaging techniques observation of integrin grouping patterns after specific electrostimulation regimes is straightforward. To augment this, sites of the integrin molecules can be mutated to remove charged moieties and explore if there are changes to integrin clustering upon electrical stimulation. This would elucidate which charged domains contribute to the observed effect, or rather if it is simply an effective charge, reducing the total charge would result in a decreased response.

5.3 Studying Subcellular Biomechanics Using Atomic Force and Super-Resolution Microscopy

In this study, current methodologies used to study cellular biomechanics were refined to account for a significant confounding variable in AFM measurements: geometry. Several studies have reported mechanical changes in aging or progeroid diseases, both at a tissue level and at a cellular level. However, the cellular studies appear to have some discordance [155], with reports showing that whole cell AFM measurements demonstrate senescent cells are softer [263], stiffer [262], or do not change [264]. These studies, however, do not specifically control for cell

geometry. One limitation of AFM studies is that specific assumptions are generally made about the object being measured. These include that the composite measurement on top of a nucleus is an accurate snapshot of any changes to the nucleus itself (other contributions are trivial), and that cellular geometry remains relatively constant [154]. However, in the context of aging, neither remains unchanged.

Cytoskeletal changes are common in senescent cells and have been reported for both replicative models [267, 270, 288] and accelerated (HGPS) models [260]. Replicative senescent cells display increases in vimentin and show alterations to the microtubule architecture. In HGPS, actin dynamics are fundamentally altered. These changes suggest, fundamentally, that the first assumption is incorrect. Furthermore, senescent cells have also been shown to have dramatic changes in their geometry. Senescent cells grow to be excessively large and have significant volume expansion [269]. Thus, the second assumption on geometry is also an incorrect assumption. To address this obstacle, we combined atomic force microscopy with super-resolution imaging to obtain each individual cells geometry to correct for these alterations. Additionally, each cell is measured twice, on top of the nucleus and far from the nucleus, in order to extract the mechanical properties of both the cytoplasm and the nucleus. Computational biomechanics using a hyperelastic model extracts the elastic modulus from the force displacement curve to arrive at the corrected material properties.

Interestingly, we observed that the raw AFM elastic moduli for all senescent cells were lower than the control counterparts. This is a counterintuitive finding which is most likely tied to the geometric observations made: all senescent cells measured were significantly larger than the isogenic control counterparts. This suggests that the large volume expansion observed in senescence may dominate the effective moduli as observed by AFM regardless of any internal cytoskeletal changes. Notably, the replicative senescent model showed no significant cytoskeletal dosing changes aside from vimentin which does not appreciably contribute to the overall stiffness. Thus, here the observed changes are largely due to structural changes. However, in HGPS, significant cytoskeletal dysregulation was observed actin was decreased, but microtubule and vimentin amounts were increased. This would suggest an overall decrease in the cytoskeletal stiffness as actin is a primary

determinant of stiffness [264, 289], and would then further be altered by any volume changes. Nuclear measurements were all lower as well, which is most likely a structural property as progeria nuclei when isolated are stiffer than control counterparts [264].

This work is ongoing currently, with biomechanical computation being optimized for each cell. Future directions will be discussed here as if this body of work was completed.

5.3.1 Elucidating Implications on Shear Sensing

The next step for this work would be to apply these newly elucidated properties to endothelial cells subject to shear stress. One such consideration is that the goal of extracting the true mechanical properties of individual cells is to study how they affect shear force transmission from the cell membrane to the nucleus importantly, the effective force measured via AFM (which would be akin to that which the environment sees so to speak) does not necessarily correlate to nuclear stiffness itself, as established by Apte et al. [264] To explore then precisely the implications of this would require new approaches tailored for studying how specific biological signaling mechanism are affected by alterations to the cellular mechanical properties. One such approach would be to use light-sheet microscopy [113] for Z-plane information on cells in a microfluidic chamber and trace a mechanosensitive, fluorescently labeled protein (in this case, YAP is a strong candidate). It is established that cytoskeletal integrity is required for appropriate YAP function [73] here the mechanical properties may provide a correlative understanding. Senescent cells do not appear to appreciably response to shear stress appropriately [258] but these mechanisms remain to be fully elucidated. It could be that the lack of response is tied uniquely to cytoskeletal structure and the altered mechanical properties are correlative to such dysfunctions, or rather there may be a synergistic effect present where excessive force transduction to the nucleus induces YAP nuclear translocation [72] to work against the normally protective effects of shear stress. The results of the computational approach would guide the conclusions made on this front: decreased nuclear force would support the former, while increased force would support the latter.

5.3.2 Addressing Approach Limitations

There are other refinements to be made to this approach as well based on the assumptions made for this work. One such avenue for improvement is modeling each individual cell as a viscoelastic material [273, 308, 309] rather than a hyperelastic one. Biological materials generally possess viscous properties in addition to their elastic properties, and adapting the protocol to account for these properties requires altering the measurement process on AFM to dynamic acquisition. This may provide additional resolution to understanding subcellular damping forces for explaining, for example, how shear stress affects intracellular structures (the nucleus). Our protocol in this work is quickly adapted from a technical perspective to this endeavor the changes required are on AFM measurement and the selected computational model. Another key assumption made in this approach lies within the continuum mechanics approach: each cellular compartment is treated as a homogenous medium. From a cell biology perspective, this is understood to be a simplification as cytoskeletal fiber distribution and connectivity vary throughout a cell, and at the nanoscale stiffness (or more accurately, bond energy) varies strongly as a function of spatial localization [115]. The information for a different treatment of the cellular continua is captured using super-resolution microscopy; actin fibers (or any other cytoskeletal filament/nuclear laminar structure) are easily visualized at high resolution, allowing for fiber-based approach using, for example, the tensegrity model [310, 311]. Nonetheless, the continuum approach has several attractive features largely tied to computational stability [114]. Other modeling approaches which forgo the assumptions of classical mechanics exist, such semi-classical or quantum mechanical molecule dynamics, which are not subject to the assumption limitations of the continuum approaches [312]. Unfortunately, these approaches are computationally expensive and require enormous processing power (and time) before any meaningful result translatable to physiology can be obtained.

5.4 Final Remarks

Here, several approaches for studying vascular mechanobiology were discussed. There are several key takeaways from this body of work. The first is that mechanobiology is a highly mul-

tidisciplinary field, highlighted by the fact that each of these studies was entirely reliant on an engineered system or pipeline to test the hypothesis in question. Second there appear to be similar paradigms for the observed patterns in literature as increased understanding of the mechanisms of biological force transduction is obtained. Illustratively, shear stress and exogenous electric fields both influence YAP behavior in endothelial cells. There is a key potential implication of this finding: convergent biology. Electric fields affecting, for example, integrin clustering itself may provide understanding for how forces influence integrin signaling to form a more complete model for biophysical signaling. Another analogous example would be ion channel signaling under shear and electrophoretic migration of ions across a membrane using an electric field ideally both would result in a similar response due to the end result (ion movement) being identical. And lastly, there is a lot of room at the bottom. Current understanding of biophysical mechanisms has a lot of room for improvement as the data guides appropriate model development. Continuum models, as an example that was used here, themselves are only one such way to describe the data and make several fundamental assumptions about the cell itself. In spite of this, these approaches as a whole have led to several important discoveries relevant to the clinic, such as interactions between fluid shear stress and matrix stiffness. Altogether, this body of work applies several approaches to study how endothelial cells respond to external forces, and how their properties and capacity to response change in disease states.

REFERENCES

[1] J. Wolff, "Das gesetz der transformation der knochen," *A Hirshwald*, vol. 1, pp. 1–152, 1892.

[2] P. F. Davies, A. Remuzzi, E. J. Gordon, C. F. Dewey, and M. A. Gimbrone, "Turbulent fluid shear stress induces vascular endothelial cell turnover in vitro," *Proceedings of the National Academy of Sciences*, vol. 83, no. 7, pp. 2114–2117, 1986.

[3] R.-P. Franke, M. Gräfe, H. Schnittler, D. Seiffge, C. Mittermayer, and D. Drenckhahn, "Induction of human vascular endothelial stress fibres by fluid shear stress," *Nature*, vol. 307, no. 5952, pp. 648–649, 1984.

[4] D. Ingber, "Mechanobiology and diseases of mechanotransduction," *Annals of medicine*, vol. 35, no. 8, pp. 564–577, 2003.

[5] D. E. Ingber, "From mechanobiology to developmentally inspired engineering," *Philosophical Transactions of the Royal Society B: Biological Sciences*, vol. 373, no. 1759, p. 20170323, 2018.

[6] T. Mammoto, A. Mammoto, and D. E. Ingber, "Mechanobiology and developmental control," *Annual review of cell and developmental biology*, vol. 29, pp. 27–61, 2013.

[7] J. Eyckmans, T. Boudou, X. Yu, and C. S. Chen, "A hitchhiker's guide to mechanobiology," *Developmental cell*, vol. 21, no. 1, pp. 35–47, 2011.

[8] S. Kim, M. Uroz, J. L. Bays, and C. S. Chen, "Harnessing mechanobiology for tissue engineering," *Developmental Cell*, 2021.

[9] B. Özkale, M. S. Sakar, and D. J. Mooney, "Active biomaterials for mechanobiology," *Biomaterials*, p. 120497, 2020.

[10] E. L. Baker and M. H. Zaman, "The biomechanical integrin," *Journal of biomechanics*, vol. 43, no. 1, pp. 38–44, 2010.

[11] E. F. Plow, T. A. Haas, L. Zhang, J. Loftus, and J. W. Smith, "Ligand binding to integrins," *Journal of Biological Chemistry*, vol. 275, no. 29, pp. 21785–21788, 2000.

[12] N. Q. Balaban, U. S. Schwarz, D. Riveline, P. Goichberg, G. Tzur, I. Sabanay, D. Mahalu, S. Safran, A. Bershadsky, and L. Addadi, "Force and focal adhesion assembly: a close relationship studied using elastic micropatterned substrates," *Nature cell biology*, vol. 3, no. 5, pp. 466–472, 2001.

[13] M. Morimatsu, A. H. Mekhdjian, A. S. Adhikari, and A. R. Dunn, "Molecular tension sensors report forces generated by single integrin molecules in living cells," *Nano letters*, vol. 13, no. 9, pp. 3985–3989, 2013.

[14] J. Cooper and F. G. Giancotti, "Integrin signaling in cancer: mechanotransduction, stemness, epithelial plasticity, and therapeutic resistance," *Cancer cell*, vol. 35, no. 3, pp. 347–367, 2019.

[15] A. Del Rio, R. Perez-Jimenez, R. Liu, P. Roca-Cusachs, J. M. Fernandez, and M. P. Sheetz, "Stretching single talin rod molecules activates vinculin binding," *Science*, vol. 323, no. 5914, pp. 638–641, 2009.

[16] C. Grashoff, B. D. Hoffman, M. D. Brenner, R. Zhou, M. Parsons, M. T. Yang, M. A. McLean, S. G. Sligar, C. S. Chen, and T. Ha, "Measuring mechanical tension across vinculin reveals regulation of focal adhesion dynamics," *Nature*, vol. 466, no. 7303, pp. 263–266, 2010.

[17] M. Michael and M. Parsons, "New perspectives on integrin-dependent adhesions," *Current opinion in cell biology*, vol. 63, pp. 31–37, 2020.

[18] B. M. Gumbiner, "Regulation of cadherin-mediated adhesion in morphogenesis," *Nature reviews Molecular cell biology*, vol. 6, no. 8, pp. 622–634, 2005.

[19] F. Van Roy and G. Berx, "The cell-cell adhesion molecule e-cadherin," *Cellular and molecular life sciences*, vol. 65, no. 23, pp. 3756–3788, 2008.

[20] J. Brasch, O. J. Harrison, G. Ahlsen, S. M. Carnally, R. M. Henderson, B. Honig, and L. Shapiro, "Structure and binding mechanism of vascular endothelial cadherin: a divergent classical cadherin," *Journal of molecular biology*, vol. 408, no. 1, pp. 57–73, 2011.

[21] E. Tzima, M. Irani-Tehrani, W. B. Kiosses, E. Dejana, D. A. Schultz, B. Engelhardt, G. Cao, H. DeLisser, and M. A. Schwartz, "A mechanosensory complex that mediates the endothelial cell response to fluid shear stress," *Nature*, vol. 437, no. 7057, pp. 426–31, 2005.

[22] D. E. Leckband, Q. le Duc, N. Wang, and J. de Rooij, "Mechanotransduction at cadherin-mediated adhesions," *Current opinion in cell biology*, vol. 23, no. 5, pp. 523–530, 2011.

[23] S. Yonemura, Y. Wada, T. Watanabe, A. Nagafuchi, and M. Shibata, "α-catenin as a tension transducer that induces adherens junction development," *Nature cell biology*, vol. 12, no. 6, pp. 533–542, 2010.

[24] D. E. Conway, M. T. Breckenridge, E. Hinde, E. Gratton, C. S. Chen, and M. A. Schwartz, "Fluid shear stress on endothelial cells modulates mechanical tension across ve-cadherin and pecam-1," *Current Biology*, vol. 23, no. 11, pp. 1024–1030, 2013.

[25] R. Goel, B. R. Schrank, S. Arora, B. Boylan, B. Fleming, H. Miura, P. J. Newman, R. C. Molthen, and D. K. Newman, "Site-specific effects of pecam-1 on atherosclerosis in ldl receptordeficient mice," *Arteriosclerosis, thrombosis, and vascular biology*, vol. 28, no. 11, pp. 1996–2002, 2008.

[26] K. S. Heo, K. Fujiwara, and J. Abe, "Shear stress and atherosclerosis," *Mol Cells*, vol. 37, no. 6, pp. 435–40, 2014.

[27] J. Ando, T. Komatsuda, and A. Kamiya, "Cytoplasmic calcium response to fluid shear stress in cultured vascular endothelial cells," *In vitro cellular & developmental biology*, vol. 24, no. 9, pp. 871–877, 1988.

[28] S.-P. Olesen, D. Claphamt, and P. Davies, "Haemodynamic shear stress activates a k+ current in vascular endothelial cells," *Nature*, vol. 331, no. 6152, pp. 168–170, 1988.

[29] J. P. Cooke, E. Rossitch, N. A. Andon, J. Loscalzo, and V. J. Dzau, "Flow activates an endothelial potassium channel to release an endogenous nitrovasodilator," *The Journal of clinical investigation*, vol. 88, no. 5, pp. 1663–1671, 1991.

[30] K. A. Gerhold and M. A. Schwartz, "Ion channels in endothelial responses to fluid shear stress," *Physiology*, vol. 31, no. 5, pp. 359–369, 2016.

[31] P. Jin, L. Y. Jan, and Y.-N. Jan, "Mechanosensitive ion channels: structural features relevant to mechanotransduction mechanisms," *Annual review of neuroscience*, vol. 43, pp. 207–229, 2020.

[32] N. Li, A. Than, X. Wang, S. Xu, L. Sun, H. Duan, C. Xu, and P. Chen, "Ultrasensitive profiling of metabolites using tyramine-functionalized graphene quantum dots," *ACS Nano*, vol. 10, no. 3, pp. 3622–9, 2016.

[33] M. Ohno, J. P. Cooke, V. J. Dzau, and G. H. Gibbons, "Fluid shear stress induces endothelial transforming growth factor beta-1 transcription and production. modulation by potassium channel blockade," *The Journal of clinical investigation*, vol. 95, no. 3, pp. 1363–1369, 1995.

[34] M. Ohno, G. H. Gibbons, V. J. Dzau, and J. P. Cooke, "Shear stress elevates endothelial cgmp. role of a potassium channel and g protein coupling," *Circulation*, vol. 88, no. 1, pp. 193–197, 1993.

[35] Z. Li, R. Sun, Y. Ni, and S. Kokot, "A novel fluorescent probe involving a graphene quantum dotenzyme hybrid system for the analysis of hydroquinone in the presence of toxic resorcinol and catechol," *Analytical Methods*, vol. 6, no. 18, 2014.

[36] H. Li, X. Yan, G. Lu, and X. Su, "Carbon dot-based bioplatform for dual colorimetric and fluorometric sensing of organophosphate pesticides," *Sensors and Actuators B: Chemical*, vol. 260, pp. 563–570, 2018.

[37] S.-S. Liang, L. Qi, R.-L. Zhang, M. Jin, and Z.-Q. Zhang, "Ratiometric fluorescence biosensor based on cdte quantum and carbon dots for double strand dna detection," *Sensors and Actuators B: Chemical*, vol. 244, pp. 585–590, 2017.

[38] J. Ge, W. Li, Q. Zhao, N. Li, M. Chen, P. Zhi, R. Li, N. Gao, B. Xiao, and M. Yang, "Architecture of the mammalian mechanosensitive piezo1 channel," *Nature*, vol. 527, no. 7576, pp. 64–69, 2015.

[39] R. Syeda, J. Xu, A. E. Dubin, B. Coste, J. Mathur, T. Huynh, J. Matzen, J. Lao, D. C. Tully, and I. H. Engels, "Chemical activation of the mechanotransduction channel piezo1," *Elife*, vol. 4, p. e07369, 2015.

[40] L. Volkers, Y. Mechioukhi, and B. Coste, "Piezo channels: from structure to function," *Pflügers Archiv-European Journal of Physiology*, vol. 467, no. 1, pp. 95–99, 2015.

[41] M. Moroni, M. R. Servin-Vences, R. Fleischer, O. Sánchez-Carranza, and G. R. Lewin, "Voltage gating of mechanosensitive piezo channels," *Nature communications*, vol. 9, no. 1, pp. 1–15, 2018.

[42] B. Xiao, "Levering mechanically activated piezo channels for potential pharmacological intervention," *Annual review of pharmacology and toxicology*, vol. 60, pp. 195–218, 2020.

[43] Q. Zhao, H. Zhou, S. Chi, Y. Wang, J. Wang, J. Geng, K. Wu, W. Liu, T. Zhang, and M.-Q. Dong, "Structure and mechanogating mechanism of the piezo1 channel," *Nature*, vol. 554, no. 7693, pp. 487–492, 2018.

[44] Q. Zhao, K. Wu, J. Geng, S. Chi, Y. Wang, P. Zhi, M. Zhang, and B. Xiao, "Ion permeation and mechanotransduction mechanisms of mechanosensitive piezo channels," *Neuron*, vol. 89, no. 6, pp. 1248–1263, 2016.

[45] J. Li, B. Hou, S. Tumova, K. Muraki, A. Bruns, M. J. Ludlow, A. Sedo, A. J. Hyman, L. McKeown, and R. S. Young, "Piezo1 integration of vascular architecture with physiological force," *Nature*, vol. 515, no. 7526, pp. 279–282, 2014.

[46] S. S. Ranade, Z. Qiu, S.-H. Woo, S. S. Hur, S. E. Murthy, S. M. Cahalan, J. Xu, J. Mathur, M. Bandell, and B. Coste, "Piezo1, a mechanically activated ion channel, is required for vascular development in mice," *Proceedings of the National Academy of Sciences*, vol. 111, no. 28, pp. 10347–10352, 2014.

[47] A. G. Solis, P. Bielecki, H. R. Steach, L. Sharma, C. C. Harman, S. Yun, M. R. de Zoete, J. N. Warnock, S. F. To, and A. G. York, "Mechanosensation of cyclical force by piezo1 is essential for innate immunity," *Nature*, vol. 573, no. 7772, pp. 69–74, 2019.

[48] W. Sun, S. Chi, Y. Li, S. Ling, Y. Tan, Y. Xu, F. Jiang, J. Li, C. Liu, and G. Zhong, "The mechanosensitive piezo1 channel is required for bone formation," *Elife*, vol. 8, p. e47454, 2019.

[49] K. Nonomura, V. Lukacs, D. T. Sweet, L. M. Goddard, A. Kanie, T. Whitwam, S. S. Ranade, T. Fujimori, M. L. Kahn, and A. Patapoutian, "Mechanically activated ion channel piezo1 is required for lymphatic valve formation," *Proceedings of the National Academy of Sciences*, vol. 115, no. 50, pp. 12817–12822, 2018.

[50] S. A. Gudipaty, J. Lindblom, P. D. Loftus, M. J. Redd, K. Edes, C. Davey, V. Krishnegowda, and J. Rosenblatt, "Mechanical stretch triggers rapid epithelial cell division through piezo1," *Nature*, vol. 543, no. 7643, pp. 118–121, 2017.

[51] K. Famm, B. Litt, K. J. Tracey, E. S. Boyden, and M. Slaoui, "A jump-start for electroceuticals," *Nature*, vol. 496, no. 7444, pp. 159–161, 2013.

[52] S. Mishra, "Electroceuticals in medicinethe brave new future," *Indian Heart Journal*, vol. 69, no. 5, pp. 685–686, 2017.

[53] S. Reardon, "Electroceuticals spark interest," *Nature*, vol. 511, no. 7507, p. 18, 2014.

[54] S. Abasi, J. R. Aggas, N. Venkatesh, I. G. Vallavanatt, and A. Guiseppi-Elie, "Design, fabrication and testing of an electrical cell stimulation and recording apparatus (ecsara) for cells in electroculture," *Biosensors and Bioelectronics*, vol. 147, p. 111793, 2020.

[55] Y. Long, H. Wei, J. Li, G. Yao, B. Yu, D. Ni, A. L. Gibson, X. Lan, Y. Jiang, and W. Cai, "Effective wound healing enabled by discrete alternative electric fields from wearable nanogenerators," *ACS nano*, vol. 12, no. 12, pp. 12533–12540, 2018.

[56] R. Nuccitelli, *Physiological electric fields can influence cell motility, growth, and polarity*, vol. 2, pp. 213–233. Elsevier, 1988.

[57] R. Nuccitelli, "A role for endogenous electric fields in wound healing," *Current topics in developmental biology*, vol. 58, no. 2, pp. 1–26, 2003.

[58] B. Song, M. Zhao, J. Forrester, and C. McCaig, "Nerve regeneration and wound healing are stimulated and directed by an endogenous electrical field in vivo," *Journal of cell science*, vol. 117, no. 20, pp. 4681–4690, 2004.

[59] G. Tai, B. Reid, L. Cao, and M. Zhao, *Electrotaxis and wound healing: experimental methods to study electric fields as a directional signal for cell migration*, pp. 77–97. Springer, 2009.

[60] M. Zhao, "Electrical fields in wound healingan overriding signal that directs cell migration," in *Seminars in cell & developmental biology*, vol. 20, pp. 674–682, Elsevier.

[61] S. Dupont, "Role of yap/taz in cell-matrix adhesion-mediated signalling and mechanotransduction," *Exp Cell Res*, vol. 343, no. 1, pp. 42–53, 2016.

[62] S. Dupont, *Regulation of YAP/TAZ Activity by Mechanical Cues: An Experimental Overview*, pp. 183–202. Springer, 2019.

[63] S. Piccolo, S. Dupont, and M. Cordenonsi, "The biology of yap/taz: hippo signaling and beyond," *Physiol Rev*, vol. 94, no. 4, pp. 1287–312, 2014.

[64] A. Totaro, T. Panciera, and S. Piccolo, "Yap/taz upstream signals and downstream responses," *Nat Cell Biol*, vol. 20, no. 8, pp. 888–899, 2018.

[65] M. Aragona, T. Panciera, A. Manfrin, S. Giulitti, F. Michielin, N. Elvassore, S. Dupont, and S. Piccolo, "A mechanical checkpoint controls multicellular growth through yap/taz regulation by actin-processing factors," *Cell*, vol. 154, no. 5, pp. 1047–1059, 2013.

[66] B. Zhao, X. Wei, W. Li, R. S. Udan, Q. Yang, J. Kim, J. Xie, T. Ikenoue, J. Yu, and L. Li, "Inactivation of yap oncoprotein by the hippo pathway is involved in cell contact inhibition and tissue growth control," *Genes & development*, vol. 21, no. 21, pp. 2747–2761, 2007.

[67] V. A. Codelia, G. Sun, and K. D. Irvine, "Regulation of yap by mechanical strain through jnk and hippo signaling," *Current biology*, vol. 24, no. 17, pp. 2012–2017, 2014.

[68] S. Dupont, L. Morsut, M. Aragona, E. Enzo, S. Giulitti, M. Cordenonsi, F. Zanconato, J. Le Digabel, M. Forcato, S. Bicciato, N. Elvassore, and S. Piccolo, "Role of yap/taz in mechanotransduction," *Nature*, vol. 474, no. 7350, pp. 179–83, 2011.

[69] K. C. Wang, Y. T. Yeh, P. Nguyen, E. Limqueco, J. Lopez, S. Thorossian, K. L. Guan, Y. J. Li, and S. Chien, "Flow-dependent yap/taz activities regulate endothelial phenotypes and atherosclerosis," *Proc Natl Acad Sci U S A*, vol. 113, no. 41, pp. 11525–11530, 2016.

[70] L. Wang, J. Y. Luo, B. Li, X. Y. Tian, L. J. Chen, Y. Huang, J. Liu, D. Deng, C. W. Lau, S. Wan, D. Ai, K. K. Mak, K. K. Tong, K. M. Kwan, N. Wang, J. J. Chiu, Y. Zhu, and Y. Huang, "Integrin-yap/taz-jnk cascade mediates atheroprotective effect of unidirectional shear flow," *Nature*, vol. 540, no. 7634, pp. 579–582, 2016.

[71] G. Brusatin, T. Panciera, A. Gandin, A. Citron, and S. Piccolo, "Biomaterials and engineered microenvironments to control yap/taz-dependent cell behaviour," *Nat Mater*, vol. 17, no. 12, pp. 1063–1075, 2018.

[72] A. Elosegui-Artola, I. Andreu, A. E. Beedle, A. Lezamiz, M. Uroz, A. J. Kosmalska, R. Oria, J. Z. Kechagia, P. Rico-Lastres, and A.-L. Le Roux, "Force triggers yap nuclear entry by regulating transport across nuclear pores," *Cell*, vol. 171, no. 6, pp. 1397–1410. e14, 2017.

[73] T. P. Driscoll, B. D. Cosgrove, S. J. Heo, Z. E. Shurden, and R. L. Mauck, "Cytoskeletal to nuclear strain transfer regulates yap signaling in mesenchymal stem cells," *Biophys J*, vol. 108, no. 12, pp. 2783–93, 2015.

[74] G. Nardone, J. Oliver-De La Cruz, J. Vrbsky, C. Martini, J. Pribyl, P. Skládal, M. Pel, G. Caluori, S. Pagliari, and F. Martino, "Yap regulates cell mechanics by controlling focal adhesion assembly," *Nature communications*, vol. 8, no. 1, pp. 1–13, 2017.

[75] B. Zhao, L. Li, Q. Lei, and K.-L. Guan, "The hippoyap pathway in organ size control and tumorigenesis: an updated version," *Genes & development*, vol. 24, no. 9, pp. 862–874, 2010.

[76] S. W. Plouffe, K. C. Lin, J. L. Moore 3rd, F. E. Tan, S. Ma, Z. Ye, Y. Qiu, B. Ren, and K.-L. Guan, "The hippo pathway effector proteins yap and taz have both distinct and overlapping functions in the cell," *Journal of Biological Chemistry*, vol. 293, no. 28, pp. 11230–11240, 2018.

[77] D. Cai, D. Feliciano, P. Dong, E. Flores, M. Gruebele, N. Porat-Shliom, S. Sukenik, Z. Liu, and J. Lippincott-Schwartz, "Phase separation of yap reorganizes genome topology for long-term yap target gene expression," *Nature cell biology*, vol. 21, no. 12, pp. 1578–1589, 2019.

[78] J. M. Franklin and K.-L. Guan, "Yap/taz phase separation for transcription," *Nature cell biology*, vol. 22, no. 4, pp. 357–358, 2020.

[79] Y. Lu, T. Wu, O. Gutman, H. Lu, Q. Zhou, Y. I. Henis, and K. Luo, "Phase separation of taz compartmentalizes the transcription machinery to promote gene expression," *Nature cell biology*, vol. 22, no. 4, pp. 453–464, 2020.

[80] O. Chaudhuri, J. Cooper-White, P. A. Janmey, D. J. Mooney, and V. B. Shenoy, "Effects of extracellular matrix viscoelasticity on cellular behaviour," *Nature*, vol. 584, no. 7822, pp. 535–546, 2020.

[81] D. E. Discher, D. J. Mooney, and P. W. Zandstra, "Growth factors, matrices, and forces combine and control stem cells," *Science*, vol. 324, no. 5935, pp. 1673–1677, 2009.

[82] A. Engler, L. Bacakova, C. Newman, A. Hategan, M. Griffin, and D. Discher, "Substrate compliance versus ligand density in cell on gel responses," *Biophysical journal*, vol. 86, no. 1, pp. 617–628, 2004.

[83] A. J. Engler, S. Sen, H. L. Sweeney, and D. E. Discher, "Matrix elasticity directs stem cell lineage specification," *Cell*, vol. 126, no. 4, pp. 677–689, 2006.

[84] N. Huebsch, P. R. Arany, A. S. Mao, D. Shvartsman, O. A. Ali, S. A. Bencherif, J. Rivera-Feliciano, and D. J. Mooney, "Harnessing traction-mediated manipulation of the cell/matrix interface to control stem-cell fate," *Nature materials*, vol. 9, no. 6, pp. 518–526, 2010.

[85] C. P. Johnson, H.-Y. Tang, C. Carag, D. W. Speicher, and D. E. Discher, "Forced unfolding of proteins within cells," *Science*, vol. 317, no. 5838, pp. 663–666, 2007.

[86] K. Y. Lee and D. J. Mooney, "Hydrogels for tissue engineering," *Chemical reviews*, vol. 101, no. 7, pp. 1869–1880, 2001.

[87] T. Matsumoto, Y. C. Yung, C. Fischbach, H. J. Kong, R. Nakaoka, and D. J. Mooney, "Mechanical strain regulates endothelial cell patterning in vitro," *Tissue engineering*, vol. 13, no. 1, pp. 207–217, 2007.

[88] J. Swift, I. L. Ivanovska, A. Buxboim, T. Harada, P. C. Dingal, J. Pinter, J. D. Pajerowski, K. R. Spinler, J. W. Shin, M. Tewari, F. Rehfeldt, D. W. Speicher, and D. E. Discher, "Nuclear lamin-a scales with tissue stiffness and enhances matrix-directed differentiation," *Science*, vol. 341, no. 6149, p. 1240104, 2013.

[89] E. E. Charrier, K. Pogoda, R. Li, C. Y. Park, J. J. Fredberg, and P. A. Janmey, "A novel method to make viscoelastic polyacrylamide gels for cell culture and traction force microscopy," *APL bioengineering*, vol. 4, no. 3, p. 036104, 2020.

[90] S. S. Hur, J. H. Jeong, M. J. Ban, J. H. Park, J. K. Yoon, and Y. Hwang, "Traction force microscopy for understanding cellular mechanotransduction," *BMB reports*, vol. 53, no. 2, p. 74, 2020.

[91] R. W. Style, R. Boltyanskiy, G. K. German, C. Hyland, C. W. MacMinn, A. F. Mertz, L. A. Wilen, Y. Xu, and E. R. Dufresne, "Traction force microscopy in physics and biology," *Soft matter*, vol. 10, no. 23, pp. 4047–4055, 2014.

[92] A. Mata, A. J. Fleischman, and S. Roy, "Characterization of polydimethylsiloxane (pdms) properties for biomedical micro/nanosystems," *Biomedical microdevices*, vol. 7, no. 4, pp. 281–293, 2005.

[93] A. Colombo, P. Cahill, and C. Lally, "An analysis of the strain field in biaxial flexcell membranes for different waveforms and frequencies," *Proceedings of the Institution of Mechanical Engineers, Part H: Journal of Engineering in Medicine*, vol. 222, no. 8, pp. 1235–1245, 2008.

[94] L. A. Matheson, N. J. Fairbank, G. N. Maksym, J. P. Santerre, and R. S. Labow, "Characterization of the flexcell uniflex cyclic strain culture system with u937 macrophage-like cells," *Biomaterials*, vol. 27, no. 2, pp. 226–233, 2006.

[95] J. Ribas, Y. S. Zhang, P. R. Pitrez, J. Leijten, M. Miscuglio, J. Rouwkema, M. R. Dokmeci, X. Nissan, L. Ferreira, and A. Khademhosseini, "Biomechanical strain exacerbates inflammation on a progeria-on-a-chip model," *Small*, vol. 13, no. 15, 2017.

[96] B. Liu, M.-J. Qu, K.-R. Qin, H. Li, Z.-K. Li, B.-R. Shen, and Z.-L. Jiang, "Role of cyclic strain frequency in regulating the alignment of vascular smooth muscle cells in vitro," *Biophysical journal*, vol. 94, no. 4, pp. 1497–1507, 2008.

[97] D. Vader, A. Kabla, D. Weitz, and L. Mahadevan, "Strain-induced alignment in collagen gels," *PloS one*, vol. 4, no. 6, p. e5902, 2009.

[98] C. Dewey Jr, S. Bussolari, M. Gimbrone Jr, and P. F. Davies, "The dynamic response of vascular endothelial cells to fluid shear stress," 1981.

[99] M. Levesque and R. Nerem, "The elongation and orientation of cultured endothelial cells in response to shear stress," 1985.

[100] M. Inglebert, L. Locatelli, D. Tsvirkun, P. Sinha, J. A. Maier, C. Misbah, and L. Bureau, "The effect of shear stress reduction on endothelial cells: A microfluidic study of the actin cytoskeleton," *Biomicrofluidics*, vol. 14, no. 2, p. 024115, 2020.

[101] M. Mohammed, P. Thurgood, C. Gilliam, N. Nguyen, E. Pirogova, K. Peter, K. Khoshmanesh, and S. Baratchi, "Studying the response of aortic endothelial cells under pulsatile flow using a compact microfluidic system," *Analytical chemistry*, vol. 91, no. 18, pp. 12077–12084, 2019.

[102] P. Thurgood, S. A. Suarez, E. Pirogova, A. R. Jex, K. Peter, S. Baratchi, and K. Khoshmanesh, "Tunable harmonic flow patterns in microfluidic systems through simple tube oscillation," *Small*, p. 2003612, 2020.

[103] F. Tovar-Lopez, P. Thurgood, C. Gilliam, N. Nguyen, E. Pirogova, K. Khoshmanesh, and S. Baratchi, "A microfluidic system for studying the effects of disturbed flow on endothelial cells," *Front Bioeng Biotechnol*, vol. 7, p. 81, 2019.

[104] G. Vázquez-Victorio, C. Peto-Gutiérrez, B. Díaz-Bello, M. Cano-Jorge, D. Pérez-Calixto, A. Jiménez-Escobar, S. Espinosa-Matías, R. L. Martínez, R. Courson, and L. Malaquin, "Building a microfluidic cell culture platform with stiffness control using loctite 3525 glue," *Lab on a Chip*, vol. 19, no. 20, pp. 3512–3525, 2019.

[105] K. H. Benam, S. Dauth, B. Hassell, A. Herland, A. Jain, K. J. Jang, K. Karalis, H. J. Kim, L. MacQueen, R. Mahmoodian, S. Musah, Y. S. Torisawa, A. D. van der Meer, R. Villenave, M. Yadid, K. K. Parker, and D. E. Ingber, "Engineered in vitro disease models," *Annu Rev Pathol*, vol. 10, pp. 195–262, 2015.

[106] S. N. Bhatia and D. E. Ingber, "Microfluidic organs-on-chips," *Nat Biotechnol*, vol. 32, no. 8, pp. 760–72, 2014.

[107] N. S. Bhise, J. Ribas, V. Manoharan, Y. S. Zhang, A. Polini, S. Massa, M. R. Dokmeci, and A. Khademhosseini, "Organ-on-a-chip platforms for studying drug delivery systems," *J Control Release*, vol. 190, pp. 82–93, 2014.

[108] A. Jain, A. D. van der Meer, A. L. Papa, R. Barrile, A. Lai, B. L. Schlechter, M. A. Otieno, C. S. Louden, G. A. Hamilton, A. D. Michelson, r. Frelinger, A. L., and D. E. Ingber, "Assessment of whole blood thrombosis in a microfluidic device lined by fixed human endothelium," *Biomed Microdevices*, vol. 18, no. 4, p. 73, 2016.

[109] L. Jia, F. Han, H. Yang, G. Turnbull, J. Wang, J. Clarke, W. Shu, M. Guo, and B. Li, "Microfluidic fabrication of biomimetic helical hydrogel microfibers for bloodvesselonachip applications," *Advanced healthcare materials*, vol. 8, no. 13, p. 1900435, 2019.

[110] T. Mathur, K. A. Singh, R. P. NK, S. H. Tsai, T. W. Hein, A. K. Gaharwar, J. M. Flanagan, and A. Jain, "Organ-on-chips made of blood: endothelial progenitor cells from blood reconstitute vascular thromboinflammation in vessel-chips," *Lab Chip*, vol. 19, no. 15, pp. 2500–2511, 2019.

[111] J. Nie, Q. Gao, Y. Wang, J. Zeng, H. Zhao, Y. Sun, J. Shen, H. Ramezani, Z. Fu, and Z. Liu, "Vesselonachip with hydrogelbased microfluidics," *Small*, vol. 14, no. 45, p. 1802368, 2018.

[112] V. Lundin, W. W. Sugden, L. N. Theodore, P. M. Sousa, A. Han, S. Chou, P. J. Wrighton, A. G. Cox, D. E. Ingber, W. Goessling, G. Q. Daley, and T. E. North, "Yap regulates hematopoietic stem cell formation in response to the biomechanical forces of blood flow," *Dev Cell*, vol. 52, no. 4, pp. 446–460 e5, 2020.

[113] C. M. Hobson, M. Kern, E. T. OBrien III, A. D. Stephens, M. R. Falvo, and R. Superfine, "Correlating nuclear morphology and external force with combined atomic force microscopy and light sheet imaging separates roles of chromatin and lamin a/c in nuclear mechanics," *Molecular biology of the cell*, vol. 31, no. 16, pp. 1788–1801, 2020.

[114] C. M. Hobson and A. D. Stephens, "Modeling of cell nuclear mechanics: Classes, components, and applications," *Cells*, vol. 9, no. 7, p. 1623, 2020.

[115] N. Mandriota, C. Friedsam, J. A. Jones-Molina, K. V. Tatem, D. E. Ingber, and O. Sahin, "Cellular nanoscale stiffness patterns governed by intracellular forces," *Nature materials*, vol. 18, no. 10, pp. 1071–1077, 2019.

[116] L. Schermelleh, P. M. Carlton, S. Haase, L. Shao, L. Winoto, P. Kner, B. Burke, M. C. Cardoso, D. A. Agard, and M. G. Gustafsson, "Subdiffraction multicolor imaging of the nuclear periphery with 3d structured illumination microscopy," *Science*, vol. 320, no. 5881, pp. 1332–1336, 2008.

[117] B. Huang, W. Wang, M. Bates, and X. Zhuang, "Three-dimensional super-resolution imaging by stochastic optical reconstruction microscopy," *Science*, vol. 319, no. 5864, pp. 810–813, 2008.

[118] J. Biteen and K. A. Willets, "Introduction: super-resolution and single-molecule imaging," *Chemical reviews*, vol. 117, no. 11, pp. 7241–7243, 2017.

[119] K. Xu, G. Zhong, and X. Zhuang, "Actin, spectrin, and associated proteins form a periodic cytoskeletal structure in axons," *Science*, vol. 339, no. 6118, pp. 452–456, 2013.

[120] F. Asphahani and M. Zhang, "Cellular impedance biosensors for drug screening and toxin detection," *Analyst*, vol. 132, no. 9, pp. 835–841, 2007.

[121] A. Han, L. Yang, and A. B. Frazier, "Quantification of the heterogeneity in breast cancer cell lines using whole-cell impedance spectroscopy," *Clinical cancer research*, vol. 13, no. 1, pp. 139–143, 2007.

[122] R. McGuinness, "Impedance-based cellular assay technologies: recent advances, future promise," *Current opinion in pharmacology*, vol. 7, no. 5, pp. 535–540, 2007.

[123] G. E. Slaughter, E. Bieberich, G. E. Wnek, K. J. Wynne, and A. Guiseppi-Elie, "Improving neuron-to-electrode surface attachment via alkanethiol self-assembly: an alternating current impedance study," *Langmuir*, vol. 20, no. 17, pp. 7189–7200, 2004.

[124] M. Zhao, B. Song, J. Pu, T. Wada, B. Reid, G. Tai, F. Wang, A. Guo, P. Walczysko, and Y. Gu, "Electrical signals control wound healing through phosphatidylinositol-3-oh kinase-γ and pten," *Nature*, vol. 442, no. 7101, pp. 457–460, 2006.

[125] A. Remuzzi, C. F. Dewey Jr, P. F. Davies, and M. A. Gimbrone Jr, "Orientation of endothelial cells in shear fields in vitro," *Biorheology*, vol. 21, no. 4, pp. 617–630, 1984.

[126] J. Ando and K. Yamamoto, "Vascular mechanobiology: endothelial cell responses to fluid shear stress," *Circ J*, vol. 73, no. 11, pp. 1983–92, 2009.

[127] J. P. Cooke, "Flow, no, and atherogenesis," *Proc Natl Acad Sci U S A*, vol. 100, no. 3, pp. 768–70, 2003.

[128] K. S. Cunningham and A. I. Gotlieb, "The role of shear stress in the pathogenesis of atherosclerosis," *Lab Invest*, vol. 85, no. 1, pp. 9–23, 2005.

[129] N. G. dela Paz, T. E. Walshe, L. L. Leach, M. Saint-Geniez, and P. A. D'Amore, "Role of shear-stress-induced vegf expression in endothelial cell survival," *J Cell Sci*, vol. 125, no. Pt 4, pp. 831–43, 2012.

[130] H. Inoguchi, T. Tanaka, Y. Maehara, and T. Matsuda, "The effect of gradually graded shear stress on the morphological integrity of a huvec-seeded compliant small-diameter vascular graft," *Biomaterials*, vol. 28, no. 3, pp. 486–95, 2007.

[131] S. Chien, "Effects of disturbed flow on endothelial cells," *Ann Biomed Eng*, vol. 36, no. 4, pp. 554–62, 2008.

[132] J.-J. Chiu and S. Chien, "Effects of disturbed flow on vascular endothelium: pathophysiological basis and clinical perspectives," *Physiological reviews*, vol. 91, no. 1, pp. 327–387, 2011.

[133] A. Dominic, P. Banerjee, D. J. Hamilton, N. T. Le, and J. I. Abe, "Time-dependent replicative senescence vs. disturbed flow-induced pre-mature aging in atherosclerosis," *Redox Biol*, vol. 37, p. 101614, 2020.

[134] K. S. Heo, B. C. Berk, and J. Abe, "Disturbed flow-induced endothelial proatherogenic signaling via regulating post-translational modifications and epigenetic events," *Antioxid Redox Signal*, vol. 25, no. 7, pp. 435–50, 2016.

[135] T. Iba and B. E. Sumpio, "Morphological response of human endothelial cells subjected to cyclic strain in vitro," *Microvascular research*, vol. 42, no. 3, pp. 245–254, 1991.

[136] J. D. Kakisis, C. D. Liapis, and B. E. Sumpio, "Effects of cyclic strain on vascular cells," *Endothelium*, vol. 11, no. 1, pp. 17–28, 2004.

[137] A. B. Howard, R. Alexander, R. M. Nerem, K. Griendling, and W. Taylor, "Cyclic strain induces an oxidative stress in endothelial cells," *American Journal of Physiology-Cell Physiology*, vol. 272, no. 2, pp. C421–C427, 1997.

[138] G. Huang, C. Luo, X. Gu, Z. Wu, Z. Wang, Z. Du, C. Hu, and L. Tang, "Mechanical strain induces expression of c-reactive protein in human blood vessels," *Journal of Pharmacology and Experimental Therapeutics*, vol. 330, no. 1, pp. 206–211, 2009.

[139] M. A. Awolesi, W. C. Sessa, and B. E. Sumpio, "Cyclic strain upregulates nitric oxide synthase in cultured bovine aortic endothelial cells," *The Journal of clinical investigation*, vol. 96, no. 3, pp. 1449–1454, 1995.

[140] N. F. Jufri, A. Mohamedali, A. Avolio, and M. S. Baker, "Mechanical stretch: physiological and pathological implications for human vascular endothelial cells," *Vascular cell*, vol. 7, no. 1, pp. 1–12, 2015.

[141] C. F. Guimarães, L. Gasperini, A. P. Marques, and R. L. Reis, "The stiffness of living tissues and its implications for tissue engineering," *Nature Reviews Materials*, pp. 1–20, 2020.

[142] J. Ohayon, A. M. Gharib, A. Garcia, J. Heroux, S. K. Yazdani, M. Malvè, P. Tracqui, M.-A. Martinez, M. Doblare, and G. Finet, "Is arterial wall-strain stiffening an additional process responsible for atherosclerosis in coronary bifurcations?: an in vivo study based on dynamic ct and mri," *American Journal of Physiology-Heart and Circulatory Physiology*, vol. 301, no. 3, pp. H1097–H1106, 2011.

[143] J. Ohayon, P. Teppaz, G. Finet, and G. Rioufol, "In-vivo prediction of human coronary plaque rupture location using intravascular ultrasound and the finite element method," *Coronary artery disease*, vol. 12, no. 8, pp. 655–663, 2001.

[144] J. Ohayon, S. K. Yazdani, M. Malvè, A. M. Gharib, A. Garcia, G. Finet, and R. I. Pettigrew, *Arterial Wall Stiffness and Atherogenesis in Human Coronaries*, pp. 193–213. Elsevier, 2017.

[145] P. Tracqui, A. Broisat, J. Toczek, N. Mesnier, J. Ohayon, and L. Riou, "Mapping elasticity moduli of atherosclerotic plaque in situ via atomic force microscopy," *Journal of structural biology*, vol. 174, no. 1, pp. 115–123, 2011.

[146] R. Akhtar, M. J. Sherratt, J. K. Cruickshank, and B. Derby, "Characterizing the elastic properties of tissues," *Mater Today (Kidlington)*, vol. 14, no. 3, pp. 96–105, 2011.

[147] A. P. Ebrahimi, "Mechanical properties of normal and diseased cerebrovascular system," *Journal of vascular and interventional neurology*, vol. 2, no. 2, p. 155, 2009.

[148] C. Palombo and M. Kozakova, "Arterial stiffness, atherosclerosis and cardiovascular risk: Pathophysiologic mechanisms and emerging clinical indications," *Vascul Pharmacol*, vol. 77, pp. 1–7, 2016.

[149] N. M. van Popele, D. E. Grobbee, M. L. Bots, R. Asmar, J. Topouchian, R. S. Reneman, A. P. Hoeks, D. A. van der Kuip, A. Hofman, and J. C. Witteman, "Association between arterial stiffness and atherosclerosis: the rotterdam study," *Stroke*, vol. 32, no. 2, pp. 454–60, 2001.

[150] J. C. Kohn, D. W. Zhou, F. Bordeleau, A. L. Zhou, B. N. Mason, M. J. Mitchell, M. R. King, and C. A. Reinhart-King, "Cooperative effects of matrix stiffness and fluid shear stress on endothelial cell behavior," *Biophys J*, vol. 108, no. 3, pp. 471–8, 2015.

[151] T. Bertero, W. M. Oldham, K. A. Cottrill, S. Pisano, R. R. Vanderpool, Q. Yu, J. Zhao, Y. Tai, Y. Tang, Y. Y. Zhang, S. Rehman, M. Sugahara, Z. Qi, r. Gorcsan, J., S. O. Vargas, R. Saggar, R. Saggar, W. D. Wallace, D. J. Ross, K. J. Haley, A. B. Waxman, V. N. Parikh, T. De Marco, P. Y. Hsue, A. Morris, M. A. Simon, K. A. Norris, C. Gaggioli, J. Loscalzo, J. Fessel, and S. Y. Chan, "Vascular stiffness mechanoactivates yap/taz-dependent glutaminolysis to drive pulmonary hypertension," *J Clin Invest*, vol. 126, no. 9, pp. 3313–35, 2016.

[152] P. B. Dieffenbach, C. M. Haeger, A. M. F. Coronata, K. M. Choi, X. Varelas, D. J. Tschumperlin, and L. E. Fredenburgh, "Arterial stiffness induces remodeling phenotypes in pulmonary artery smooth muscle cells via yap/taz-mediated repression of cyclooxygenase-2," *Am J Physiol Lung Cell Mol Physiol*, vol. 313, no. 3, pp. L628–L647, 2017.

[153] K. Geng, J. Wang, P. Liu, X. Tian, H. Liu, X. Wang, C. Hu, and H. Yan, "Electrical stimulation facilitates the angiogenesis of human umbilical vein endothelial cells through mapk/erk signaling pathway by stimulating fgf2 secretion," *American Journal of Physiology-Cell Physiology*, vol. 317, no. 2, pp. C277–C286, 2019.

[154] J. Lammerding, "Mechanics of the nucleus," *Comprehensive physiology*, vol. 1, no. 2, pp. 783–807, 2011.

[155] J. M. Phillip, I. Aifuwa, J. Walston, and D. Wirtz, "The mechanobiology of aging," *Annual review of biomedical engineering*, vol. 17, pp. 113–141, 2015.

[156] D. E. Ingber, "Mechanobiology and diseases of mechanotransduction," *Ann Med*, vol. 35, no. 8, pp. 564–77, 2003.

[157] T. T. van Sloten, M. T. Schram, K. van den Hurk, J. M. Dekker, G. Nijpels, R. M. Henry, and C. D. Stehouwer, "Local stiffness of the carotid and femoral artery is associated with incident cardiovascular events and all-cause mortality: the hoorn study," *Journal of the American College of Cardiology*, vol. 63, no. 17, pp. 1739–1747, 2014.

[158] S. Xu, M. Koroleva, M. Yin, and Z. G. Jin, "Atheroprotective laminar flow inhibits hippo pathway effector yap in endothelial cells," *Transl Res*, vol. 176, pp. 18–28 e2, 2016.

[159] W. Hong and K. L. Guan, "The yap and taz transcription co-activators: key downstream effectors of the mammalian hippo pathway," *Semin Cell Dev Biol*, vol. 23, no. 7, pp. 785–93, 2012.

[160] J. S. Warren, Y. Xiao, and J. M. Lamar, "Yap/taz activation as a target for treating metastatic cancer," *Cancers*, vol. 10, no. 4, p. 115, 2018.

[161] H. L. Kim and S. H. Kim, "Pulse wave velocity in atherosclerosis," *Front Cardiovasc Med*, vol. 6, p. 41, 2019.

[162] S. L. Diamond, "Systems analysis of thrombus formation," *Circ Res*, vol. 118, no. 9, pp. 1348–62, 2016.

[163] T. Panciera, L. Azzolin, M. Cordenonsi, and S. Piccolo, "Mechanobiology of yap and taz in physiology and disease," *Nat Rev Mol Cell Biol*, vol. 18, no. 12, pp. 758–770, 2017.

[164] K. Gold, A. K. Gaharwar, and A. Jain, "Emerging trends in multiscale modeling of vascular pathophysiology: Organ-on-a-chip and 3d printing," *Biomaterials*, vol. 196, pp. 2–17, 2019.

[165] B. Zhang, A. Korolj, B. F. L. Lai, and M. Radisic, "Advances in organ-on-a-chip engineering," *Nature Reviews Materials*, vol. 3, no. 8, pp. 257–278, 2018.

[166] A. D. van der Meer, V. V. Orlova, P. ten Dijke, A. van den Berg, and C. L. Mummery, "Three-dimensional co-cultures of human endothelial cells and embryonic stem cell-derived pericytes inside a microfluidic device," *Lab Chip*, vol. 13, no. 18, pp. 3562–8, 2013.

[167] N. K. R. Pandian, R. G. Mannino, W. A. Lam, and A. Jain, "Thrombosis-on-a-chip: Prospective impact of microphysiological models of vascular thrombosis," *Current Opinion in Biomedical Engineering*, vol. 5, pp. 29–34, 2018.

[168] N. Gavara and R. S. Chadwick, "Determination of the elastic moduli of thin samples and adherent cells using conical atomic force microscope tips," *Nature nanotechnology*, vol. 7, no. 11, pp. 733–736, 2012.

[169] R. D. Barber, D. W. Harmer, R. A. Coleman, and B. J. Clark, "Gapdh as a housekeeping gene: analysis of gapdh mrna expression in a panel of 72 human tissues," *Physiological genomics*, vol. 21, no. 3, pp. 389–395, 2005.

[170] Z. Püspöki, M. Storath, D. Sage, and M. Unser, *Transforms and operators for directional bioimage analysis: a survey*, pp. 69–93. Springer, 2016.

[171] J. D. Hunter, "Matplotlib: A 2d graphics environment," *Computing in Science & Engineering*, vol. 9, no. 3, pp. 90–95, 2007.

[172] S. M. McCormick, S. G. Eskin, L. V. McIntire, C. L. Teng, C. M. Lu, C. G. Russell, and K. K. Chittur, "Dna microarray reveals changes in gene expression of shear stressed human umbilical vein endothelial cells," *Proc Natl Acad Sci U S A*, vol. 98, no. 16, pp. 8955–60, 2001.

[173] T. Nagel, N. Resnick, W. J. Atkinson, J. Dewey, C. F., and J. Gimbrone, M. A., "Shear stress selectively upregulates intercellular adhesion molecule-1 expression in cultured human vascular endothelial cells," *J Clin Invest*, vol. 94, no. 2, pp. 885–91, 1994.

[174] D. C. Chappell, S. E. Varner, R. M. Nerem, R. M. Medford, and R. W. Alexander, "Oscillatory shear stress stimulates adhesion molecule expression in cultured human endothelium," *Circ Res*, vol. 82, no. 5, pp. 532–9, 1998.

[175] J. J. Chiu and S. Chien, "Effects of disturbed flow on vascular endothelium: pathophysiological basis and clinical perspectives," *Physiol Rev*, vol. 91, no. 1, pp. 327–87, 2011.

[176] N. E. Ajami, S. Gupta, M. R. Maurya, P. Nguyen, J. Y. Li, J. Y. Shyy, Z. Chen, S. Chien, and S. Subramaniam, "Systems biology analysis of longitudinal functional response of endothelial cells to shear stress," *Proc Natl Acad Sci U S A*, vol. 114, no. 41, pp. 10990–10995, 2017.

[177] C. M. Potter, M. H. Lundberg, L. S. Harrington, C. M. Warboys, T. D. Warner, R. E. Berson, A. V. Moshkov, J. Gorelik, P. D. Weinberg, and J. A. Mitchell, "Role of shear stress in endothelial cell morphology and expression of cyclooxygenase isoforms," *Arterioscler Thromb Vasc Biol*, vol. 31, no. 2, pp. 384–91, 2011.

[178] S. Zhao, A. Suciu, T. Ziegler, J. Moore, J. E., E. Burki, J. J. Meister, and H. R. Brunner, "Synergistic effects of fluid shear stress and cyclic circumferential stretch on vascular endothelial cell morphology and cytoskeleton," *Arterioscler Thromb Vasc Biol*, vol. 15, no. 10, pp. 1781–6, 1995.

[179] M. I. Cybulsky, K. Iiyama, H. Li, S. Zhu, M. Chen, M. Iiyama, V. Davis, J.-C. Gutierrez-Ramos, P. W. Connelly, and D. S. Milstone, "A major role for vcam-1, but not icam-1, in early atherosclerosis," *The Journal of clinical investigation*, vol. 107, no. 10, pp. 1255–1262, 2001.

[180] P. Doddapattar, N. Dhanesha, M. R. Chorawala, C. Tinsman, M. Jain, M. K. Nayak, J. M. Staber, and A. K. Chauhan, "Endothelial cellderived von willebrand factor, but not platelet-derived, promotes atherosclerosis in apolipoprotein edeficient mice," *Arteriosclerosis, thrombosis, and vascular biology*, vol. 38, no. 3, pp. 520–528, 2018.

[181] S. J. Hwang, C. M. Ballantyne, A. R. Sharrett, L. C. Smith, C. E. Davis, J. Gotto, A. M., and E. Boerwinkle, "Circulating adhesion molecules vcam-1, icam-1, and e-selectin in carotid atherosclerosis and incident coronary heart disease cases: the atherosclerosis risk in communities (aric) study," *Circulation*, vol. 96, no. 12, pp. 4219–25, 1997.

[182] K. Ley and Y. Huo, "Vcam-1 is critical in atherosclerosis," *The Journal of clinical investigation*, vol. 107, no. 10, pp. 1209–1210, 2001.

[183] P. S. Tsao, R. Buitrago, J. R. Chan, and J. P. Cooke, "Cellular and molecular cardiovascular disease: Fluid flow inhibits endothelial adhesiveness nitric oxide and transcriptional regulation of vcam-1," *Circulation*, vol. 94, no. 7, pp. 1682–1689, 1996.

[184] P. S. Tsao, R. Buitrago, J. R. Chan, and J. P. Cooke, "Fluid flow inhibits endothelial adhesiveness: nitric oxide and transcriptional regulation of vcam-1," *Circulation*, vol. 94, no. 7, pp. 1682–1689, 1996.

[185] I. Fleming, B. Fisslthaler, M. Dixit, and R. Busse, "Role of pecam-1 in the shear-stress-induced activation of akt and the endothelial nitric oxide synthase (enos) in endothelial cells," *J Cell Sci*, vol. 118, no. Pt 18, pp. 4103–11, 2005.

[186] E. Gee, M. Milkiewicz, and T. L. Haas, "p38 mapk activity is stimulated by vascular endothelial growth factor receptor 2 activation and is essential for shear stressinduced angiogenesis," *Journal of cellular physiology*, vol. 222, no. 1, pp. 120–126, 2010.

[187] Z. G. Jin, H. Ueba, T. Tanimoto, A. O. Lungu, M. D. Frame, and B. C. Berk, "Ligand-independent activation of vascular endothelial growth factor receptor 2 by fluid shear stress regulates activation of endothelial nitric oxide synthase," *Circ Res*, vol. 93, no. 4, pp. 354–63, 2003.

[188] P. Nigro, J. Abe, and B. C. Berk, "Flow shear stress and atherosclerosis: a matter of site specificity," *Antioxid Redox Signal*, vol. 15, no. 5, pp. 1405–14, 2011.

[189] J. L. Tuttle, R. D. Nachreiner, A. S. Bhuller, K. W. Condict, B. A. Connors, B. P. Herring, M. C. Dalsing, and J. L. Unthank, "Shear level influences resistance artery remodeling: wall dimensions, cell density, and enos expression," *Am J Physiol Heart Circ Physiol*, vol. 281, no. 3, pp. H1380–9, 2001.

[190] I. Cicha, A. Yilmaz, M. Klein, D. Raithel, D. R. Brigstock, W. G. Daniel, M. Goppelt-Struebe, and C. D. Garlichs, "Connective tissue growth factor is overexpressed in complicated atherosclerotic plaques and induces mononuclear cell chemotaxis in vitro," *Arteriosclerosis, thrombosis, and vascular biology*, vol. 25, no. 5, pp. 1008–1013, 2005.

[191] I. Cicha, A. Yilmaz, Y. Suzuki, N. Maeda, W. G. Daniel, M. Goppelt-Struebe, and C. D. Garlichs, "Connective tissue growth factor is released from platelets under high shear stress and is differentially expressed in endothelium along atherosclerotic plaques," *Clinical hemorheology and microcirculation*, vol. 35, no. 1-2, pp. 203–206, 2006.

[192] W. H. Fan, M. Pech, and M. J. Karnovsky, "Connective tissue growth factor (ctgf) stimulates vascular smooth muscle cell growth and migration in vitro," *Eur J Cell Biol*, vol. 79, no. 12, pp. 915–23, 2000.

[193] N. Niu, S. Xu, Y. Xu, P. J. Little, and Z. G. Jin, "Targeting mechanosensitive transcription factors in atherosclerosis," *Trends Pharmacol Sci*, vol. 40, no. 4, pp. 253–266, 2019.

[194] K. Brodowska, A. Al-Moujahed, A. Marmalidou, M. M. zu Horste, J. Cichy, J. W. Miller, E. Gragoudas, and D. G. Vavvas, "The clinically used photosensitizer verteporfin (vp) in-

hibits yap-tead and human retinoblastoma cell growth in vitro without light activation," *Experimental eye research*, vol. 124, pp. 67–73, 2014.

[195] J. Feng, J. Gou, J. Jia, T. Yi, T. Cui, and Z. Li, "Verteporfin, a suppressor of yap-tead complex, presents promising antitumor properties on ovarian cancer," *Onco Targets Ther*, vol. 9, pp. 5371–81, 2016.

[196] C. Wang, X. Zhu, W. Feng, Y. Yu, K. Jeong, W. Guo, Y. Lu, and G. B. Mills, "Verteporfin inhibits yap function through up-regulating 14-3-3σ sequestering yap in the cytoplasm," *American journal of cancer research*, vol. 6, no. 1, p. 27, 2016.

[197] H. Wei, F. Wang, Y. Wang, T. Li, P. Xiu, J. Zhong, X. Sun, and J. Li, "Verteporfin suppresses cell survival, angiogenesis and vasculogenic mimicry of pancreatic ductal adenocarcinoma via disrupting the yap-tead complex," *Cancer Sci*, vol. 108, no. 3, pp. 478–487, 2017.

[198] Y. W. Ma, Y. Z. Liu, and J. X. Pan, "Verteporfin induces apoptosis and eliminates cancer stem-like cells in uveal melanoma in the absence of light activation," *Am J Cancer Res*, vol. 6, no. 12, pp. 2816–2830, 2016.

[199] A. Dominic, D. Hamilton, and J.-i. Abe, "Mitochondria and chronic effects of cancer therapeutics: The clinical implications," *Journal of Thrombosis and Thrombolysis*, pp. 1–6, 2020.

[200] G. Sorrentino, N. Ruggeri, V. Specchia, M. Cordenonsi, M. Mano, S. Dupont, A. Manfrin, E. Ingallina, R. Sommaggio, S. Piazza, A. Rosato, S. Piccolo, and G. Del Sal, "Metabolic control of yap and taz by the mevalonate pathway," *Nat Cell Biol*, vol. 16, no. 4, pp. 357–66, 2014.

[201] T. Bertero, K. A. Cottrill, Y. Lu, C. M. Haeger, P. Dieffenbach, S. Annis, A. Hale, B. Bhat, V. Kaimal, Y. Y. Zhang, B. B. Graham, R. Kumar, R. Saggar, R. Saggar, W. D. Wallace, D. J. Ross, S. M. Black, S. Fratz, J. R. Fineman, S. O. Vargas, K. J. Haley, A. B. Waxman, B. N. Chau, L. E. Fredenburgh, and S. Y. Chan, "Matrix remodeling promotes pulmonary hypertension through feedback mechanoactivation of the yap/taz-mir-130/301 circuit," *Cell Rep*, vol. 13, no. 5, pp. 1016–32, 2015.

[202] D. Gomez and G. K. Owens, "Smooth muscle cell phenotypic switching in atherosclerosis," *Cardiovasc Res*, vol. 95, no. 2, pp. 156–64, 2012.

[203] R. Ross and J. A. Glomset, "Atherosclerosis and the arterial smooth muscle cell: Proliferation of smooth muscle is a key event in the genesis of the lesions of atherosclerosis," *Science*, vol. 180, no. 4093, pp. 1332–9, 1973.

[204] E. W. Young, A. R. Wheeler, and C. A. Simmons, "Matrix-dependent adhesion of vascular and valvular endothelial cells in microfluidic channels," *Lab Chip*, vol. 7, no. 12, pp. 1759–66, 2007.

[205] N. K. Rajeeva Pandian, B. K. Walther, R. Suresh, J. P. Cooke, and A. Jain, "Microengineered human veinchip recreates venous valve architecture and its contribution to thrombosis," *Small*, vol. 16, no. 49, p. 2003401, 2020.

[206] J. D. Welsh, M. H. Hoofnagle, S. Bamezai, M. Oxendine, L. Lim, J. D. Hall, J. Yang, S. Schultz, J. D. Engel, T. Kume, G. Oliver, J. M. Jimenez, and M. L. Kahn, "Hemodynamic regulation of perivalvular endothelial gene expression prevents deep venous thrombosis," *J Clin Invest*, vol. 129, no. 12, pp. 5489–5500, 2019.

[207] M. P. Hughes, *Nanoelectromechanics in engineering and biology*. CRC press, 2002.

[208] G. W. Stone, *Electro-Biology: or, the Electrical science of life*. Willmer & Smith, 1850.

[209] D. J. Blackiston, K. A. McLaughlin, and M. Levin, "Bioelectric controls of cell proliferation: ion channels, membrane voltage and the cell cycle," *Cell cycle*, vol. 8, no. 21, pp. 3527–3536, 2009.

[210] B. P. Bean, "The action potential in mammalian central neurons," *Nature Reviews Neuroscience*, vol. 8, no. 6, pp. 451–465, 2007.

[211] B. Naundorf, F. Wolf, and M. Volgushev, "Unique features of action potential initiation in cortical neurons," *Nature*, vol. 440, no. 7087, pp. 1060–1063, 2006.

[212] A. Verkhratsky and C. Steinhäuser, "Ion channels in glial cells," *Brain research reviews*, vol. 32, no. 2-3, pp. 380–412, 2000.

[213] M. R. Boyett, H. Honjo, and I. Kodama, "The sinoatrial node, a heterogeneous pacemaker structure," *Cardiovascular research*, vol. 47, no. 4, pp. 658–687, 2000.

[214] D. F. Clayton, "The genomic action potential," *Neurobiology of learning and memory*, vol. 74, no. 3, pp. 185–216, 2000.

[215] R. D. Fields, F. Eshete, B. Stevens, and K. Itoh, "Action potential-dependent regulation of gene expression: temporal specificity in ca2+, camp-responsive element binding proteins, and mitogen-activated protein kinase signaling," *Journal of Neuroscience*, vol. 17, no. 19, pp. 7252–7266, 1997.

[216] H. Irisawa, H. Brown, and W. Giles, "Cardiac pacemaking in the sinoatrial node," *Physiological reviews*, vol. 73, no. 1, pp. 197–227, 1993.

[217] B. Stankovi and E. Davies, "Both action potentials and variation potentials induce proteinase inhibitor gene expression in tomato," *Febs Letters*, vol. 390, no. 3, pp. 275–279, 1996.

[218] J. M. Benarroch and M. Asally, "The microbiologists guide to membrane potential dynamics," *Trends in Microbiology*, vol. 28, no. 4, pp. 304–314, 2020.

[219] A. G. Kléber, "Resting membrane potential, extracellular potassium activity, and intracellular sodium activity during acute global ischemia in isolated perfused guinea pig hearts," *Circulation Research*, vol. 52, no. 4, pp. 442–450, 1983.

[220] S. H. Wright, "Generation of resting membrane potential," *Advances in physiology education*, vol. 28, no. 4, pp. 139–142, 2004.

[221] X.-J. Yuan, "Voltage-gated k+ currents regulate resting membrane potential and [ca2+] i in pulmonary arterial myocytes," *Circulation research*, vol. 77, no. 2, pp. 370–378, 1995.

[222] L. Abdul Kadir, M. Stacey, and R. Barrett-Jolley, "Emerging roles of the membrane potential: action beyond the action potential," *Frontiers in physiology*, vol. 9, p. 1661, 2018.

[223] E. D. Kirson, V. Dbalý, F. Tovary, J. Vymazal, J. F. Soustiel, A. Itzhaki, D. Mordechovich, S. Steinberg-Shapira, Z. Gurvich, and R. Schneiderman, "Alternating electric fields arrest cell proliferation in animal tumor models and human brain tumors," *Proceedings of the National Academy of Sciences*, vol. 104, no. 24, pp. 10152–10157, 2007.

[224] Y. Lu, S. Qi, H. Ouyang, H. Li, Y. Liu, and Y. Song, "Surgical and therapeutic strategies of malignant gliomas in refractory sites," *Chin. J. Contemp. Neurol Neurosurg*, vol. 12, pp. 682–690, 2012.

[225] T. Voloshin, R. S. Schneiderman, A. Volodin, R. R. Shamir, N. Kaynan, E. Zeevi, L. Koren, A. Klein-Goldberg, R. Paz, and M. Giladi, "Tumor treating fields (ttfields) hinder cancer cell motility through regulation of microtubule and acting dynamics," *Cancers*, vol. 12, no. 10, p. 3016, 2020.

[226] G. Gregoratos, M. D. Cheitlin, A. Conill, A. E. Epstein, C. Fellows, T. B. Ferguson, R. A. Freedman, M. A. Hlatky, G. V. Naccarelli, and S. Saksena, "Acc/aha guidelines for implantation of cardiac pacemakers and antiarrhythmia devices: a report of the american college of cardiology/american heart association task force on practice guidelines (committee on pacemaker implantation)," *Journal of the American College of Cardiology*, vol. 31, no. 5, pp. 1175–1209, 1998.

[227] C. Members, G. Gregoratos, J. Abrams, A. E. Epstein, R. A. Freedman, D. L. Hayes, M. A. Hlatky, R. E. Kerber, G. V. Naccarelli, and M. H. Schoenfeld, "Acc/aha/naspe 2002 guideline update for implantation of cardiac pacemakers and antiarrhythmia devices: summary article: a report of the american college of cardiology/american heart association task force on practice guidelines (acc/aha/naspe committee to update the 1998 pacemaker guidelines)," *Circulation*, vol. 106, no. 16, pp. 2145–2161, 2002.

[228] B. Honig and A. Nicholls, "Classical electrostatics in biology and chemistry," *Science*, vol. 268, no. 5214, pp. 1144–1149, 1995.

[229] J. B. Lansman, T. J. Hallam, and T. J. Rink, "Single stretch-activated ion channels in vascular endothelial cells as mechanotransducers?," *Nature*, vol. 325, no. 6107, pp. 811–813, 1987.

[230] C. Alcaino, G. Farrugia, and A. Beyder, *Mechanosensitive piezo channels in the gastrointestinal tract*, vol. 79, pp. 219–244. Elsevier, 2017.

[231] B. Coste, B. Xiao, J. S. Santos, R. Syeda, J. Grandl, K. S. Spencer, S. E. Kim, M. Schmidt, J. Mathur, and A. E. Dubin, "Piezo proteins are pore-forming subunits of mechanically activated channels," *Nature*, vol. 483, no. 7388, pp. 176–181, 2012.

[232] M. Zhao, H. Bai, E. Wang, J. V. Forrester, and C. D. McCaig, "Electrical stimulation directly induces pre-angiogenic responses in vascular endothelial cells by signaling through vegf receptors," *Journal of cell science*, vol. 117, no. 3, pp. 397–405, 2004.

[233] A. Stefanovska, M. Bracic, and H. D. Kvernmo, "Wavelet analysis of oscillations in the peripheral blood circulation measured by laser doppler technique," *IEEE Trans Biomed Eng*, vol. 46, no. 10, pp. 1230–9, 1999.

[234] P. Libby, P. M. Ridker, and A. Maseri, "Inflammation and atherosclerosis," *Circulation*, vol. 105, no. 9, pp. 1135–1143, 2002.

[235] P. Libby, "Inflammation in atherosclerosis," *Arterioscler Thromb Vasc Biol*, vol. 32, no. 9, pp. 2045–51, 2012.

[236] L. B. Gordon, M. E. Kleinman, J. Massaro, R. B. DAgostino Sr, H. Shappell, M. Gerhard-Herman, L. B. Smoot, C. M. Gordon, R. H. Cleveland, and A. Nazarian, "Clinical trial of the protein farnesylation inhibitors lonafarnib, pravastatin, and zoledronic acid in children with hutchinson-gilford progeria syndrome," *Circulation*, vol. 134, no. 2, pp. 114–125, 2016.

[237] R. Varga, M. Eriksson, M. R. Erdos, M. Olive, I. Harten, F. Kolodgie, B. C. Capell, J. Cheng, D. Faddah, and S. Perkins, "Progressive vascular smooth muscle cell defects in a mouse model of hutchinsongilford progeria syndrome," *Proceedings of the National Academy of Sciences*, vol. 103, no. 9, pp. 3250–3255, 2006.

[238] C. Sekirnjak, P. Hottowy, A. Sher, W. Dabrowski, A. Litke, and E. Chichilnisky, "Electrical stimulation of mammalian retinal ganglion cells with multielectrode arrays," *Journal of neurophysiology*, vol. 95, no. 6, pp. 3311–3327, 2006.

[239] N. Tandon, C. Cannizzaro, P.-H. G. Chao, R. Maidhof, A. Marsano, H. T. H. Au, M. Radisic, and G. Vunjak-Novakovic, "Electrical stimulation systems for cardiac tissue engineering," *Nature protocols*, vol. 4, no. 2, p. 155, 2009.

[240] G. M. Xiong, A. T. Do, J. K. Wang, C. L. Yeoh, K. S. Yeo, and C. Choong, "Development of a miniaturized stimulation device for electrical stimulation of cells," *Journal of biological engineering*, vol. 9, no. 1, pp. 1–10, 2015.

[241] S. Abasi, J. R. Aggas, and A. Guiseppi-Elie, "Physiochemical and morphological dependent growth of nih/3t3 and pc-12 on polyaniline-chloride/chitosan bionanocomposites," *Materials Science and Engineering: C*, vol. 99, pp. 1304–1312, 2019.

[242] L. Ghasemi-Mobarakeh, M. P. Prabhakaran, M. Morshed, M. H. Nasr-Esfahani, and S. Ramakrishna, "Electrical stimulation of nerve cells using conductive nanofibrous scaffolds for nerve tissue engineering," *Tissue Engineering Part A*, vol. 15, no. 11, pp. 3605–3619, 2009.

[243] A. Guiseppi-Elie, "Electroconductive hydrogels: synthesis, characterization and biomedical applications," *Biomaterials*, vol. 31, no. 10, pp. 2701–2716, 2010.

[244] M. P. Prabhakaran, L. Ghasemi-Mobarakeh, G. Jin, and S. Ramakrishna, "Electrospun conducting polymer nanofibers and electrical stimulation of nerve stem cells," *Journal of bioscience and bioengineering*, vol. 112, no. 5, pp. 501–507, 2011.

[245] H. Yuk, B. Lu, and X. Zhao, "Hydrogel bioelectronics," *Chemical Society Reviews*, vol. 48, no. 6, pp. 1642–1667, 2019.

[246] R. Burla, M. La Torre, and I. Saggio, "Mammalian telomeres and their partnership with lamins," *Nucleus*, vol. 7, no. 2, pp. 187–202, 2016.

[247] J. R. Aggas, B. K. Walther, S. Abasi, C. N. Kotanen, O. Karunwi, A. M. Wilson, and A. Guiseppi-Elie, "On the intersection of molecular bioelectronics and biosensors: 20 years of c3b," *Biosensors and Bioelectronics*, p. 112889, 2020.

[248] T. P. Driscoll, B. D. Cosgrove, S.-J. Heo, Z. E. Shurden, and R. L. Mauck, "Cytoskeletal to nuclear strain transfer regulates yap signaling in mesenchymal stem cells," *Biophysical journal*, vol. 108, no. 12, pp. 2783–2793, 2015.

[249] L. Resutek and A. H. Hsieh, "The vacuolated morphology of chordoma cells is dependent on cytokeratin intermediate filaments," *Journal of Cellular Physiology*, vol. 234, no. 4, pp. 3458–3468, 2019.

[250] N. Wang and D. Stamenovic, "Contribution of intermediate filaments to cell stiffness, stiffening, and growth," *American Journal of Physiology-Cell Physiology*, vol. 279, no. 1, pp. C188–C194, 2000.

[251] L. Lin, X. Song, Y. Chen, M. Rong, T. Zhao, Y. Wang, Y. Jiang, and X. Chen, "Intrinsic peroxidase-like catalytic activity of nitrogen-doped graphene quantum dots and their application in the colorimetric detection of h2o2 and glucose," *Anal Chim Acta*, vol. 869, pp. 89–95, 2015.

[252] M. M. Pathak, J. L. Nourse, T. Tran, J. Hwe, J. Arulmoli, T. L. Dai Trang, E. Bernardis, L. A. Flanagan, and F. Tombola, "Stretch-activated ion channel piezo1 directs lineage choice in human neural stem cells," *Proceedings of the National Academy of Sciences*, vol. 111, no. 45, pp. 16148–16153, 2014.

[253] H. Liu, T. Ye, and C. Mao, "Fluorescent carbon nanoparticles derived from candle soot," *Angew Chem Int Ed Engl*, vol. 46, no. 34, pp. 6473–5, 2007.

[254] P. Scaffidi and T. Misteli, "Lamin a-dependent nuclear defects in human aging," *Science*, vol. 312, no. 5776, pp. 1059–1063, 2006.

[255] B. Zhao, L. Li, L. Wang, C.-Y. Wang, J. Yu, and K.-L. Guan, "Cell detachment activates the hippo pathway via cytoskeleton reorganization to induce anoikis," *Genes & development*, vol. 26, no. 1, pp. 54–68, 2012.

[256] Y. Li, G. Zhou, I. G. Bruno, N. Zhang, S. Sho, E. Tedone, T. P. Lai, J. P. Cooke, and J. W. Shay, "Transient introduction of human telomerase mrna improves hallmarks of progeria cells," *Aging Cell*, vol. 18, no. 4, p. e12979, 2019.

[257] H. J. Jung, C. Coffinier, Y. Choe, A. P. Beigneux, B. S. Davies, S. H. Yang, n. Barnes, R. H., J. Hong, T. Sun, S. J. Pleasure, S. G. Young, and L. G. Fong, "Regulation of prelamin a but not lamin c by mir-9, a brain-specific microrna," *Proc Natl Acad Sci U S A*, vol. 109, no. 7, pp. E423–31, 2012.

[258] S. Osmanagic-Myers, A. Kiss, C. Manakanatas, O. Hamza, F. Sedlmayer, P. L. Szabo, I. Fischer, P. Fichtinger, B. K. Podesser, M. Eriksson, and R. Foisner, "Endothelial progerin expression causes cardiovascular pathology through an impaired mechanoresponse," *J Clin Invest*, vol. 129, no. 2, pp. 531–545, 2019.

[259] H. T. Gilbert and J. Swift, "The consequences of ageing, progeroid syndromes and cellular senescence on mechanotransduction and the nucleus," *Experimental cell research*, vol. 378, no. 1, pp. 98–103, 2019.

[260] X. Mu, C. Tseng, W. S. Hambright, P. Matre, C. Lin, P. Chanda, W. Chen, J. Gu, S. Ravuri, and Y. Cui, "Cytoskeleton stiffness regulates cellular senescence and innate immune response in hutchinsongilford progeria syndrome," *Aging cell*, vol. 19, no. 8, p. e13152, 2020.

[261] V. L. Verstraeten, J. Y. Ji, K. S. Cummings, R. T. Lee, and J. Lammerding, "Increased mechanosensitivity and nuclear stiffness in hutchinsongilford progeria cells: effects of farnesyltransferase inhibitors," *Aging cell*, vol. 7, no. 3, pp. 383–393, 2008.

[262] A. P. Cabrera, A. Bhaskaran, J. Xu, X. Yang, H. A. Scott, U. Mohideen, and K. Ghosh, "Senescence increases choroidal endothelial stiffness and susceptibility to complement in-

jury: implications for choriocapillaris loss in amd," *Investigative ophthalmology & visual science*, vol. 57, no. 14, pp. 5910–5918, 2016.

[263] J. T. Zahn, I. Louban, S. Jungbauer, M. Bissinger, D. Kaufmann, R. Kemkemer, and J. P. Spatz, "Agedependent changes in microscale stiffness and mechanoresponses of cells," *Small*, vol. 7, no. 10, pp. 1480–1487, 2011.

[264] K. Apte, R. Stick, and M. Radmacher, "Mechanics in human fibroblasts and progeria: Lamin a mutation e145k results in stiffening of nuclei," *Journal of Molecular Recognition*, vol. 30, no. 2, p. e2580, 2017.

[265] A. J. Ford and P. Rajagopalan, "Measuring cytoplasmic stiffness of fibroblasts as a function of location and substrate rigidity using atomic force microscopy," *ACS Biomaterials Science & Engineering*, vol. 4, no. 12, pp. 3974–3982, 2018.

[266] E. K. Dimitriadis, F. Horkay, J. Maresca, B. Kachar, and R. S. Chadwick, "Determination of elastic moduli of thin layers of soft material using the atomic force microscope," *Biophysical journal*, vol. 82, no. 5, pp. 2798–2810, 2002.

[267] O. Moujaber, F. Fishbein, N. Omran, Y. Liang, I. Colmegna, J. F. Presley, and U. Stochaj, "Cellular senescence is associated with reorganization of the microtubule cytoskeleton," *Cellular and Molecular Life Sciences*, vol. 76, no. 6, pp. 1169–1183, 2019.

[268] O. Moujaber and U. Stochaj, "The cytoskeleton as regulator of cell signaling pathways," *Trends in biochemical sciences*, vol. 45, no. 2, pp. 96–107, 2020.

[269] G. E. Neurohr, R. L. Terry, J. Lengefeld, M. Bonney, G. P. Brittingham, F. Moretto, T. P. Miettinen, L. P. Vaites, L. M. Soares, and J. A. Paulo, "Excessive cell growth causes cytoplasm dilution and contributes to senescence," *Cell*, vol. 176, no. 5, pp. 1083–1097. e18, 2019.

[270] K. Nishio, A. Inoue, S. Qiao, H. Kondo, and A. Mimura, "Senescence and cytoskeleton: overproduction of vimentin induces senescent-like morphology in human fibroblasts," *Histochemistry and cell biology*, vol. 116, no. 4, pp. 321–327, 2001.

[271] L. Hayflick and P. S. Moorhead, "The serial cultivation of human diploid cell strains," *Experimental cell research*, vol. 25, no. 3, pp. 585–621, 1961.

[272] Y. Ding, G.-K. Xu, and G.-F. Wang, "On the determination of elastic moduli of cells by afm based indentation," *Scientific reports*, vol. 7, no. 1, pp. 1–8, 2017.

[273] Y. M. Efremov, W.-H. Wang, S. D. Hardy, R. L. Geahlen, and A. Raman, "Measuring nanoscale viscoelastic parameters of cells directly from afm force-displacement curves," *Scientific reports*, vol. 7, no. 1, pp. 1–14, 2017.

[274] P. D. Garcia, C. R. Guerrero, and R. Garcia, "Nanorheology of living cells measured by afm-based forcedistance curves," *Nanoscale*, vol. 12, no. 16, pp. 9133–9143, 2020.

[275] P.-H. Wu, D. R.-B. Aroush, A. Asnacios, W.-C. Chen, M. E. Dokukin, B. L. Doss, P. Durand-Smet, A. Ekpenyong, J. Guck, and N. V. Guz, "A comparison of methods to assess cell mechanical properties," *Nature methods*, vol. 15, pp. 491–498, 2018.

[276] J. N. Reddy, *Introduction to the finite element method*. McGraw-Hill Education, 2019.

[277] A. I. Gómez-Varela, D. R. Stamov, A. Miranda, R. Alves, C. Barata-Antunes, D. Dambournet, D. G. Drubin, S. Paiva, and P. A. De Beule, "Simultaneous co-localized super-resolution fluorescence microscopy and atomic force microscopy: combined sim and afm platform for the life sciences," *Scientific reports*, vol. 10, no. 1, pp. 1–10, 2020.

[278] L. M. Hirvonen, R. J. Marsh, G. E. Jones, and S. Cox, "Combined afm and super-resolution localisation microscopy: Investigating the structure and dynamics of podosomes," *European Journal of Cell Biology*, vol. 99, no. 7, p. 151106, 2020.

[279] A. Miranda, A. I. Gómez-Varela, A. Stylianou, L. M. Hirvonen, H. Sánchez, and P. A. De Beule, "How did correlative atomic force microscopy and super-resolution microscopy evolve in the quest for unravelling enigmas in biology?," *Nanoscale*, vol. 13, no. 4, pp. 2082–2099, 2021.

[280] S. Vichare, S. Sen, and M. M. Inamdar, "Cellular mechanoadaptation to substrate mechanical properties: contributions of substrate stiffness and thickness to cell stiffness measurements using afm," *Soft matter*, vol. 10, no. 8, pp. 1174–1181, 2014.

[281] M. G. Gustafsson, "Surpassing the lateral resolution limit by a factor of two using structured illumination microscopy," *Journal of microscopy*, vol. 198, no. 2, pp. 82–87, 2000.

[282] E. Abbe, "Vii.on the estimation of aperture in the microscope," *Journal of the Royal Microscopical Society*, vol. 1, no. 3, pp. 388–423, 1881.

[283] M. G. Gustafsson, "Nonlinear structured-illumination microscopy: wide-field fluorescence imaging with theoretically unlimited resolution," *Proceedings of the National Academy of Sciences*, vol. 102, no. 37, pp. 13081–13086, 2005.

[284] L. Shao, P. Kner, E. H. Rego, and M. G. Gustafsson, "Super-resolution 3d microscopy of live whole cells using structured illumination," *Nature methods*, vol. 8, no. 12, pp. 1044–1046, 2011.

[285] C. McQuin, A. Goodman, V. Chernyshev, L. Kamentsky, B. A. Cimini, K. W. Karhohs, M. Doan, L. Ding, S. M. Rafelski, and D. Thirstrup, "Cellprofiler 3.0: Next-generation image processing for biology," *PLoS biology*, vol. 16, no. 7, p. e2005970, 2018.

[286] B. C. Russell, A. Torralba, K. P. Murphy, and W. T. Freeman, "Labelme: a database and web-based tool for image annotation," *International journal of computer vision*, vol. 77, no. 1-3, pp. 157–173, 2008.

[287] L. Ding and A. Goshtasby, "On the canny edge detector," *Pattern Recognition*, vol. 34, no. 3, pp. 721–725, 2001.

[288] K. Nishio and A. Inoue, "Senescence-associated alterations of cytoskeleton: extraordinary production of vimentin that anchors cytoplasmic p53 in senescent human fibroblasts," *Histochemistry and cell biology*, vol. 123, no. 3, pp. 263–273, 2005.

[289] C. Rotsch and M. Radmacher, "Drug-induced changes of cytoskeletal structure and mechanics in fibroblasts: an atomic force microscopy study," *Biophysical journal*, vol. 78, no. 1, pp. 520–535, 2000.

[290] K. N. Dahl, P. Scaffidi, M. F. Islam, A. G. Yodh, K. L. Wilson, and T. Misteli, "Distinct structural and mechanical properties of the nuclear lamina in hutchinsongilford progeria syndrome," *Proceedings of the National Academy of Sciences*, vol. 103, no. 27, pp. 10271–10276, 2006.

[291] X. Zhang, X. Hu, H. Lei, J. Hu, and Y. Zhang, "Mechanical force-induced polymerization and depolymerization of f-actin at water/solid interfaces," *Nanoscale*, vol. 8, no. 11, pp. 6008–6013, 2016.

[292] Y. Ling, C. Li, K. Feng, R. Duncan, R. Eisma, Z. Huang, and G. Nabi, "Effects of fixation and preservation on tissue elastic properties measured by quantitative optical coherence elastography (oce)," *Journal of biomechanics*, vol. 49, no. 7, pp. 1009–1015, 2016.

[293] L. L. Cooper, S. K. Musani, J. A. Moore, V. A. Clarke, Y. Yano, K. Cobbs, C. W. Tsao, J. Butler, M. E. Hall, and N. M. Hamburg, "Clinical associations of vascular stiffness, microvascular dysfunction, and prevalent cardiovascular disease in a black cohort: The jackson heart study," *Journal of the American Heart Association*, vol. 9, no. 18, p. e017018, 2020.

[294] L. Hansen and W. R. Taylor, "Is increased arterial stiffness a cause or consequence of atherosclerosis?," *Atherosclerosis*, vol. 249, pp. 226–227, 2016.

[295] C. Vlachopoulos, K. Aznaouridis, and C. Stefanadis, "Prediction of cardiovascular events and all-cause mortality with arterial stiffness: a systematic review and meta-analysis," *Journal of the American College of Cardiology*, vol. 55, no. 13, pp. 1318–1327, 2010.

[296] S. J. Zieman, V. Melenovsky, and D. A. Kass, "Mechanisms, pathophysiology, and therapy of arterial stiffness," *Arteriosclerosis, thrombosis, and vascular biology*, vol. 25, no. 5, pp. 932–943, 2005.

[297] M. R. Bennett, S. Sinha, and G. K. Owens, "Vascular smooth muscle cells in atherosclerosis," *Circulation research*, vol. 118, no. 4, pp. 692–702, 2016.

[298] C. Collins, L. D. Osborne, C. Guilluy, Z. Chen, E. T. OBrien, J. S. Reader, K. Burridge, R. Superfine, and E. Tzima, "Haemodynamic and extracellular matrix cues regulate the mechanical phenotype and stiffness of aortic endothelial cells," *Nature communications*, vol. 5, no. 1, pp. 1–12, 2014.

[299] N. L. Sehgel, Y. Zhu, Z. Sun, J. P. Trzeciakowski, Z. Hong, W. C. Hunter, D. E. Vatner, G. A. Meininger, and S. F. Vatner, "Increased vascular smooth muscle cell stiffness: a novel mechanism for aortic stiffness in hypertension," *American Journal of Physiology-Heart and Circulatory Physiology*, vol. 305, no. 9, pp. H1281–H1287, 2013.

[300] X. Li, L. Liu, X. Zhang, and T. Xu, "Research and development of 3d printed vasculature constructs," *Biofabrication*, vol. 10, no. 3, p. 032002, 2018.

[301] X.-F. Ming, C. Barandier, H. Viswambharan, B. R. Kwak, F. Mach, L. Mazzolai, D. Hayoz, J. Ruffieux, S. Rusconi, and J.-P. Montani, "Thrombin stimulates human endothelial arginase enzymatic activity via rhoa/rock pathway: implications for atherosclerotic endothelial dysfunction," *Circulation*, vol. 110, no. 24, pp. 3708–3714, 2004.

[302] M. E. Safar, R. Asmar, A. Benetos, J. Blacher, P. Boutouyrie, P. Lacolley, S. Laurent, G. London, B. Pannier, and A. Protogerou, "Interaction between hypertension and arterial stiffness: an expert reappraisal," *Hypertension*, vol. 72, no. 4, pp. 796–805, 2018.

[303] M. Levin, T. Thorlin, K. R. Robinson, T. Nogi, and M. Mercola, "Asymmetries in h+/k+-atpase and cell membrane potentials comprise a very early step in left-right patterning," *Cell*, vol. 111, no. 1, pp. 77–89, 2002.

[304] D. K. Lieu, P. A. Pappone, and A. I. Barakat, "Differential membrane potential and ion current responses to different types of shear stress in vascular endothelial cells," *American Journal of Physiology-Cell Physiology*, vol. 286, no. 6, pp. C1367–C1375, 2004.

[305] E. G. Lakatta, V. A. Maltsev, and T. M. Vinogradova, "A coupled system of intracellular ca2+ clocks and surface membrane voltage clocks controls the timekeeping mechanism of the hearts pacemaker," *Circulation research*, vol. 106, no. 4, pp. 659–673, 2010.

[306] G. Thrivikraman, S. K. Boda, and B. Basu, "Unraveling the mechanistic effects of electric field stimulation towards directing stem cell fate and function: A tissue engineering perspective," *Biomaterials*, vol. 150, pp. 60–86, 2018.

[307] L. Falkovsky, "Optical properties of graphene," in *Journal of Physics: conference series*, vol. 129, p. 012004, IOP Publishing.

[308] A. R. Bausch, W. Möller, and E. Sackmann, "Measurement of local viscoelasticity and forces in living cells by magnetic tweezers," *Biophysical journal*, vol. 76, no. 1, pp. 573–579, 1999.

[309] P. Kollmannsberger, C. T. Mierke, and B. Fabry, "Nonlinear viscoelasticity of adherent cells is controlled by cytoskeletal tension," *Soft Matter*, vol. 7, no. 7, pp. 3127–3132, 2011.

[310] D. E. Ingber, N. Wang, and D. Stamenovic, "Tensegrity, cellular biophysics, and the mechanics of living systems," *Rep Prog Phys*, vol. 77, no. 4, p. 046603, 2014.

[311] N. Wang, K. Naruse, D. Stamenovi, J. J. Fredberg, S. M. Mijailovich, I. M. Toli-Nørrelykke, T. Polte, R. Mannix, and D. E. Ingber, "Mechanical behavior in living cells consistent with the tensegrity model," *Proceedings of the National Academy of Sciences*, vol. 98, no. 14, pp. 7765–7770, 2001.

[312] M. Karplus and J. A. McCammon, "Molecular dynamics simulations of biomolecules," *Nature structural biology*, vol. 9, no. 9, pp. 646–652, 2002.

APPENDIX

SUPPLEMENTARY MATERIAL*

Vessel-on-a-Chip Cell Extraction: Trypsinizing cells from the vessel-on-a-chip system for processing and later use in experimentation required a modified protocol for consistent results, which is laid out here for reproducibility. After removal of the chip from the experimental conditions (connections, syringe pump, etc.), place an empty pipette tip (200 ţL is the lower limit since this protocol relies on gravity flow, but higher volume tips are acceptable) on one of the two ports of the microfluidic chamber. In the other, still open port, fill a pipette tip to full volume with PBS and place it on the other port. Remove the tip from the pipettor without pushing any of the PBS through the chamber and place it in the incubator for 3-5 minutes. This serves as the PBS wash step. After the short incubation, check to see PBS flow-through on the other side, indicating that PBS is now the fluid volume in the channel. Remove both pipette tips from all ports. Repeat the steps for a wash with 0.25% trypsin. However, for this step, incubate within the cell incubator for 2 minutes. Remove the chips after and observed under a microscope to detect cell detachment. If cells are not fully detached, the chamber may be gently percussed to facilitate detachment. Afterwards, in the chamber, if cells are not present, they are now detached, and the fluid may be removed from the chamber. To do so, prime a pipette for suction by pressing the top dispensation plunger all the way down and connect it to the pipette tip with the lower volume. Let go of the plunger and suction the cells in the trypsin through. Once a majority of the volume is withdrawn, remove the tip and add the trypsin to an equivalent or greater volume of cell media in a centrifuge tube. Media may be perfused through the chamber after to pick up any cells not obtained through the first suction. The tube may be centrifuged for a pellet, and any subsequent protocol may be performed. It is important to note that trypsinization rapidly deactivates YAP, though gene expression is dependent on the mRNA half-life. Thus, all trypsinization steps to RNA extraction should be kept to under

10 minutes to ensure preservation of the phenotype and not introduce artifacts.

*Text and figures reprinted with permission from "Mechanotransduction-on-chip: vessel-chip model of endothelial YAP mechanobiology reveals matrix stiffness impedes shear response" by B.K. Walther, N.K.R. Pandian, K.A. Gold, E.S. Kiliç, V. Sama, J. Gu, A.K. Gaharwar, A. Guiseppi-Elie, J.P. Cooke, A. Jain, 2021. *Lab on a Chip*, 21, 1738-1751, Copyright 2021 by the Royal Society of Chemistry.